Fatigue Behavior of Thin Cu Films: Film Thickness and Interface Effects

Dong Wang

Institut für Materialforschung

Fatigue Behavior of Thin Cu Films:
Film Thickness and Interface Effects

Dong Wang

Institut für Materialforschung

Zur Erlangung des akademischen Grades eines

Doktors der Ingenieurwissenschaften

von der Fakultät für Maschinenbau

der Universität Karlsruhe (TH) genehmigte Dissertation

Fatigue Behavior of Thin Cu Films:
Film Thickness and Interface Effects

Zur Erlangung des akademischen Grades eines

Doktors der Ingenieurwissenschaften

von der Fakultät für Maschinenbau der

Universität Karlsruhe (TH)

genehmigte

Dissertation

von

Dong Wang M. Sc.

aus Nei Mongol, China

Tag der mündlichen Prüfung: 28. Juni 2007

Hauptreferent: Prof. Dr. rer. nat. O. Kraft

Korreferent: Prof. Dr. rer. nat. P. Gumbsch

Abstract

The mechanical properties of thin metal films are strongly influenced by size through the films thickness and grain size. The best known example of a length scale effect in film mechanical properties is the increase in yield stress with decreasing film thickness or grain size. This effect is usually attributed to the inhibition of dislocation motion and nucleation in small volumes. In addition, previous work indicates a length scale effect on fatigue behavior in thin Cu films. Therefore, this study will present a systematic investigation of the effect of length scale on fatigue life and damage formation in thin Cu films at both room temperature and 200°C and with and without surrounding Ta layers.

Fatigue testing of Cu films with thicknesses between 50 nm and 3.0 µm on Kapton substrate has been performed and the fatigue damage has been investigated using scanning electron and ion beam microscopy. It is observed that the extrusions decrease in number and size with decreasing film thickness or grain size, while the cracks increase in number. The fatigue life is also clearly influenced by size in that a higher strain range or more cycles are required in thinner films to form damage and cause failure. This transition in damage morphology and fatigue life with length scale is explained by a transition in mechanism from dislocation controlled plasticity in the thicker films to cracking along interfaces and boundaries in the thinner films. In order to gain better insight into the deformation mechanisms, synchrotron diffraction studies were performed on the thin films during cyclic loading.
The fatigue damage of the Cu films loaded at 200°C is similar to that at room temperature, except that the extrusions are more rounded and the grain boundary grooves are larger. This indicates that diffusion processes play an important role during fatigue damage formation and likely account for the clearly reduced fatigue life at 200°C.

The presence of surrounding Ta layers has a clear influence on the fatigue behavior of the Cu films. A Ta under-layer does not change much in the Cu film fatigue behavior, but a Ta over-layer leads to a dramatic improvement in fatigue life in the thicker Cu films. This is likely due to the observed inhibition of extrusion formation by the presence of the over-layer. In contrast, the Ta over-layer has little effect on the fatigue life of the thinner Cu films. This is presumably an indication that the Ta over-layer does not influence crack formation and is consistent with the transition to failure by crack growth in the thinner films.

Ermüdungsverhalten dünner Cu-Schichten: Größeneffekte und Grenzflächeneffekte

Kurzzusammenfassung

Größeneffekte in Bezug auf die mechanischen Eigenschaften von Werkstoffen zeigen sich an vielen Stellen. Ein prominentes Beispiel ist die Zunahme der Fließspannung dünner Metallschichten mit Abnahme der Schichtdicke. Diese wird in der Regel durch eine Behinderung der Versetzungsbewegung und limitierte Versetzungsbildung in eingeschränkten Dimensionen erklärt. Darüber hinaus wurde auch ein Größeneffekt für das Ermüdungsverhalten dünner Metallschichten gefunden. Im Rahmen der vorgelegten Arbeit sollte deshalb das Ermüdungsverhalten dünner Cu-Schichten systematisch in Bezug auf Lebensdauer und Schädigung in Abhängigkeit von der Schichtdicke (50 nm bis 3,0 μm) bei Raumtemperatur und erhöhten Temperaturen sowie der Einfluss einer Deckschicht untersucht werden.

Die mikroskopischen Arbeiten, die mithilfe der Rasterelektronen- und Focused Ion Beam-Mikroskopie durchgeführt wurden, zeigen, dass sich die Schädigungsmorphologie in Abhängigkeit von der Schichtdicke deutlich verändert, und zwar nimmt die Zahl und die Größe von Extrusionen, die sich durch die zyklische Verformung bilden, mit Abnahme der Schichtdicke und Korngröße ab. Auf der anderen Seite wurden mehr Risse in den dünneren Schichten beobachtet. Der Größeneffekt auf die Lebensdauer ist ebenfalls sehr deutlich ausgeprägt. Es wurde nachgewiesen, dass deutlich höhere Dehnungsamplitude aufgebracht werden müssen um in dünneren Schichten eine Schädigung zu erzeugen. Auf Grund der Änderung in der Schädigungsmorphologie und der Lebensdauer, wird ein Wechsel im Ermüdungsmechanismus von versetzungsgetragener Extrusionsbildung zu einer Rissbildung an existierenden Defekten vorgeschlagen. Um hier einen besseren Einblick in das Verformungsverhalten zu erlangen, wurden Röntgenmessungen an einer Synchrotronquelle durchgeführt.

Des Weiteren wurde beobachtet, dass das Ermüdungsverhalten der dünnen Cu-Schichten bei 200°C ähnlich ist wie bei Raumtemperatur, aber Extrusionen weniger scharfe Kanten aufweisen und an Korngrenzen Furchen entstehen. Das deutet darauf hin, dass Diffusionsprozesse eine wichtige Rolle bei der Schädigungsentstehung spielen, wobei die Lebensdauer deutlich reduziert ist.

Auch eine Ta-Deckschicht hat einen offensichtlichen Einfluss auf das Ermüdungsverhalten der Cu-Schichten. Mit der Ta-Deckschicht werden in einer 1 µm dicken Ta/Cu/Ta-Schicht weniger und kleinere Extrusionen als in Cu-Schichten gleicher Dicke beobachtet. Dabei wird die Lebensdauer dramatisch erhöht. Dieser Effekt ist für die Lebensdauer eines Ta/Cu/Ta Schichtstapel mit 100 nm dicken Cu weit weniger ausgeprägt, da vermutlich die Extrusionsbildung hier eine viel kleinere Rolle spielt und die Lebensdauer durch Rissbildung bestimmt wird. Diese Beobachtungen sind in Einklang mit dem vorgeschlagenen Mechanismuswechsel.

Danksagung

Die vorliegende Doktorarbeit wurde zwischen Mai 2004 und Mai 2007 am Institut für Materialforschung II des Forschungszentrums Karlsruhe angefertigt. Den Personen, die für den Fortgang dieser Arbeit von besonderer Bedeutung waren möchte ich hier danken:

Herrn Prof. Dr. O. Kraft für die Stellung dieses Promotionsthemas, sein Interesse an der Arbeit, viele wichtige und hilfreiche Diskussion sowie die Übernahme des Hauptreferats.

Herrn Prof. Dr. P. Gumbsch für die freundliche Übernahme des Korreferats.

Frau Dr. C.A. Volkert für die fördernde Betreuung, viele wichtige Anregungen, Vorschläge und Diskussion sowie Hilfen bei Verbesserung meiner Schreibfähigkeit in englische Sprache.

Herrn Dr. P. Gruber (Max-Planck Institut für Metallforschung) für die freundliche Hilfen bei der Spannungsmessungen mittels Synchrotron X-Ray und viele wertvolle Diskussionen.

Herrn Dr. B. Okolo und Herrn Prof. Dr. A. Wanner (Universität Karlsruhe) für die freundliche Hilfen bei XRD Messungen.

Frau D. Exner für die ausführliche Einschulung am DMA.

Herrn W. Schwan für die ausführliche Einschulung am FIB.

Herrn Dr. T. Wagner und Herrn F. Thiele (Max-Planck Institut für Metallforschung) für die Herstellung der untersuchten Schichten.

Herrn M. Klotz für die Auslagerung von der Proben.

Allen Mitgliedern am IMF II, besonders an der Abteilung WMI für die angenehme und kooperative Arbeitsatmosphäre.

Meine Frau für die beste Unterstützung und Ermunterung.

Vor allem möchte ich mich bei Gott für die Führung meines Lebens herzlich bedanken.

Contents

1 Introduction

With the rapid development of microelectronics (ME), micro-electro-mechanical systems (MEMS), and macroelectronics (such as flexible displays), thin metal films have been placed under increasingly demanding conditions over the last several decades in their application as interconnects and components. The reliability of such devices or systems depends partially on the mechanical properties of the thin metal films or structures. Many investigations of thin films show clearly different mechanical behavior from that of their bulk counterparts. In particular it is observed that flow stress increases with decreasing film thickness and/or grain size which is attributed to the inhibition of dislocation motion and nucleation stressing small volumes. Furthermore, surrounding films or materials also have a large influence on the mechanical response of thin films since they also typically hinder dislocation motion in the film.

Recently, mechanical studies of thin films have been extended to fatigue studies. The results show that there are length scale effects here as well, namely thinner films need either more cycles or higher applied strain or stress range to cause failure. Moreover, such studies show that characteristic fatigue dislocation structures and surface damage morphology change as the films are made thinner. Therefore, investigations of fatigue behavior in thin metal films give not only direct indication of reliability threats in various applications, but also give important insights in basic material science at small length scales.

In Chapter 2, a brief overview of thin film mechanical testing methods and fatigue behavior in bulk metals and thin metal films will be introduced. Chapter 3 depicts fabrication of the samples and the experimental methods. All representative experimental results are described in Chapter 4. In the first section of Chapter 4, the microstructure of the thin films is described. In the second section, results of systematic studies of high cycle fatigue behavior in Cu films with different thickness (50 nm to 3.0 μm) are given. The third section shows the results of stress

determination using synchrotron x-ray in fatigued films. The fourth section present results of fatigue behavior of thin Cu films at 200°C. Results of investigations of the effects of Ta over- and under-layers on fatigue behavior of thin Cu film will be summarized in last section. The implications and proposed explanations of these results will be presented in Chapter 5.

2 Literature Review

There are clear differences between the mechanical and fatigue behavior of thin metal films and their bulk counterparts. In this chapter, a brief overview of mechanical testing methods and properties of thin films will be summarized from recent literature, with a focus on length scale effects in yield stress. Then, a summary of the extensive literature on fatigue behavior in bulk metals will be introduced and compared with the recent literature on fatigue in thin metal films.

2.1 Mechanical testing and properties of thin metal films

With the development of the microelectronics industry in the last several decades, more and more attention has been devoted to investigating mechanical properties of thin films. Novel testing methods have been developed to investigate the mechanical properties of thin films. In this section, mechanical testing and mechanical properties from the literature are briefly reviewed, and the applicability of the mechanical testing techniques to fatigue testing is discussed.

2.1.1 Mechanical testing of thin films

Mechanical properties of thin films can not be simply deduced from those of their bulk counterparts due the constraint of dimension and microstructure on various processes such as dislocation activation [Nix1989, Arzt1998]. Therefore, it is necessary to experimentally investigate the length scale effects and microstructure effects on mechanical behavior in thin films, and several specialized testing techniques have been developed [Nix1989, Brotzen1994, and Kraft2001a].

The wafer curvature method was developed for stress measurement during a temperature change, when film and substrate have different thermal expansion coefficients [Flinn1987, Keller1998, Keller1999, and Venkatraman1992]. The radius of curvature of the substrate is used to calculate the stress in the film. If the

temperature change is cyclically repeated, the thermal fatigue behavior of thin film can be studied [Mönig2004].

Bulge test is also a specialized method for thin films, in which a freestanding film is pressurized from one side and the resultant bulge height is measured to determine both elastic and plastic behavior [Vlassak1992, Xiang2002, and Xiang2005]. Fig. 2-1 illustrates the bulge test of thin film. Special fabrication processes are required for this method and it is not clear that is applicable to fatigue testing.
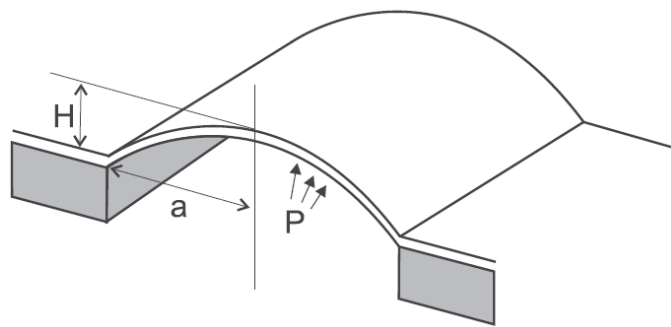

Fig. 2-1 Schematic illustration of a bulge test on thin film.

Microbeam bending is used to investigate elasticity, plasticity and fracture in thin films [Weihs1988, Florando2005]. Normally the specimen is fabricated using deposition, lithography, etching and other microfabrication techniques. Fig. 2-2 depicts the set-up of the bending test. As the microbeam is repeatedly loaded, fatigue behavior of thin films can be studied with this method [Schwaiger1999].

Microtensile testing can also be used for thin films. Both freestanding films and films on substrates can be used. Tests with freestanding films have higher requirements of specimen preparation and handling, but the stress can be determined directly. Films on substrates are much easier to handle, but extra steps must be taken to determine the stress in the film. In some cases, x-ray diffraction is used to measure the elastic strain in the thin film, from which the stress can be calculated [Hommel1999, Hommel2001, and Boehm2004]. If the substrate is sufficiently thin and compliant, the stress of the metal film can be obtained by subtracting the contribution of the substrate from the total force [Yu2004]. In addition, an obvious difference between tests on freestanding films and on films deposited on substrate is

that freestanding films can only be stressed in tension, while films on substrate can be stressed in both tension and compression [Hommel1999]. Fatigue behavior of thin Cu films on Kapton substrate has been studied using the cyclic tensile testing [Schwaiger2003, Kraft2001, Kraft2002, Zhang2003, Zhang2005, and Zhang2006].
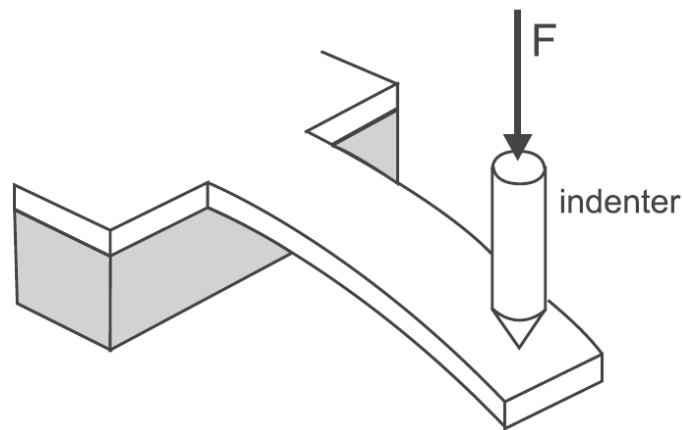
Fig. 2-2 Schematic illustration of set-up for bending test.

Indentation is also a widely used method to determine the mechanical properties for thin films. However it leads to very inhomogeneous stresses and strains and is difficult to use for quantitative determination of fatigue behavior. A more detailed review of mechanical testing of thin films is given in [Nix1989, Brotzen1994, and Kraft2001a].

2.1.2 Mechanical properties of thin films

Mechanical properties of thin metal films are different from those of their bulk counterparts due to length scale effects. The small sample dimensions and grain sizes of thin films inhibit dislocation motion and limit dislocation nucleation, leading to an increase in yield stress [Nix1989, Arzt1998]. Several literature results for the yield stress of Cu thin films are summarized in Fig. 2-3 [Hommel2001, Yu2004, and Nicola2006]. The size effect is seen in the increase in the yield stress with decreasing film thickness (and corresponding decreasing grain size). Over-layers also increase the strength, due to constraint of dislocation motion at the interface produced with the over-layer [Keller1998, Arzt1998, and Nicola2006].

Fig. 2-3 Yield stress at 0.1% plastic strain [Hommel2001] and 0.2% plastic strain [Yu2004, Nicola2006] in thin Cu films.
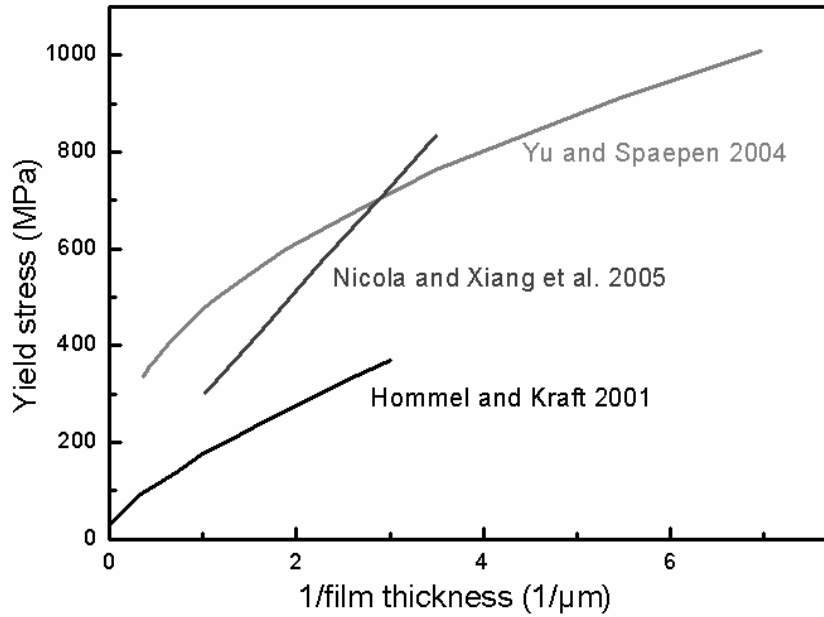
Different models have been developed to describe the increasing strength in thinner films. The Nix model depicts the confinement effects based on dislocation channeling through the thickness [Nix1989, Nix1998]. As response to applied stress, the threading segment of dislocation moves forward to reduce strain energy, while the deposited segment of dislocation becomes longer and costs energy. This leads to a threshold stress for dislocation motion, and as result, the driving stress to move the threading segment scales with inverse of film thickness. When grain size is similar to thickness, grain size decreases with decreasing film thickness. Hall-Petch effect is also considered for the strengthening due to dislocation pile-up at grain boundaries. This means that strength increases with decrease of film thickness/grain size. Thompson extended the Nix model to include the deposition of dislocations at grain boundaries, creating an additional term to describe the grain size effect on yield stress of polycrystalline thin films [Thompson1993]. In fact, a separation of thickness effect and grain size effect in strengthening was studied by [Venkatraman1992]. Further more, the classical Taylor relation between the strength and dislocation density was also applied in thin films to study work hardening [Keller1998]. A comparison of strengthening due to Nix dimensional constraint, Hall-Petch effect and Taylor relation was summarized by [Baker2001]. More over, it is argued that

dislocation sources are limited in thin film or small dimensional structures and thereby the strength increases with decrease of thickness [Arzt2001, Blanckenhagen2001, and Blanckenhagen2003]. As film thickness decreases, dislocation nucleation becomes more difficult and plasticity is source-limited.

Freestanding thin metal films rupture at small strain (<2%) [Huang2000]. Thin Cu films on Kapton substrate can sustain much larger strain (>7%) without the presence of cracks [Gruber2004]. This is proposed to be due to that the strain localization (necking) which causes a local elongation is on the order of the film thickness, while the substrate inhibits strain localization when the film is on a substrate [Li2005]. Cracking in films on a substrate depends on the stress and mechanical properties of substrate and film and, as a result, is very complicated. Extensive reviews of research work of crack in film on substrate using fracture mechanics are given in [Hutchinson1991, Evens1995]. In addition, Xiang and his colleagues [Xiang2005a] have reported that the rupture strains of Cu films are sensitive to their adhesion to the polyimide substrate. This implies that the rupture strain depends on the interface quality. Furthermore, it is reported that patterned thin metal films on polymer substrates have a better stretchability than unpatterned thin metal films on polymer substrates [Li2005, Lacour2006].

Besides the plastic and fracture properties, Young's modulus in thin films or multilayer was often observed to be smaller than that of their bulk counterparts [Huang2000, Kalkman2001, and Yu2004]. Modulus deficit results presumably from more compliant grain boundaries [Huang2000], grain boundary sliding [Kalkman2001] or reversible microplasticity [Huang2000, Nucci2005].

2.2 Fatigue in bulk metals

Fatigue is understood as damage or failure in materials due to suffering a repeated load. It can be termed mechanical fatigue or thermal fatigue and others according to loading type. But generally fatigue is referred as mechanical fatigue, in which a repeated stresses or strains are applied. The fatigue behavior has an important implication on the reliability of a material.

2.2.1 Fatigue life approaches

Fatigue life, defined as the total number of cycles until failure, is mainly studied by two approaches, the stress-life approach and the strain-life approach. The stress-life approach was first introduced by Wöhler in the 1860s [Woehler1860], where the stress amplitude is controlled during cyclic loading of a specimen.

Fatigue cycles of sinusoidal waveform with nonzero mean stress are shown schematically in Fig. 2-4. In this case, the stress parameters, namely the stress range, $\Delta\sigma$, the stress amplitude, σ_a, and the mean stress, σ_m, which all affect the fatigue life, are defined as:

$$\Delta\sigma = \sigma_{max} - \sigma_{min} \tag{2.1}$$

$$\sigma_a = \frac{\sigma_{max} - \sigma_{min}}{2} \tag{2.2}$$

$$\sigma_m = \frac{\sigma_{max} + \sigma_{min}}{2} \tag{2.3}$$

In a fully reversed, constant amplitude fatigue test, the relation of the stress amplitude, σ_a to fatigue life, $2N_f$ is expressed by Basquin equation [Basquin1910]:

$$\frac{\Delta\sigma}{2} = \sigma_a = \sigma'_f \, (2N_f)^b \tag{2.4}$$

where σ'_f is the fatigue strength coefficient, b the fatigue strength exponent.
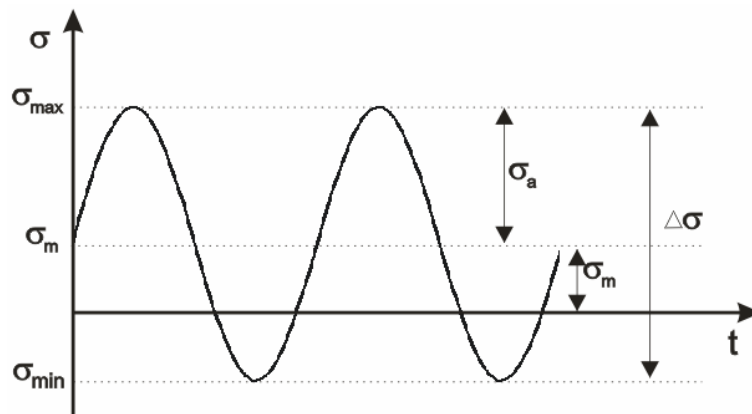

Fig. 2-4 Nomenclature for stress parameters. The variation of stress σ with time t is shown.

As the stress amplitude increases, fatigue life is reduced, which is schematically shown in Fig. 2-5. Here, the stress amplitude of an uniaxial fatigue test is plotted versus the fatigue life, number of cycles to failure $2N_f$, for metallic materials. This is because crack initiation as well as crack propagation is faster with larger stress amplitudes. In addition, there is a mean stress effect on fatigue life. Different S-N (stress amplitude - life) responses are induced by different mean stress level, σ_{m1}, σ_{m2}, σ_{m3}. Generally, fatigue life decreases with increasing mean stress value.
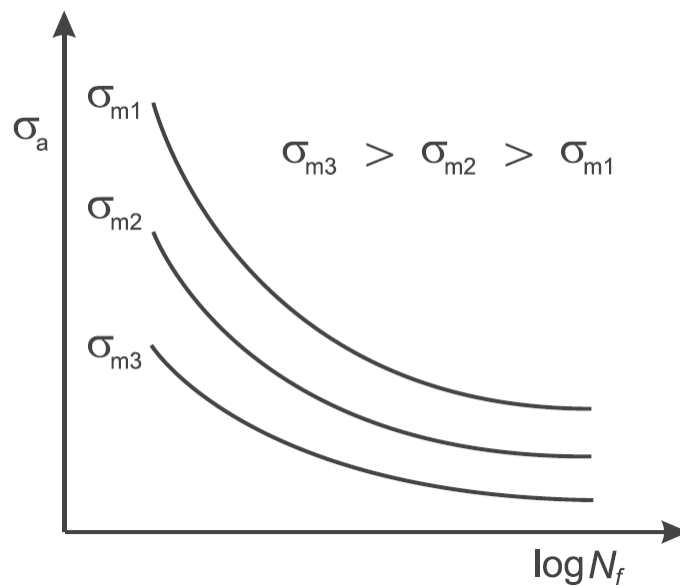
Fig. 2-5 Typical stress amplitude - life plot showing mean stress effect on fatigue life.

In analogy, in the strain-life approach, the strain amplitude is controlled to test for the fatigue life. Independently in 1954, Coffin and Manson proposed to characterize fatigue life based on the relation with the plastic strain in low cycle fatigue regime [Coffin1954, Manson1954]. This relation can be written as

$$\frac{\Delta \varepsilon_p}{2} = \varepsilon'_f \left(2N_f\right)^c \tag{2.5}$$

where $\Delta\varepsilon_p/2$ is the plastic strain amplitude, ε'_f the fatigue ductility coefficient and c the fatigue ductility exponent.

The total strain amplitude $\Delta\varepsilon/2$ can be rewritten as the sum of elastic strain amplitude, $\Delta\varepsilon_e/2$, and plastic strain amplitude, $\Delta\varepsilon_p/2$:

$$\frac{\Delta\varepsilon}{2} = \frac{\Delta\varepsilon_e}{2} + \frac{\Delta\varepsilon_p}{2} \qquad (2.6)$$

using Basquin equation (Eq. 2.4) and noting that

$$\frac{\Delta\varepsilon_e}{2} = \frac{\Delta\sigma}{2E} + \frac{\varepsilon_a}{E} \qquad (2.7)$$

where E is Young's modulus, it is found that

$$\frac{\Delta\varepsilon_e}{2} = \frac{\sigma'_f}{E}(2N_f)^b \qquad (2.8)$$

Combining Eqs. 2.5, 2.6 and 2.8 one obtains

$$\frac{\Delta\varepsilon}{2} = \frac{\Delta\varepsilon_e}{2} + \frac{\Delta\varepsilon_p}{2} = \frac{\sigma'_f}{E}(2N_f)^b + \varepsilon'_f(2N_f)^c \qquad (2.9)$$
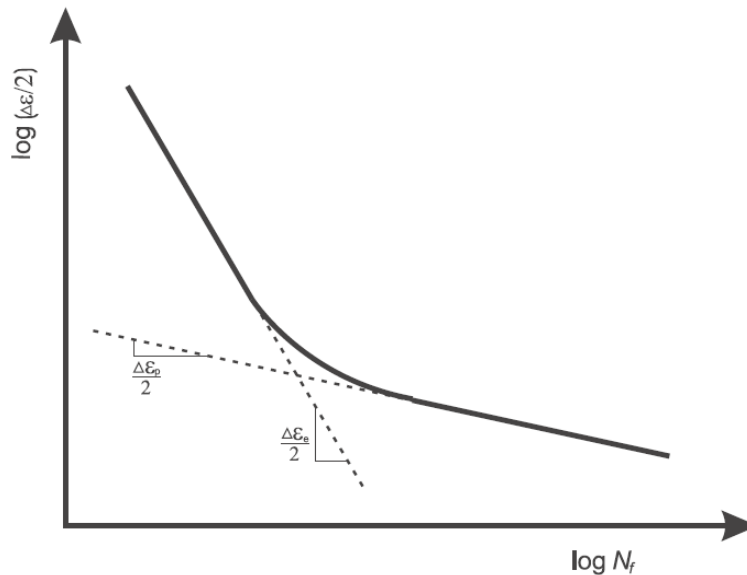
Fig. 2-6 The total strain amplitude Δε/2 versus fatigue life. The variations of elastic and plastic strain amplitude, Δε$_e$/2, andΔε$_p$/2, leading to transition in the relation.

On the right side of Eq. 2.9, the first and second term are the fatigue lives with respect to the elastic and plastic component in the total strain, respectively. A schematic representation of Eq. 2.9 is given in Fig. 2-6. For low cycle fatigue, the macroscopic strain is predominantly plastic and the first term in Eq. 2.9 is dominant. For high cycle fatigue, the macroscopic strain is elastic and the second term becomes dominant. Fig. 2-6 describes the logarithmic relation between total strain amplitude and fatigue life, showing a clear transition from low cycle regime to high cycle

regime. For most metallic materials, the transition between the two regimes occurs at about 10^4 cycles.

2.2.2 Fatigue damage

Fatigue damage, particularly in face-centered cubic (f.c.c.) metals, includes the formation of characteristic dislocation structures, surface damage and fatigue cracks.

Dislocation structures, such as persistent slip bands (PSBs), labyrinth structures and dislocation cells, form by self-ordering of dislocations over long distances in a crystal with typical feature dimensions in the micrometer regime. They form due to dislocation interaction in the early fatigue stage of cyclic deformation in both single and polycrystalline f.c.c. bulk metals [Mughrabi1979, Ackermann1984]. For example, Fig. 2-7 shows a TEM micrograph of dislocation structures (PSBs) in a fatigued Cu crystal [Mughrabi1979]. The exact nature of the dislocation structure is very complicated and depends on crystal orientation, strain/stress amplitude and number of cycles.

Fig. 2-7 TEM image of dislocation structures (PSBs) in a fatigued Cu crystal [Mughrabi1979].

Detailed investigations show the surface damage (extrusion and intrusion) is associated with PSBs [Lukáš2004], which represent zones of cyclic plastic strain localization. This is shown schematically in Fig. 2-8. More slip activity can occur in

the plastic PSBs than in the surrounding matrix. While coarse slips cause extrusion and intrusion formation at the intersection of PSBs with the surface, fine slip leads to only to much smaller slip traces at the surface of the matrix.
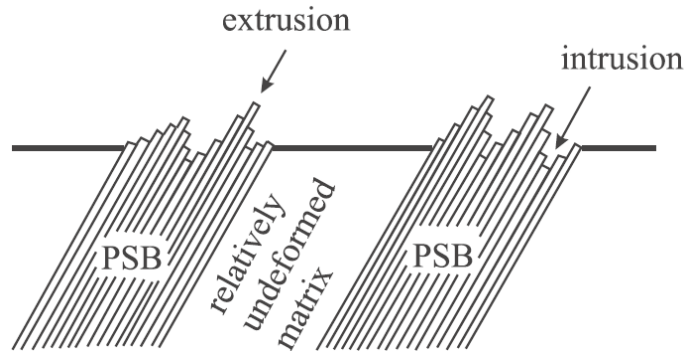

Fig. 2-8 A rough surface consisting of hill and valleys produced by cyclic plastic strain [Suresh1998].

In the next stage of fatigue, such extrusions/intrusions lead to the formation of cracks from surface intrusions, leading eventually to failure [Essmann1981, Ma1989]. Another mode is that cracks are initiated at grain boundaries, where PSBs impinge [Essmann1981, Zhang1999]. Heinz and Neumann have also reported twin boundaries as crack initiation sites in high cycle fatigued austenitic stainless steel [Heinz1990]. Twin boundaries are regarded as stress raisers due to the elastic anisotropy between the crystals on either side of the twin boundary. In addition, the twin boundary orientation strongly influences the density and propagation of twin boundary cracks [Blochwitz2003, Blochwitz2005]. Twin boundaries are also observed as preferred sites for early PSB nucleation [Llanes1992, Peralta1994].

In summary, bulk metals come to fatigue failure in following sequence: (i) formation of dislocation microstructures (like PSBs), (ii) surface roughening in terms of surface extrusions and intrusions induced by intersecting dislocation structures at the surface, (iii) crack initiation at surface intrusion, (iv) stable growth of cracks with characteristic crack face striations, and (v) rapture of the whole specimen.

2.3 Fatigue behavior of thin metal films

In recent years several studies have been focused on the fatigue behavior of thin metal films [Read1998, Kraft2001, Kraft2002, Schwaiger2003, Schwaiger2003a, Zhang2003, Zhang2005, and Zhang2006]. Thermal fatigue of thin Cu films due to repeated temperature change has also been studied [Moenig2004, Park2006, and Park2007]. Besides, fatigue behavior of thin metal films was studied at ultra high frequency based on surface acoustic wave (SAW) technique [Eberl2006, Eberl2006a].
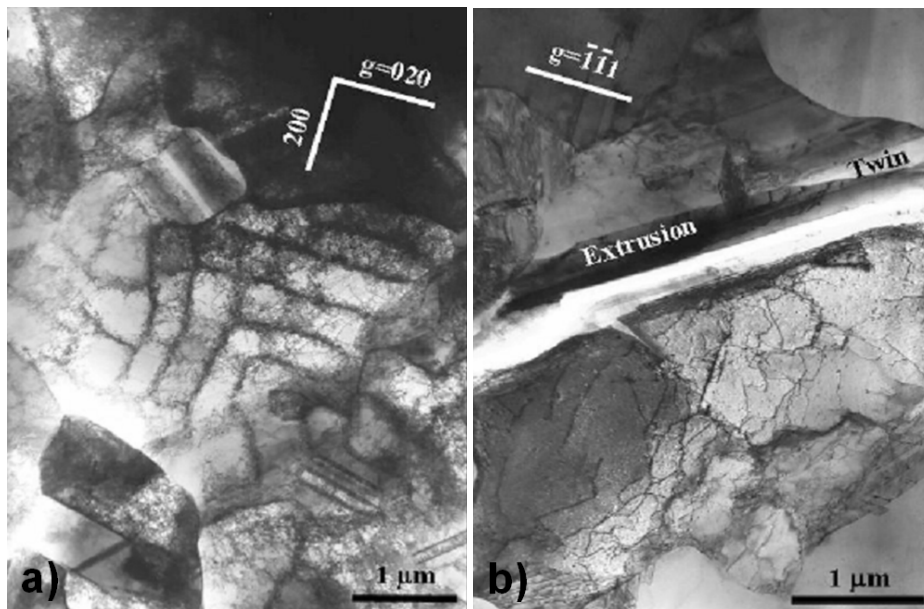
Fig. 2-9 TEM observations of dislocation structures in fatigued Cu thin films: (a) 3.0 μm thick film with a [001] zone axis, (b) 0.4 μm thick film with [123] zone axis [Zhang2003].

These studies have shown that size effects in fatigue are significant at the micrometer and sub-micrometer length scale. As the film thickness or grain size is reduced, the fatigue life at constant applied total strain is increased [Kraft2002, Schwaiger2003a, and Moenig2004]. Similarly, characteristic fatigue dislocation structures are not present in thin films for thickness or grain size below 1 μm [Zhang2003, Zhang2005, and Zhang2006]; instead just single dislocations are found. This is illustrated in Fig. 2-9 (a) and (b), which show the TEM images of fatigued 3.0

μm thick and 0.4 μm Cu films, respectively. Furthermore, the surface extrusions decrease in size and number with decreasing film thickness or grain size and are replaced by cracks along boundaries in mechanical fatigue [Zhang2003, Zhang2005, and Zhang2006], and grain boundary grooves in thermal fatigue [Moenig2004, Park2006, and Park2007].

2.4 Perspectives of this work

Thin metal films show very different mechanical and fatigue behavior than their bulk counterparts. The previous literature on fatigue in thin Cu films shows a clear effect of film thickness or grain size on fatigue damage and suggests that fatigue life increases with decreasing film thickness.

In this work, the fatigue behavior of thin Cu films of different thicknesses (50 nm to 3.0 μm) and with Ta under- and over-layers has been investigated. The goal is to understand the effects of film thickness, grain size, and surrounding layers (or interface quality) on fatigue damage evolution and fatigue life. These studies differ from previous studies in that they extend the investigations to: (1) higher cycle numbers and lower total strains, which are closer to the conditions present in technological applications; (2) thinner films and smaller grains; (3) quantitative analysis of damage evolution for different applied strains; (4) fatigue behavior of thin Cu films at 200°C; (5) fatigue behavior in Cu films with Ta under- and over-layers; and (6) studies of the stress-strain response during fatigue testing using synchrotron x-ray diffraction. The plastic strain is real driving force for fatigue, and the determination of plastic strain using synchrotron x-ray diffraction technique will help to understand the fatigue mechanism in thin metal films.

3 Experimental Details

3.1 Fabrication of thin film samples

Kapton (polyimide) has been shown to be a suitable substrate material for mechanical testing of thin metal films [Hommel1999, Kraft2000, and Hommel2001], because it is compliant and can be deformed homogeneously and reversibly up to large strains (>3%) [Hommel2001]. By using a reversibly deformable substrate, one can study the behavior of thin films not only in tension, but also in compression [Hommel1999]. As long as the film adheres to the substrate, which is the case for Cu on Kapton [Hommel1999], removing the external load after plastic deformation of the films under tension allows contraction of the elastic substrate and drives the film into compression. For the samples studied here, 125 μm thick dog-bone shaped Kapton-HN (DuPont) sheets were used as the substrate for all thin film samples. The sample geometry is depicted schematically in Fig. 3-1 and the schematic stress-strain response during cyclic tensile testing is shown in Fig. 3-2.
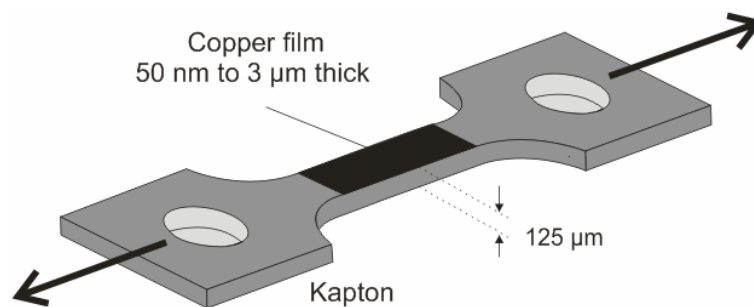

Fig. 3-1 Schematic illustration of sample geometry.

Two series of samples were fabricated and investigated in this work. In the series A, Cu films with thicknesses between 50 nm and 3.0 μm were deposited on the Kapton substrates at the Thin Film Central Facility of the Max-Planck-Institute for Metal Research in Stuttgart. The Kapton substrates had been machined into dog-bone

shaped tensile specimens (gauge lengths of 9 and 20 mm). The Cu films were deposited by Ar sputtering under UHV conditions (base pressure: 10^{-8} mbar) at a power of 100 W. Different thicknesses of Cu (50 nm, 100 nm, 200 nm, 500 nm, 1.0 µm, 3.0 µm) were deposited by controlling the sputtering time. After deposition, the specimens were annealed at 400 °C in vacuum for 2 hours to allow for grain growth. Several specimens of 100 nm thick Cu film were annealed 40 minutes more.
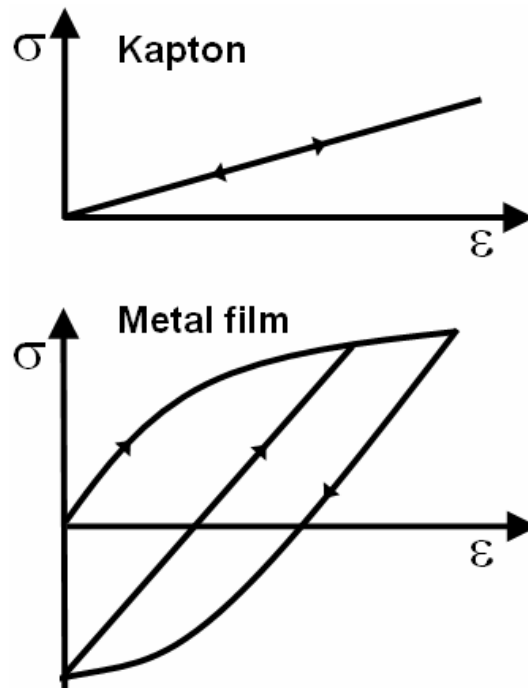
Fig. 3-2 Schematic illustration of the stress-strain responses of the Kapton substrate and the adherent metal film during tensile testing.

In the series B samples, different Cu, Cu/Ta and Ta/Cu/Ta thin film stacks, shown schematically in Fig. 3-3, were deposited on the Kapton substrates also at the Thin Film Central Facility of the Max-Planck-Institute for Metal Research. The Ta layers and Cu films were deposited without breaking vacuum by Ar sputtering under UHV conditions (base pressure: 10^{-8} mbar) at a power of 150 W and 100 W, respectively. The goal of fabrication of this series of samples is to study the influence of under- and over-layers on the fatigue behavior in thin Cu films. Ta was chosen for the under- and over-layer material because it had already been shown to adhere well to Kapton and Cu and to not significantly modify the microstructure of the Cu layer [Gruber2004]. Cu film thicknesses in the series B were 1.0 µm and 100 nm thick and

the Ta over- and under-layers were 10 nm thick. The gauge length and width of the samples with 1.0 μm thick Cu films were 12 mm and 3 mm, respectively, while these were 9 mm and 2 mm for the 100 nm thick Cu film samples.
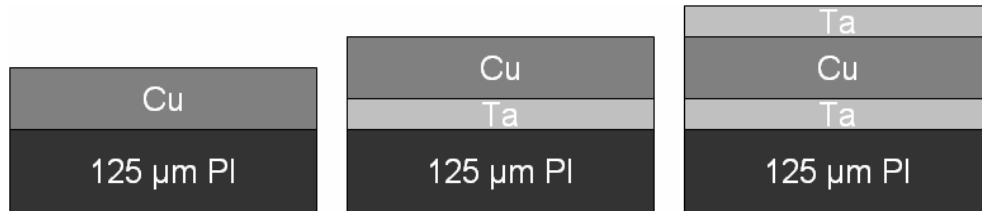
Fig. 3-3 Schematic illustration of the Cu, Cu/Ta and Ta/Cu/Ta thin film stacks on Kapton substrate.
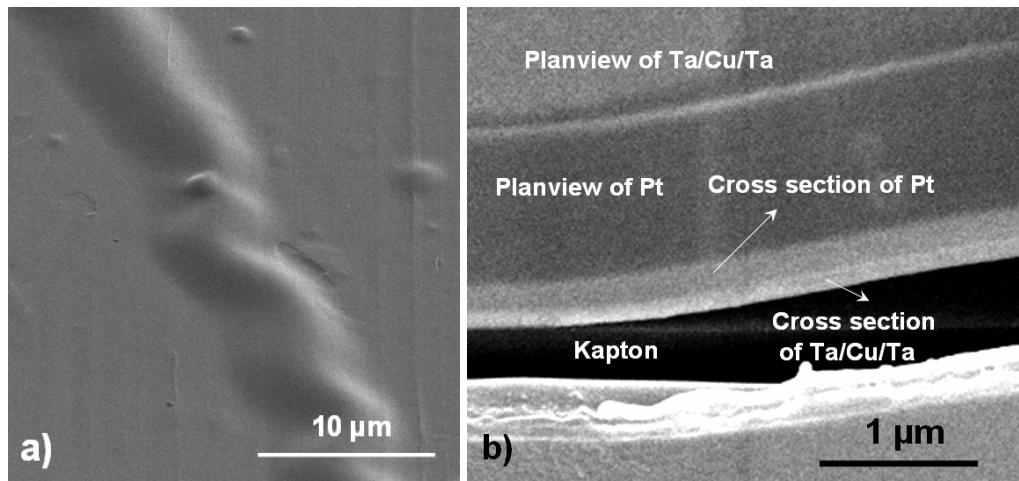
Fig. 3-4 SEM images at 52° tilt of delamination and buckling in a Ta/100 nm Cu/Ta sample after annealing at 400°C for 2 hours in vacuum: (a) surface image showing "telephone cord" buckling and (b) image of a FIB cross-section through the sample showing that delamination has occurred at the Ta/Kapton interface. The Pt layer was deposited to protect the sample during FIB cross-sectioning (see Section 3.2 for more details).

After deposition, the 1.0 μm thick Cu films with and without Ta layers were annealed at 400 °C in vacuum for 2 hours to allow for grain growth. The 100 nm thick Cu films with and without Ta layers were annealed at a lower temperature of 350°C in vacuum for 0.5 hours. This lower temperature was used since annealing the Ta/100 nm Cu/Ta samples at 400°C caused delamination at the Ta/Kapton interface

17

and "telephone cord" buckling (Fig. 3-4). No delamination was observed in the 100 nm thick Cu film stack samples after annealing at 350°C (or in the 1.0 µm thick Cu film stack samples after annealing at 400°C).

3.2 Microstructure characterization

The microstructure of the films was characterized using scanning electron microscopy (SEM) and focused ion beam (FIB) microscopy in a Dual Beam Workstation (FEI Nova NanoLab 200), which reveals the grain structure through crystal channeling contrast. FIB images were obtained at four different tilt angles (0°, 7°, 12°,17°) and overlaid to determine the grain boundary locations accurately. Fig. 3-5 shows a typical FIB image of the grain structure in a 1.0 µm thick Cu film. Both grains and twins can be easily recognized. The grain size was determined by the linear intercept method without taking twin boundaries into account.

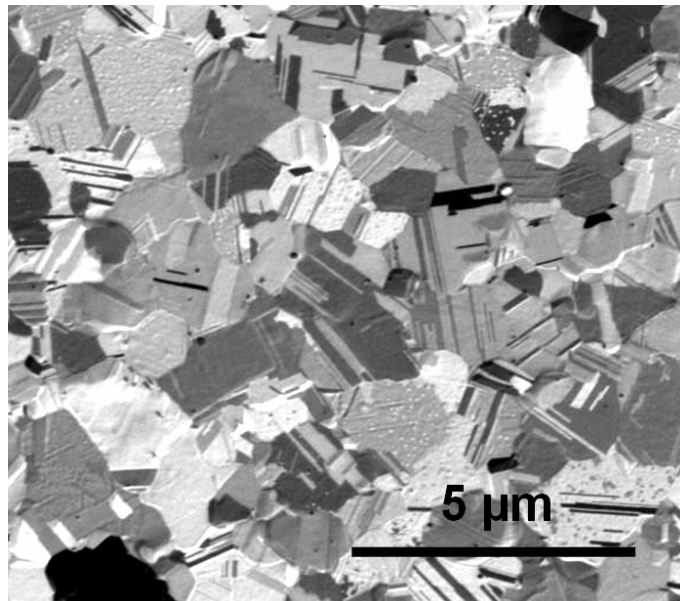Fig. 3-5 FIB image of a 1.0 µm thick Cu film showing grain and twin contrast.

The out-of-plane crystallographic texture of the Cu films was estimated using x-ray diffraction (XRD) with help from Prof. Alexander Wanner and Dr. Brando Okolo (IWK1, University Karlsruhe). θ-2θ XRD measurements were performed in a Seifert virtual axes type diffractometer. Cu-Kα x-rays were generated from a rotating

anode source allowing for a high intensity parallel beam. The diffraction scans were conducted over the 2θ range 38° to 95°.

3.3 Fatigue tests

For the series A samples, most of the fatigue tests were performed using a Dynamical Mechanical Analyzer (DMA) (Netzsch DMA 242), which load cell is driven from an oscillator. The samples were mounted in a tensile test holder and fatigue tests were performed under displacement control at a frequency of 100 Hz. Mounting of the samples had to be performed with care to avoid inhomogeneous stresses in the sample during testing. The homogeneity has been confirmed by the observation that fatigue-induced surface damage is distributed homogenously over the surface of the film. To minimize oxidation of the Cu during both room temperature and 200 °C tests, the furnace chamber enclosing the sample and the grips was supplied with a steady flow of nitrogen gas (flow rate of 100 ml/min) throughout the tests.

Film thickness	Strain range $\Delta\varepsilon$ (%), RT	Strain range $\Delta\varepsilon$ (%), 200 °C
3.0 μm	0.2/0.4	0.2
1.0 μm	0.15/0.2/0.4	0.2
500 nm	0.2/0.4/0.8	0.4
200 nm	0.2/0.3/0.4/0.6/0.8	0.6
100 nm	0.4/0.8/1.0	0.6 (2x)
50 nm	0.8/1.0/1.2	0.6

Table 3.1 Mechanical fatigue tests performed on the series A Cu film samples at room temperature (RT) and 200 °C. The number of tests performed at a particular strain is indicated in parentheses, if more than one.

In order to investigate fatigue damage formation in the Cu films, the fatigue tests were periodically interrupted and the films were studied using dual-beam (scanning electron microscopy (SEM) and FIB) microscopy (FEI Nova NanoLab). Interruption intervals of less than 10^4 cycles were not possible with DMA at 100 Hz;

longer intervals were often chosen to allow for sufficient damage development. Fatigue damage was studied using both surface imaging as well as using FIB cross-sections. Following damage characterization, the samples were remounted in the DMA and fatigue testing was continued. These interruptions were performed iteratively to record the damage evolution during the fatigue process. Table 3.1 lists the strain ranges that were used for the fatigue experiments on the first series of Cu films.

Cu film thickness	Sample type	Strain range $\Delta\varepsilon$ (%)
1.0 μm	Cu	0.2/0.3
	Cu/Ta	0.2/0.3
	Ta/Cu/Ta	0.2/0.3/0.4
100 nm	Cu	1.0
	Cu/Ta	0.8/1.0
	Ta/Cu/Ta	0.8/1.0

Table 3.2 Mechanical fatigue tests performed on the series B Cu film samples (with and without 10 nm thick Ta under- and over-layers) at room temperature.

For a few of the fatigue tests, an electro-mechanical testing apparatus (EnduraTEC ELF 3200) was used. This machine has a magnetically driven load cell and was used instead of the DMA because it can accommodate the larger samples (20 mm gauge length) necessary for the in-situ synchrotron x-ray diffraction determination of the film stress. These tests were displacement controlled.

The series B samples (with Ta layers) were tested using the DMA under the same loading conditions as used for the first series of Cu film samples (displacement control, loading at 100 Hz, nitrogen gas flow). As in the tests on the first series of samples, the damage evolution was characterized by periodically interrupting the fatigue tests for SEM and FIB microscopy. Table 3.2 lists the strain ranges that were used for the fatigue tests on the second series of Cu film samples.

Fatigue failure in bulk samples is usually defined as macroscopic rupture or fracture. However, this criterion cannot be used as a measure of fatigue failure for thin films on substrates, since the load is transferred to the substrate as the film

deteriorates. In the work presented here, a qualitative criterion for thin film failure is defined by the number of cycles when the evolution of extrusions or cracks begins to saturate. This will be described and discussed in later sections.

3.4 Stress determination

Fatigue damage formation and failure is driven by plastic strain. The plastic strain experienced by a film for a given applied strain depends on the yield stress of the film. Since the yield stress depends on film thickness and grain structure, the stresses and plastic strains need to be determined experimentally.

However, the stresses in thin films on compliant substrates are difficult to measure. The wafer curvature method [Keller1998, Keller1999, and Venkatraman1992] is not accurate for compliant substrates and although the load applied to the Cu/Kapton film specimens can be measured, the contribution from the film is difficult to resolve when the films are thin and substrates are thick [Yu2004]. Recently, a synchrotron-based x-ray diffraction technique to determine stress in very thin metal films on compliant substrates has been developed [Boehm2004]. The "$\sin^2\varphi$" method is used to measure the lattice strains of <111> out-of-plane-oriented grains in the metal films as they are loaded under a controlled displacement in a microtensile tester. The lattice strains are converted to stresses using the known elastic constants for the metal, so that a stress-strain curve for the metal film can be obtained. But the strain is measured for the whole film containing not only <111> out-of-plane-oriented grains.

In collaboration with Mr. Patric Gruber (Max-Planck-Institute for Metal Research) this method has been used to determine stress-strain curves at the ANKA synchrotron source (Forschungszentrum Karlsruhe). In these experiments, the samples (gauge length 20 mm) were mounted in the microtensile tester and strained in discrete steps to a maximum strain before unloading. At each step on loading and unloading, the total sample strain was measured using a laser extensometer (Fiedler Optoelektronik GmbH, Germany) and the change in stress in the film was determined using x-ray diffraction (absolute stress and lattice strains were not determined). The goal of these tests is to estimate the magnitude of the plastic strain

in the Cu films, to determine the effect of cyclic loading on the stress-strain behavior of the films, and to look for evidence of cyclic work hardening or softening.

Experimental series	Film thickness (nm)	Cycle in which measured
1	100	2 and 2×10^6
	500	2 and 2×10^6
2	100	2×10^4
	500	5×10^4
3	100	1 and 30
	500	1 and 30
4	500	1 through 14
	100	1 through 14

Table 3.3 Sample conditions used for stress-strain measurements performed by x-ray diffraction at ANKA.

Several series of in-situ x-ray experiments were performed on 500 and 100 nm thick Cu film samples, as summarized in Table 3.3. In the first and second series of experiments, samples were first fatigue tested in the ELF before mounting in the microtensile tester at ANKA to determine the stress during a subsequent cycle with a comparable total strain. This was done because the microtensile tests at ANKA are too slow to reach the large cycle numbers that were desired. The third and forth series of experiments were performed entirely in-situ with the microtensile tester at ANKA.

4 Experimental Results

Experimental observations and results will be summarized in this chapter, starting with the sample microstructure (Section 4.1) and continuing with the fatigue behavior at room temperature (Section 4.2), the stress-strain response during fatigue testing (Section 4.3), the fatigue behavior at 200°C (Section 4.4), and finally the effect of Ta under-and over-layers on fatigue behavior (Section 4.5).

4.1 Initial sample microstructure

The mean grain sizes for all films in the series A and B samples (with and without Ta under- and over-layers) are summarized in Fig. 4-1 and listed in Tables 4.1 and 4.2. They vary from 110 nm to 1.63 μm with increasing film thickness. The grain size of the 3.0 μm thick film is smaller than the film thickness and is non-columnar; all other films have a columnar structure. The grain sizes of the series B Cu films are the same as those in the series A indicating that the mean size is not influenced by the Ta under- and over-layers. In order to determine the mean grain sizes of the Ta/Cu/Ta film stacks, the Ta over-layer was first removed by ion sputtering in the FIB to expose the Cu film.

FIB images of the grain structure in 3.0 μm and 500 nm thick Cu films (series A) are shown in Fig. 4-2. The thinner film has smaller grains, as well as thinner twins and a higher twin density than the thicker film. This trend in microstructure with film thickness was observed for all films in the series A and B and has been reported before for Cu films [Yu2004].
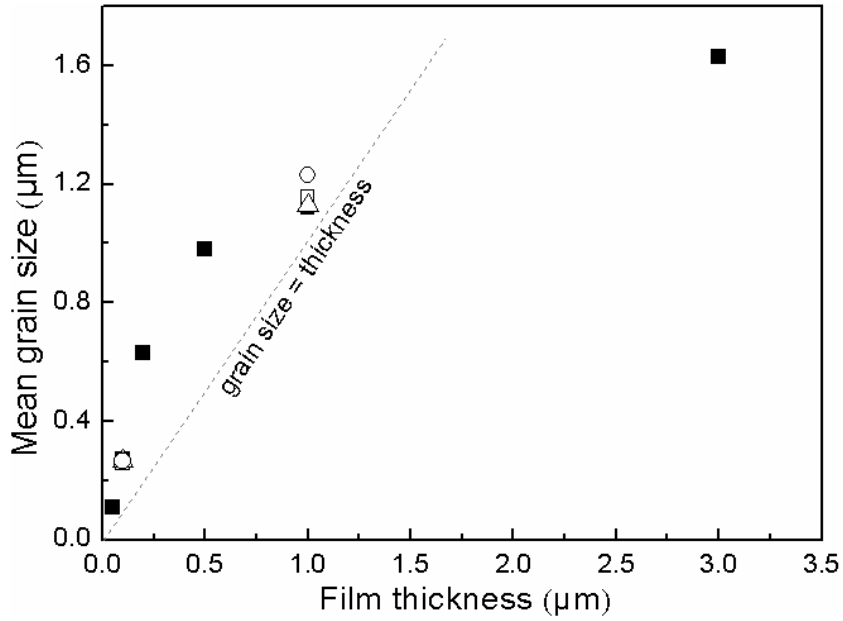
Fig. 4-1 Mean grain size of both annealed series A (■) and series B (□ for Cu, Δ for Cu/Ta, and ○ for Ta/Cu/Ta) Cu films as a function of thickness. The sketches indicate the regions of columnar and non-columnar structures.

Thickness (μm)	3.0	1.0	0.5	0.2	0.1	0.05
Grain size (μm)	1.63	1.12	0.98	0.63	0.27	0.11

Table 4.1 Mean grain size of series A Cu films.

Thickness of Cu film	Mean grain size of Cu films (μm)		
	Cu	Cu/Ta	Ta/Cu/Ta
1.0 μm	1.16	1.13	1.23
100 nm	0.26	0.27	0.27

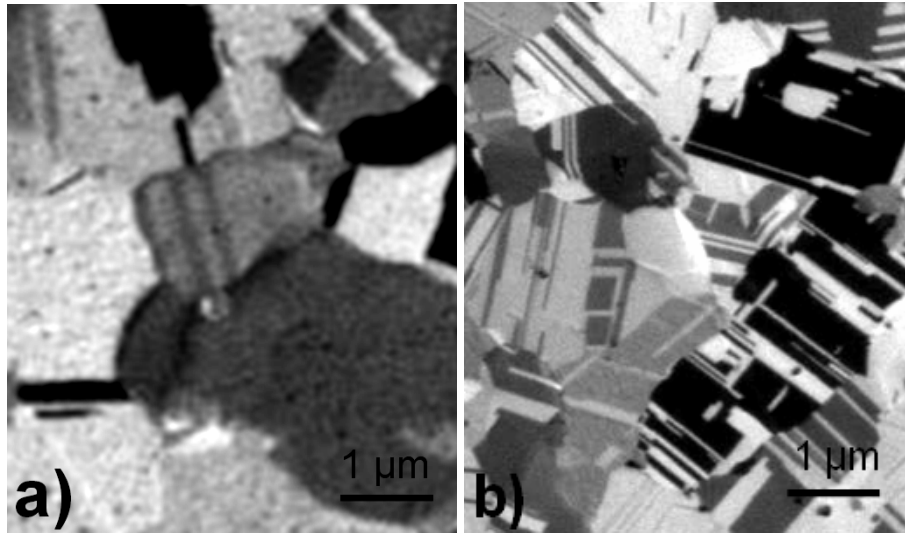Table 4.2 Mean grain size of series B Cu films with and without Ta under- and over-layers.

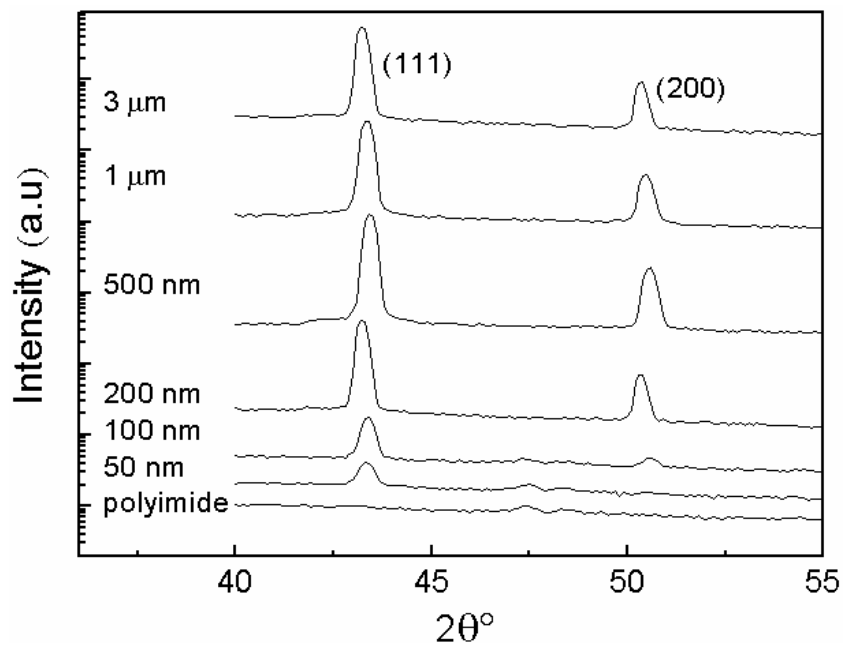Fig. 4-2 FIB images showing the grain structure in 3.0 μm (a) and 500 nm (b) thick Cu films (series A).

Fig. 4-3 θ-2θ XRD scans from the series A Cu/Kapton samples and from bare Kapton. The intensity is scaled logarithmically and displaced vertically for clarity.

The results from θ-2θ XRD scans on the different series A Cu films are shown in Fig. 4-3. Only (111) and (200) peaks are present indicating that the films contain <111> and <100> out-of-plane-oriented grains. The twin orientation peaks are expected at higher 2θ angles than accessed in these scans. An XRD measurement

was also performed on a bare Kapton substrate and accounts for the features observed in the scans at $2\theta \sim 47.5°$ in the thinnest films.

After subtracting the background from the θ-2θ XRD scans, the ratio of the integrated peak intensities $I_{(111)}/I_{(200)}$ was calculated and is shown in Fig. 4-4 for the series A samples. The data of the texture-free Cu powder sample with a value of 2.3 is included taken from [Otte1961]. The plot shows that all the Cu thin films have a {111} texture since the values of their (111)/(200) ratio lie above that from a texture-free sample. The ratio remains constant from 3.0 μm to 200 nm thick films, and then increases with decreasing film thickness. This suggests that the thinnest films (50 and 100 nm thick) have a larger volume fraction of <111> out-of-plane-oriented grains than the thicker films (200 nm and thicker).
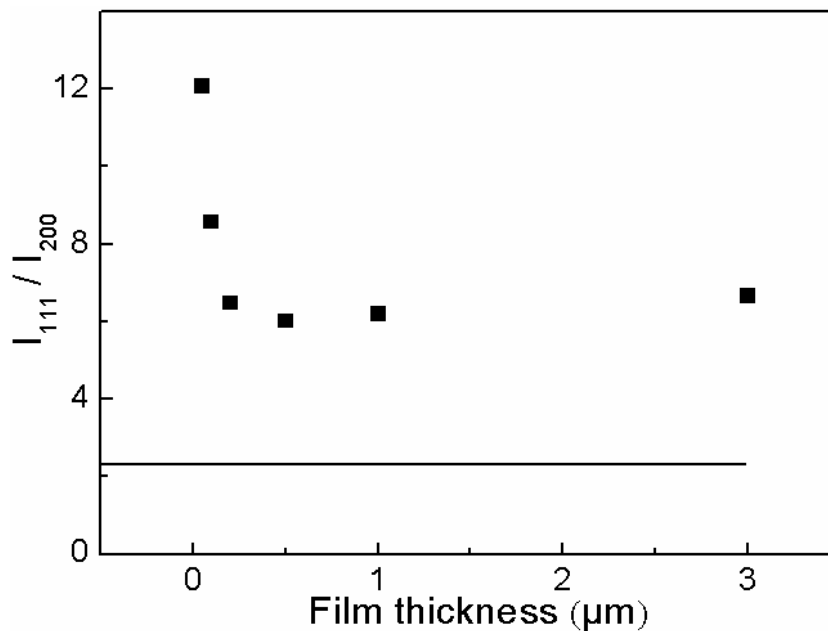

Fig. 4-4 Ratio of intensities of the (111) and (200) peaks obtained from θ-2θ scans of the series A Cu films. The solid horizontal line represents intensity ratio (111)/(200) for texture-free Cu powder sample [Otte1961].

X-ray diffraction measurements were not performed on the series B samples, but based on previous measurements it is expected that the Cu films with Ta under-layers will have a sharper <111> out-of-plane texture than the films without this under-layer [Gruber2004]. This sharpening of {111} texture may be driven by

energy minimization due to a proposed increase in energy of the Ta/Cu interface relative to the Kapton/Cu interface [Park2006a]. The Ta layers are expected to consist of the tetragonal β-Ta-phase [Lee1999] and are immiscible with Cu [Lee1999].

In the series B samples for 1.0 μm thick Cu films, the surface roughness decreases from the Cu films over the Cu/Ta film stacks to the Ta/Cu/Ta film stacks, which quite smooth. This difference in surface roughness can be distinguished qualitatively in SEM images (Fig. 4-5). In contrast, the surface roughness of all films with 100 nm thickness, Cu, Cu/Ta and Ta/Cu/Ta film stacks, is similar.
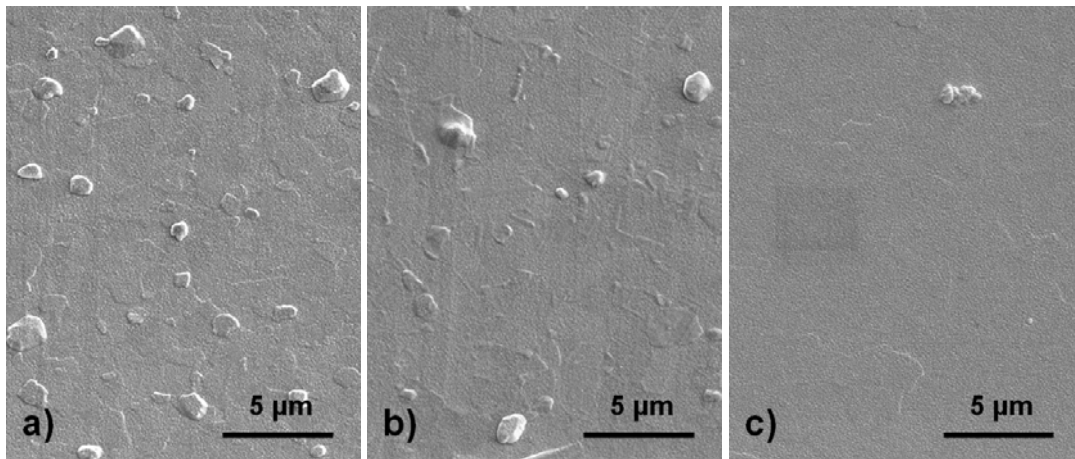

Fig. 4-5 SEM images at 30° tilt of three types of film stacks (series B) with 1.0 μm thick Cu film: (a) Cu; (b) Cu/Ta; (c) Ta/Cu/Ta.

4.2 Fatigue behavior of thin Cu films at room temperature

4.2.1 Fatigue damage

The effect of fatigue testing on the evolution of damage in a 1.0 μm thick Cu film is shown in Fig. 4-6. At the early stage of cyclic testing, the surface looks something different from that before the fatigue testing. Comparing with the film surface before fatigue testing showed in Fig. 4-6 (a), Fig. 4-6 (b) shows that surface features such as grain boundary grooves become sharper after 5.4×10^4 cycles. This increase in the sharpness of the surface relief is observed in all thickness films in early stage of cyclic testing before any other fatigue surface damage.
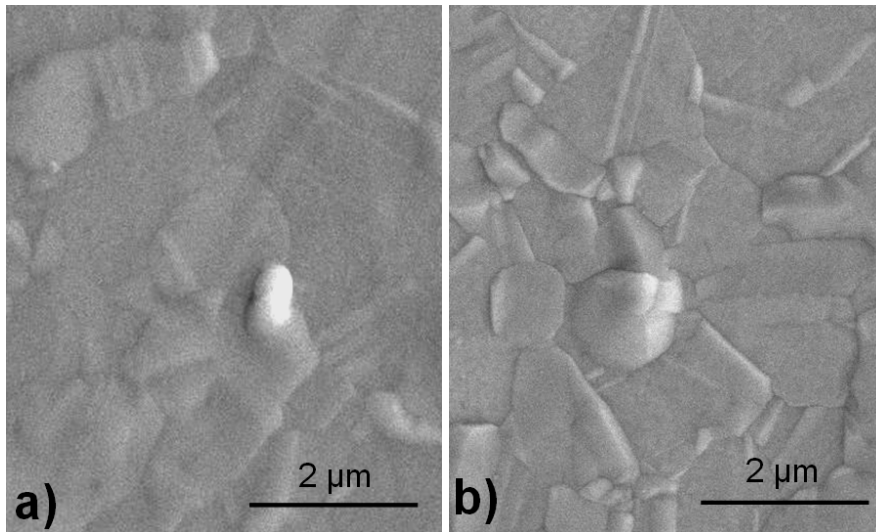
Fig. 4-6 SEM images of a series A 1.0 μm thick Cu film (first series): (a) before fatigue testing and (b) after 5.4×10^4 cycles (strain range 0.2%).
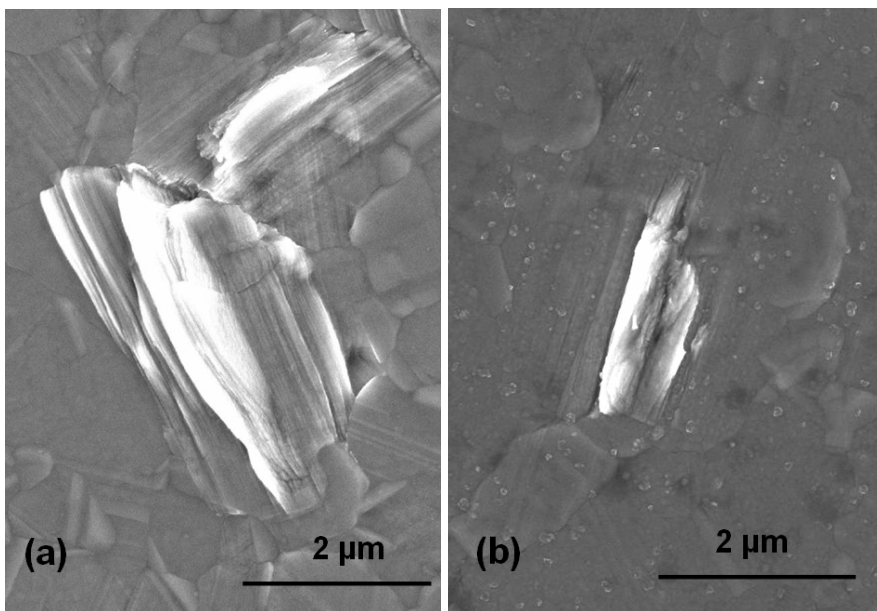
tensile axis

Fig. 4-7 SEM images of extrusions in (a) a series A 1.0 μm thick fatigued film (strain range 0.2%, 2.7×10^5 cycles) and (b) a series A 500 nm thick fatigued film (strain range 0.2%, 5.28×10^5 cycles).

As the number of cycles is increased at a given applied strain range, surface extrusions and cracks begin to form and evolve at the surface of the Cu films. In general, extrusions decrease in size and number with decreasing film thickness, while

cracks increase in number but decrease in length. Fig. 4-7 is SEM images of surface extrusions in fatigued 1.0 μm and 500 nm thick Cu films illustrating the smaller size of extrusions in thinner films.

Fig. 4-8 shows SEM images of typical fatigue damage in a 1.0 μm thick film. A single extrusion is shown in Fig. 4-8 (a), which is representative of the early damage that forms in the thicker films (200 nm, 500 nm, 1.0 μm and 3.0 μm). The individual extrusions are contained within single grains and typically run from one side of the grain to another. As the number of loading cycles is increased, neighboring grains form extrusions and the extrusions link up to form short chains such as shown in Fig. 4-8 (b). Eventually, a crack forms along the extrusion chain, such as shown in Fig. 4-8 (c). Once a crack is formed, it often propagates beyond the existing extrusion chain, accompanied by the formation of new extrusions. The individual extrusions, extrusion chains, and cracks all form roughly perpendicular to the tensile axis, which is horizontal in the images.
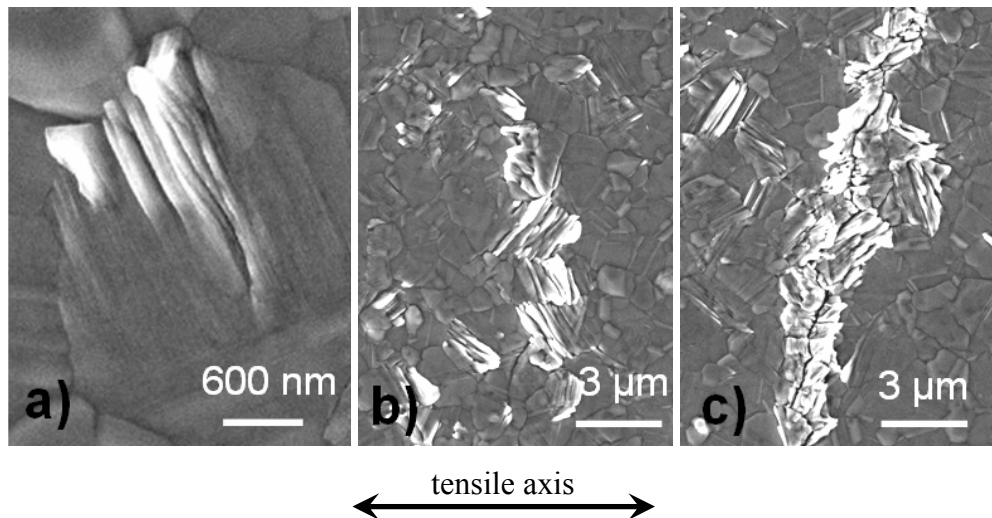

Fig. 4-8 SEM images of extrusions and cracks in a series A fatigued 1.0 μm thick Cu film (applied strain range 0.2%). (a) A single extrusion (after 2.7×10^5 cycles), (b) a short chain of extrusions and (c) a longer chain of extrusions surrounding a crack (after 3.24×10^5 cycles). The tensile axis is horizontal in the images.
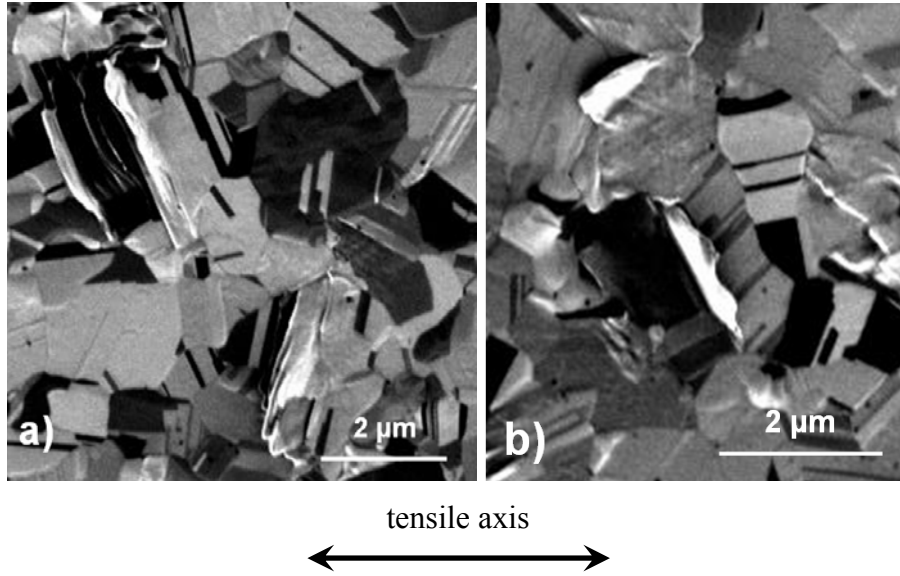
tensile axis

Fig. 4-9 Ion images of a series A fatigued 1.0 μm thick Cu film (strain range 0.2%, 2.7×10^5 cycles; room temperature).

Fig. 4-9 is ion images of a fatigued 1.0 μm thick Cu film. Extrusions form preferentially near and parallel to twin (Fig. 4-9 (a)) and grain (Fig. 4-9 (b)) boundaries. This reveals the boundaries play an important role for extrusion formation.

In order to investigate the extrusions in detail, several were cross-sectioned perpendicular to the extrusion lamella using FIB. Before cutting, platinum was deposited on the film surface in the FIB to protect the Cu during ion sputtering. Fig. 4-10 shows SEM images of cross-sections in a fatigued 1.0 μm thick film. The extrusions (with heights up to about 400 nm above the original surface of the 1.0 μm thick film) are paired with intrusions of a similar size at the film/substrate interface. In Fig. 4-10 (a) several coherent twin boundaries can be seen within the film and are parallel to the slip direction of the extrusion/intrusion pairs. It is believed that crack initiates from extrusion/intrusion pair in thicker films [Kraft2002], and here Fig. 4-10 (b) shows the direct evidence that a fine crack line indicated with arrow started from intrusion propagates along the slip plane to surface.
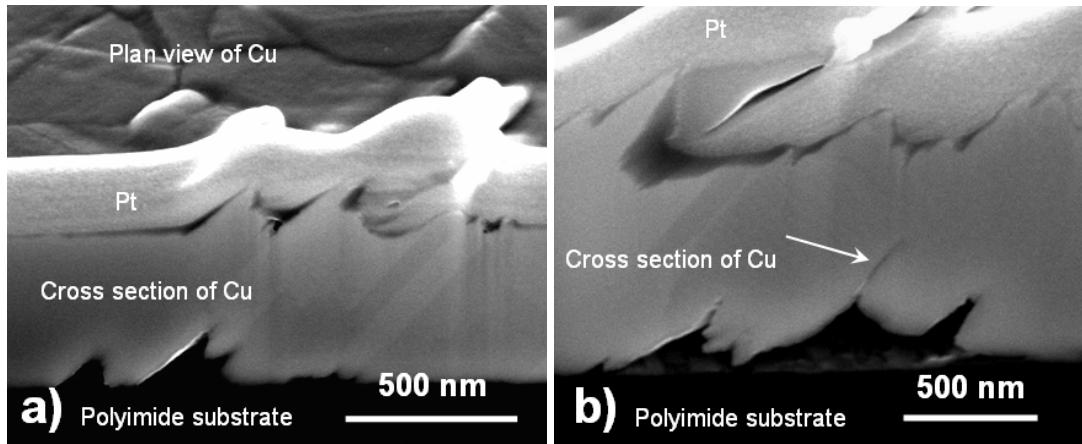
tensile axis

Fig. 4-10 SEM images at 52° tilt of cross-sectioned extrusions (both (a) and (b)) in a series A fatigued 1.0 µm thick Cu film (strain range 0.2%; 3.78x10^5 cycles; room temperature). The arrow indicates a fine crack that has formed at an intrusion. In (b) under the intrusion, there is a very thin Cu layer adhered to the polyimide substrate, which is probably the consequence of re-deposition from the ion milling process.

tensile axis
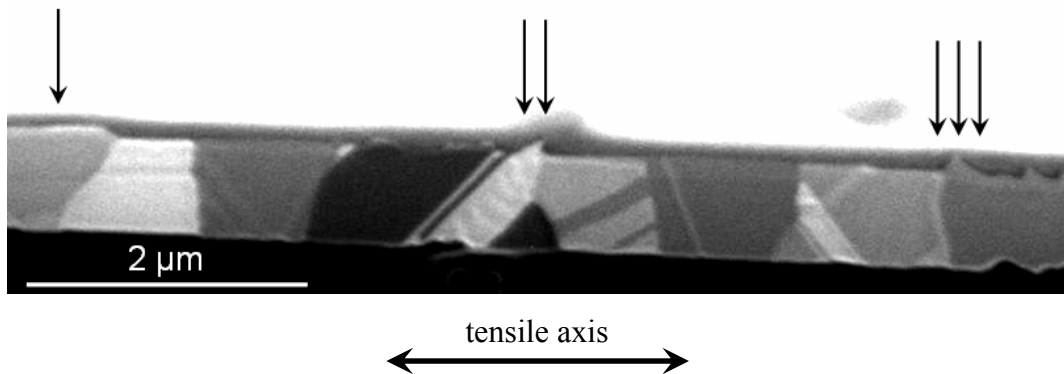
Fig. 4-11 FIB image at 52° tilt of cross-sectioned extrusions in a series A fatigued 1.0 µm thick Cu film (strain range 0.2%; 3.78x10^5 cycles; room temperature).

A long cross-section through several extrusions was made in a fatigued 1.0 µm thick film and imaged by FIB (Fig. 4-11). Before ion milling, Pt was deposited on the film in FIB for protection. Extrusions are observed both in a grain parallel and next to twin boundaries (indicated with double arrows) and in twin-free grain (indicated with tri-arrows). Intrusions are paired with extrusion at the interface. Several other grains contain also twins, but no extrusion/intrusion pair is observed in such grains. This indicates, when the primary slip system of dislocation is parallel to

a twin boundary, it may impel the formation of extrusions. In contrast, twin boundaries play a much smaller role for extrusion formation for the case of the primary slip system not being parallel to twin boundaries. A hillock indicated with a single arrow is seen near a grain boundary. The hillock does not have sharp crystallographic definition of the extrusions.

While extrusions decrease in size with decreasing film thickness or grain size, the damage under extrusion of thinner films also differs somewhat from that of thicker films. Fig. 4-12 (a) and Fig. 4-12 (b) are SEM images of cross-sectioned extrusions in a fatigued 500 nm thick film. Fig. 4-12 (a) shows an extrusion with a height up to 380 nm above the original surface. Under the extrusion two very sharp wedge-like intrusions are observed. Fig. 4-12 (b) shows a cross-sectioned extrusion with a height of about 250 nm above the original surface. An intrusion at the film/substrate interface with a quite large volume extends under the extrusion almost through the thickness of the film.
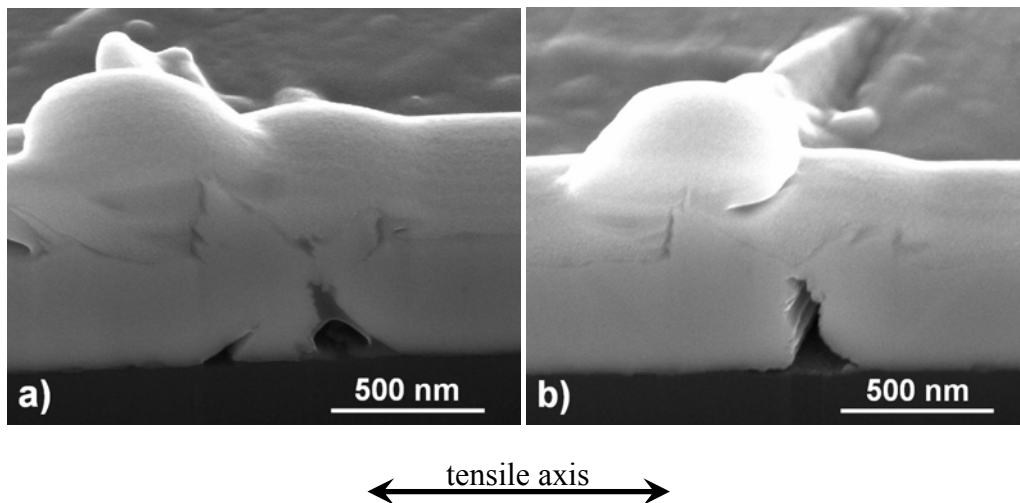
Fig. 4-12 SEM images at 52° tilt of cross-sectioned extrusions in a series A fatigued 500 nm (strain range 0.2%; (a) 3.54×10^5, (b) 5.28×10^5 cycles; room temperature). Under the left intrusion a very thin Cu layer adhered to the substrate is observed just like the case observed in Fig. 4-10 (b) due the re-deposition from the ion milling process.

Fig. 4-13 (a) and Fig. 4-13 (b) are SEM and FIB images, respectively, of the same cross-sectioned extrusions, with heights up to 100 nm above the original

surface in a fatigued 200 nm thick film. Smaller intrusions, with size of about 60 nm above the interface, are found under the extrusion at the interface between film and substrate. Additionally, a fine crack line from the intrusion to surface is seen. The FIB image (Fig. 4-13 (b)) shows that extrusions are near to the twin boundaries.
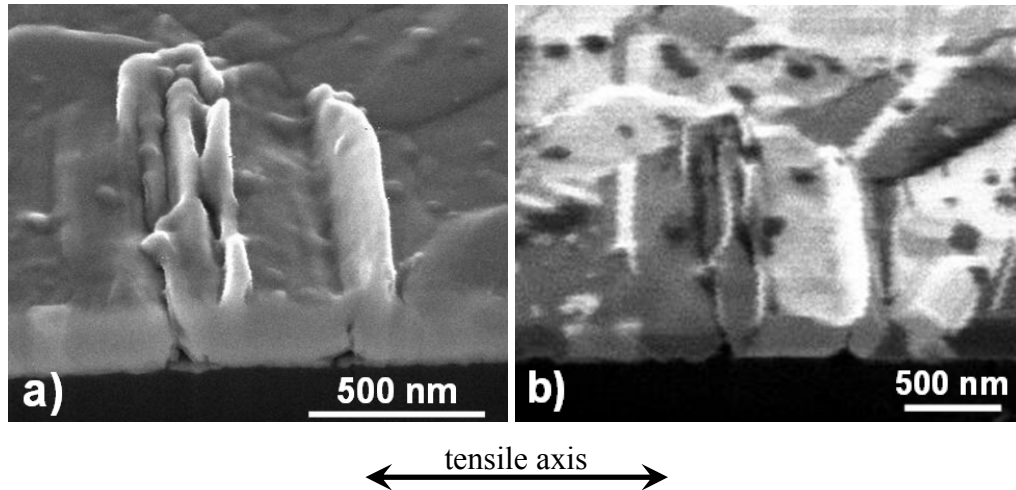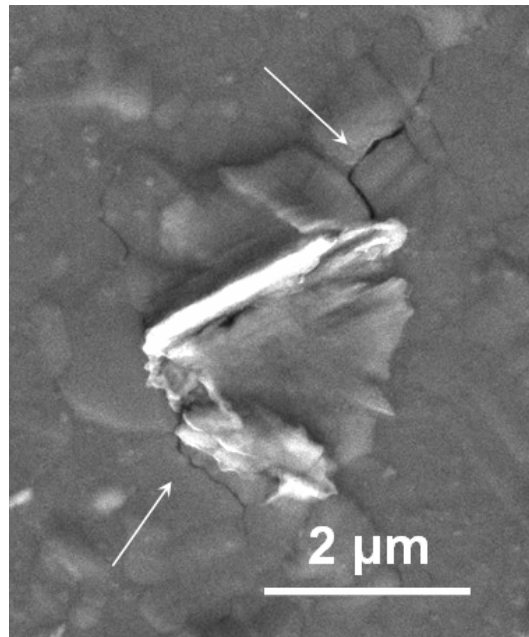

Fig. 4-13 SEM (a) and FIB (b) images at 52° tilt of the same cross-sectioned extrusion in a series A fatigued 200 nm thick film (strain range 0.6%; 3.48×10^5 cycles; room temperature).

As shown in Fig. 4-8, extrusion formation is the dominant fatigue damage mechanism and cracks are formed at the chain of connected extrusions in 3.0 and 1.0 films. As thickness is down to 500 nm and 200 nm, fewer extrusions appeared and cracks through the thickness were observed even in grains with single extrusions. Besides, cracks propagate intergranularly from single extrusions in to both directions perpendicular to the tensile axis, as shown in Fig. 4-14 for a fatigued 200 nm Cu film. The arrows indicate intergranular cracking.

Fig. 4-15 shows an SEM image of cracks in a fatigued 100 nm thick Cu film. Well defined extrusions can be observed along cracks, which are observed along grain or twin boundaries. In some places along the crack, hillocks marked by arrows are observed. These hillocks do not have the sharp crystallographic definition of the extrusions observed in the 1.0 μm thick films, and are thus believed to be oxidized Cu [Zhang2005] and localized deformation caused by friction and wear of the crack faces after crack formation.

tensile axis

Fig. 4-14 SEM image of a surface extrusion in a series A fatigued 200 nm thick film (strain range 0.6%, 9.48×10^5 cycles, room temperature). The arrows mark the occurrence of fine intergranular cracks.
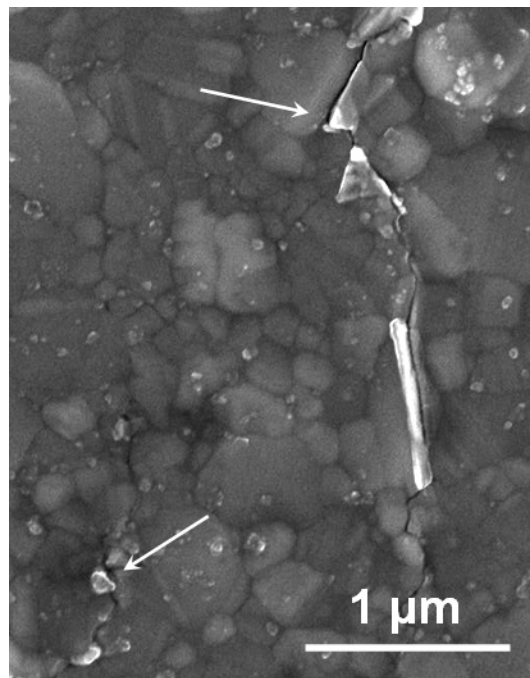
tensile axis

Fig. 4-15 SEM image of a crack in a series A fatigued 100 nm thick Cu film (strain range 0.8%, 1.62×10^6 cycles, room temperature).

For the first time, fatigue in a 50 nm thin Cu film has been studied. Fig. 4-16 shows a crack in a fatigued 50 nm thick Cu film. Well defined extrusions indicated with black arrow can be observed along cracks, which are typically observed along grain or twin boundaries. Similar hillocks as observed in fatigued 100 nm thick film are found here and marked with white arrows. This is first time illustration of fatigue damage in 50 nm thick Cu film. More investigations have supported that the damage of 50 nm thick film evolves in a similar way as the 100 nm thick films.

Both plan-view and cross-sectional images support the idea that the cracks in the 100 nm and 50 nm thick films often initiate at existing defects (such as particles present on the substrate or created during deposition) or at the grain boundaries of large grains after higher cycle numbers. Once formed, the cracks propagate along grain or twin boundaries. Extrusions form after crack initiation and during crack propagation.
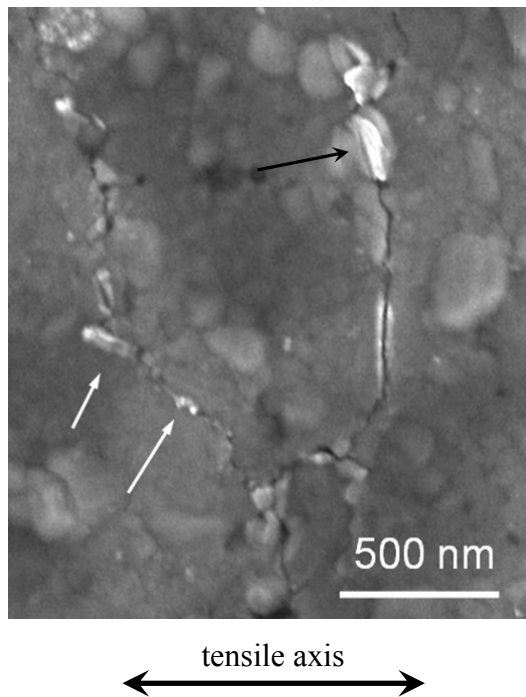

tensile axis

Fig. 4-16 SEM image of a crack in a series A fatigued 50 nm thick Cu film (strain range 1.2%, 2.4×10^4 cycles, room temperature)..

Several SEM images of fatigue cracks are shown in Fig. 4-17. The cracks in the thicker films (1.0 and 3.0 μm) are always surrounded by extrusions, such as shown in Fig. 4-8 (c) and Fig. 4-17 (a). In somewhat thinner films, such as the 200

nm thick Cu film in Fig. 4-17 (b), the cracks connect up isolated extrusions. There are very few extrusions (marked by arrow) along cracks in the 100 nm thick Cu film (Fig. 4-17 (c)). Extrusion formation can be considered as a result of plastic deformation.
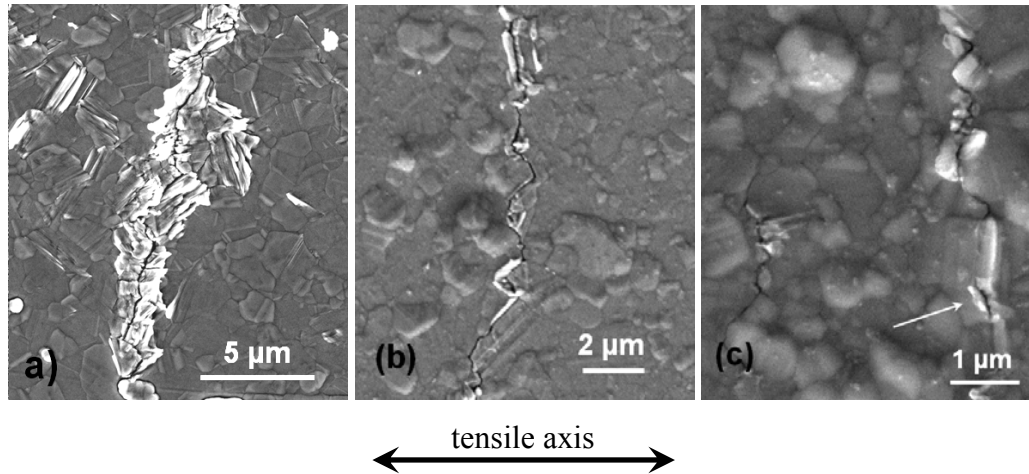

tensile axis

Fig. 4-17 Fatigue cracks in (a) 1.0 μm (strain range 0.2%; 3.24×10^5 cycles; room temperature), (b) 200 nm (strain range 0.6%; 9.48×10^5 cycles; room temperature), and (c) 100 nm (strain range 0.8%; 1.08×10^6 cycles; room temperature) thick series A Cu films. The tensile axis is horizontal in the images.

Extrusions decrease in width, height and number with decreasing film thickness. The same trend was also reported in [Zhang2006]. It is also noted that in the thickest films, there is extensive extrusion formation before crack formation (1.0 and 3.0 μm thick). Here, extrusions form first within single grains, and the extrusion lamella tend to lie perpendicular to the tensile axis. As fatigue proceeds in the 1.0 and 3.0 μm thick films, new extrusions form in more single grains and also in neighboring grains and connect to form a line of extrusions. As more and more extrusions connect to each other, the crack initiates at the location of an extrusion/intrusion pair. Once cracks form along the extrusion chains, the extrusion chain and crack proceed cooperatively. In thinner films (200 and 500 nm thick), cracks initiate even at single extrusions and then propagate along grain or twin boundaries accompanied by the formation of additional extrusions. In the 200 nm thick films, a formation of extrusions is hardly observed at all. In the thinnest films (50 and 100 nm), the cracks initiate at existing defects or boundaries of large grains

without assistance of extrusion/intrusion pair and once formed, propagate along grain and twin boundaries, occasionally accompanied by formation of small extrusions and hillocks.

4.2.2 Damage analysis

Quantitative analyses of the evolution of extrusion density, crack density, and mean crack length were performed during fatigue testing. The extrusion density is defined as the number of extrusions per unit film area as estimated from SEM images. Within a chain of extrusions, the extrusion within each grain counts as a single extrusion. Extrusion densities were only measured in the thickest films (200 nm to 3.0 μm) where they were large enough to be easily seen. The crack density is defined as the number of cracks (either with or without accompanying extrusion chains) having their midpoints within a given film area as estimated from SEM images. The mean crack length is the total length of cracks in a given area divided by the number of cracks. Crack length is defined as the distance between the ends of a crack, which is somewhat smaller than the true crack length since the cracks are not straight.

The fatigue failure of a bulk material in cyclic uniaxial tensile testing can be defined as rupture or fracture of specimen. It is difficult to define fatigue failure because sample of thin film on substrate will not rupture due to constraint of the compliant substrate. Fatigue failure of thin films on Kapton can be defined as transition in mechanical energy loss decreases [Kraft2002]. However, the mechanical energy loss was too small to be measured in all but the thickest films and an alternative definition based on the damage evolution is used in this work.

Representative examples of the evolution of extrusion and crack densities are shown in Fig. 4-18. The extrusion density in a 1.0 μm thick film (Fig. 4-18 (a)) increases after an initial incubation period until saturation, whereas crack growth only starts when the extrusion density has saturated. In a 200 nm thick film (Fig. 4-18 (b)), both extrusion density and crack density increase linearly with the number of cycles until they reach saturation at a similar number of cycles. This indicates that the extrusions and cracks are formed simultaneously and that there is no clear period of extrusion formation before crack initiation. The crack density in a 100 nm thick film (Fig. 4-18 (c)) increases linearly with cycle number before reaching saturation. The extrusion density has not been systematically measured in this film because the

extrusions are too small to be identified unambiguously. Nevertheless, one data point was measured for the maximum number of cycles and a qualitative indication of extrusion evolution is indicated with the dashed curve. Extrusions are formed after crack initiation and during crack propagation.

Fatigue failure is defined as onset of saturation of extrusion or crack density according to the construction shown in Fig. 4-18. Extrusion density for 500 nm, 1.0 µm and 3.0 µm thick films and crack density for the 50 nm, 100 nm, and 200 nm thick films were chosen, respectively, because damage is dominated by extrusions in the thicker films and by cracks in the thinner films. Determination of other films is enclosed in Appendix A and a summary of all fatigue lives is shown in Fig. 4-22 (Section 4.2.3).

We have seen both extrusion density for thicker films and crack density for thinner films will reach saturation with increasing number of cycles (Fig. 4-18). Here the evolution of the mean crack length for all film thickness with increasing number of cycles is plotted in Fig. 4-19. Because of different applied strain ranges, films with different thickness come to failure in the similar range between 10^5 and 10^6 cycles. Crack lengths of all film thickness keeps constant with cycle number within the accuracy of the measurement, and to increase with film thickness. By the investigation of damage we have observed that existing cracks became longer while new cracks initiated with small crack length simultaneous. This leads to the mean crack length does not change much or even remains constant.

The extrusion densities (200 nm to 3.0 µm) and crack densities at saturation (50 nm to 200 nm) and mean crack lengths are plotted as a function of film thickness in Fig. 4-20. The extrusion density at saturation increases with both applied strain range (1.0 µm and 3.0 µm) and with film thickness (200 nm to 3.0 µm). However, the influence of strain range on extrusion formation is clearly smaller than that of film thickness. Crack density at saturation increases with applied strain range and with decreasing film thickness. For the cracks, it is not clear whether the increase in crack density is a thickness effect or a result of the increased strain range. The crack densities in the thicker films are not shown since the total number of cracks was very low. However, the mean crack length could be determined for all film thickness and was observed to increase with film thickness.
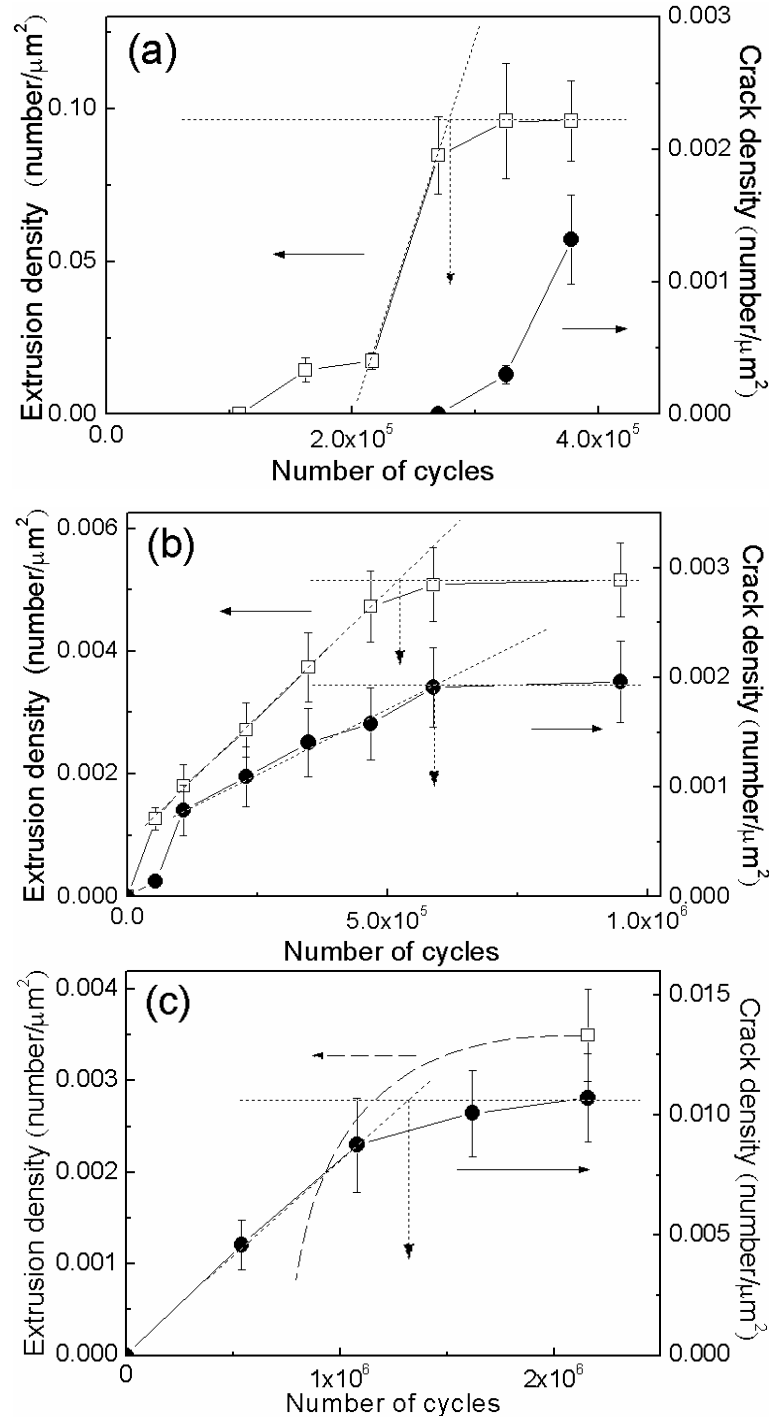
Fig. 4-18 Extrusion (□) and crack (●) densities in (a) 1.0 μm, (b) 200 nm and (c) 100 nm thick series A films (strain range: 0.2 %, 0.6% and 0.8%, respectively) as a function of cycle number. The onset of saturation, which is used as the criterion for failure, is indicated by vertical arrows. The error bars are calculated with in extrusion density and crack density dividing square roots of number of extrusions or cracks represent the uncertainties due to finite sampling size.
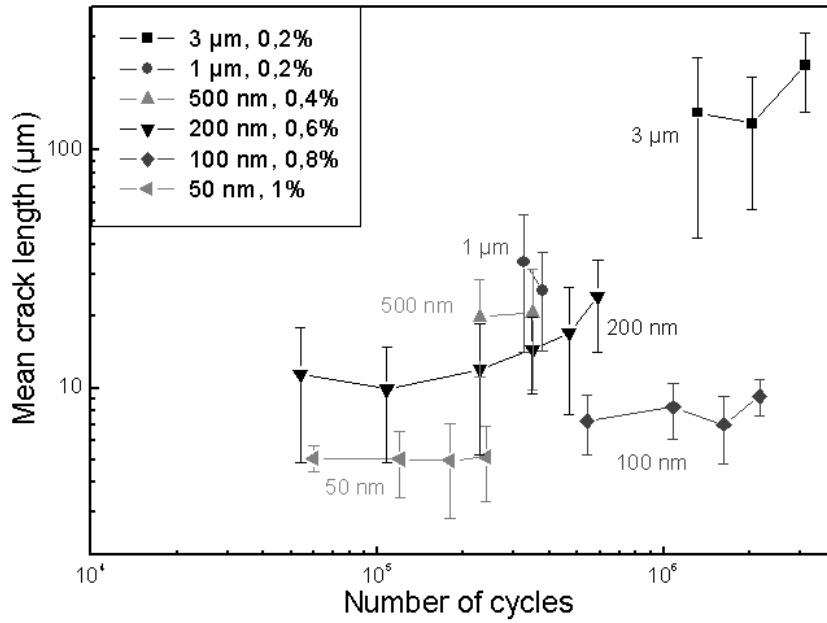
Fig. 4-19 Mean crack length perpendicular to the tensile axis as a function of cycle number. Thickness and applied strain ranges are shown next to data points. Error bars for mean crack length are estimated standard deviation.

Fig. 4-20 Extrusion density (■) and crack density (Δ) at saturation, and mean crack length (●) as a function of film thickness. Applied strain ranges are shown next to each data point. Error bars for mean crack length are estimated standard deviation.
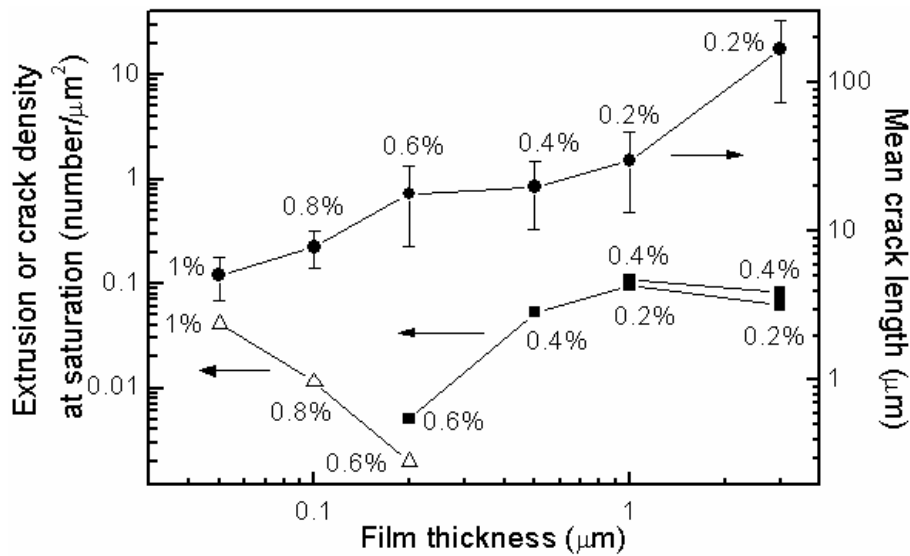
Although extrusions decrease in size and height with decreasing thickness, the ratio of extrusion height to film thickness seems not to have the same trend. Fig.

4-21 is the plot of the ratio of extrusion height to film thickness versus film thickness and applied total strain range. As film thickness decreases from 3.0 μm to 200 nm, the ratio of extrusion height to film thickness increases. Due to difficulty to recognize extrusions in thinner films (like 100 nm and 50 nm), the ratio of extrusion height to film thickness for these films cannot be determined. Moreover, the ratio increases with decreasing applied strain range in 3.0 μm thick films (non-columnar structure), while there is no clear strain range effect on the ratio in other thickness films (columnar structure).
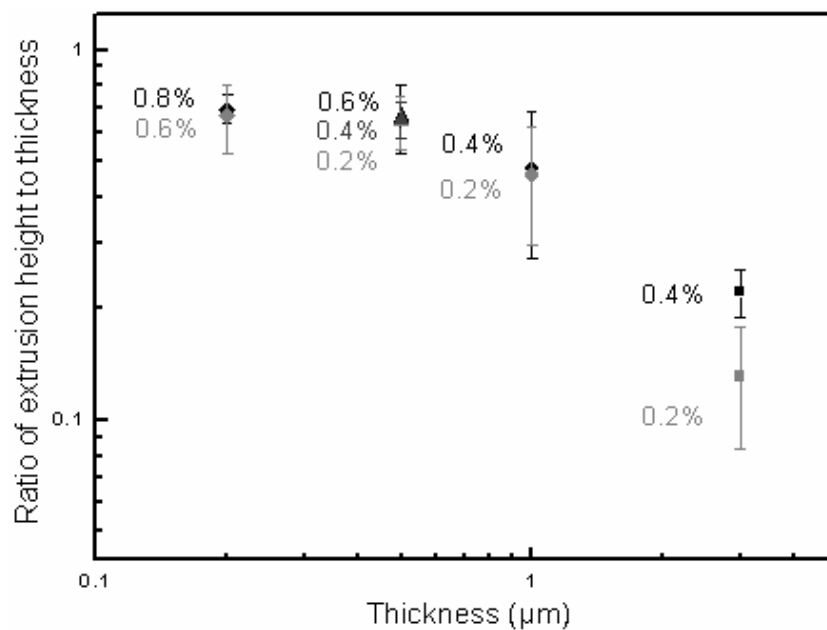
Fig. 4-21 Ratio of extrusion height to film thickness versus film thickness. The given numbers refer to the applied total strain range.

4.2.3 Fatigue life

The determined fatigue lives of all films are summarized in Fig. 4-22. Applied total strain ranges were plotted as function of fatigue lives. The points (filled symbols) are the numbers of cycles required to cause failure of the thin Cu films. Data from the literature for Cu films [Kraft2002] and bulk Cu [Lukáš1987] are also included for comparison. The points with arrows indicate that the corresponding strain and cycle number did not cause observable surface damage in the films. Other than for the 1.0 μm thick films, which show a slightly shorter fatigue life than the 3.0

µm thick films, there is a clear trend of increasing fatigue life with decreasing film thickness and/or grain size. In other words, either higher strain ranges or more cycles are required to bring the thinner films to failure. Even though we have used a rather qualitative failure criterion, it is shown that no damage occurs in thinner films at small strain ranges (data points with arrows), while thicker films have failed under these conditions. All this indicates a clear length scale effect on fatigue life.
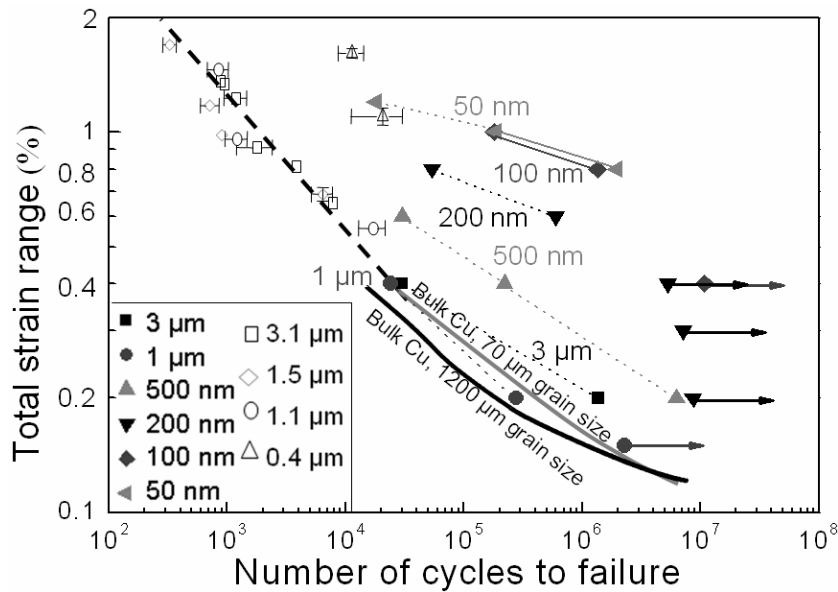
Fig. 4-22 Fatigue life diagram for Cu. Data from high cycle fatigue of the thin Cu films on Kapton are shown as filled symbols. Low cycle fatigue data from Cu on Kapton samples (open symbols) [Kraft2002] and from large grained bulk Cu (solid lines) [Lukáš1987] are included for comparison.

4.3 Stress determination

The change in stress during cyclic loading was measured in some of the series A samples (gauge length 20 mm) using x-ray diffraction and the method described in Section 3.4. The stress-strain curves were used to estimate the plastic strain in the films during cyclic loading and to look for evidence of cyclic strain hardening or softening. In all experiments the absolute stress could not be determined and, therefore, the yield stress was not evaluated.

Fig. 4-23 through Fig. 4-25 show the stress-strain behavior of 500 nm and 100 nm thick Cu films determined by x-ray diffraction during micro-tensile testing at ANKA. Both the stress along the tensile direction, σ_1, and the stress perpendicular to the tensile direction, σ_2, are plotted. The initial residual stress state in the film before any loading is unknown but assumed to be equibiaxial. The stress along the loading direction σ_1 becomes more tensile on applying tensile strain. On unloading, σ_1 decreases and a slight hysteresis in the stress-strain behavior is observed indicating that plasticity has occurred in the Cu films. The values of the transverse stresses σ_2 are small and do not change much during straining. This reveals that the difference between the Poisson ratios of the Cu and Kapton is small, although the slight positive slope shows that the Kapton Poisson ratio is smaller than that the Cu films. Poisson ratio is 0.34 for Kapton and $(-2S_{11}-10S_{12}+S_{44})/(6S_{11}+6S_{12}+3S_{44}) = 0.5$ for <111> out-of-plane-oriented Cu grains.

Fig. 4-23 Series A 500 nm thick Cu film: (a) In-situ stress-strain curves of samples previously loaded to 2, 5×10^4, and 2×10^6 cycles; (b) SEM images of sample surfaces after 2 cycles (upper) and after 2×10^6 cycles (lower).

The stresses in the 500 nm thick film are slightly higher after 5×10^4 cycles than after 2 cycles, whereas there is no difference in the stress-strain behavior of the

100 nm thick Cu films that have experienced 2 and $2x10^4$ cycles. SEM images of the films show that there are no cracks present after $2x10^4$ cycles (100 nm thick film) and $5x10^4$ cycles (500 nm thick film). It is not clear if the slight increase in stress in the 500 nm thick film is a real effect or due to a problem with measurement reproducibility. In contrast, the stresses along the tensile direction in both 100 and 500 nm thick films are much lower after $2x10^6$ cycles and the slope of transverse stresses σ_2 decreases and even becomes slight negative. SEM images of the film surfaces after $2x10^6$ cycles show that many cracks have developed in both 100 and 500 nm thick films perpendicular to the tensile direction during fatigue loading. These cracks have certainly led to a reduction in the stiffness of the films and, as a result, to a reduced average film stress.
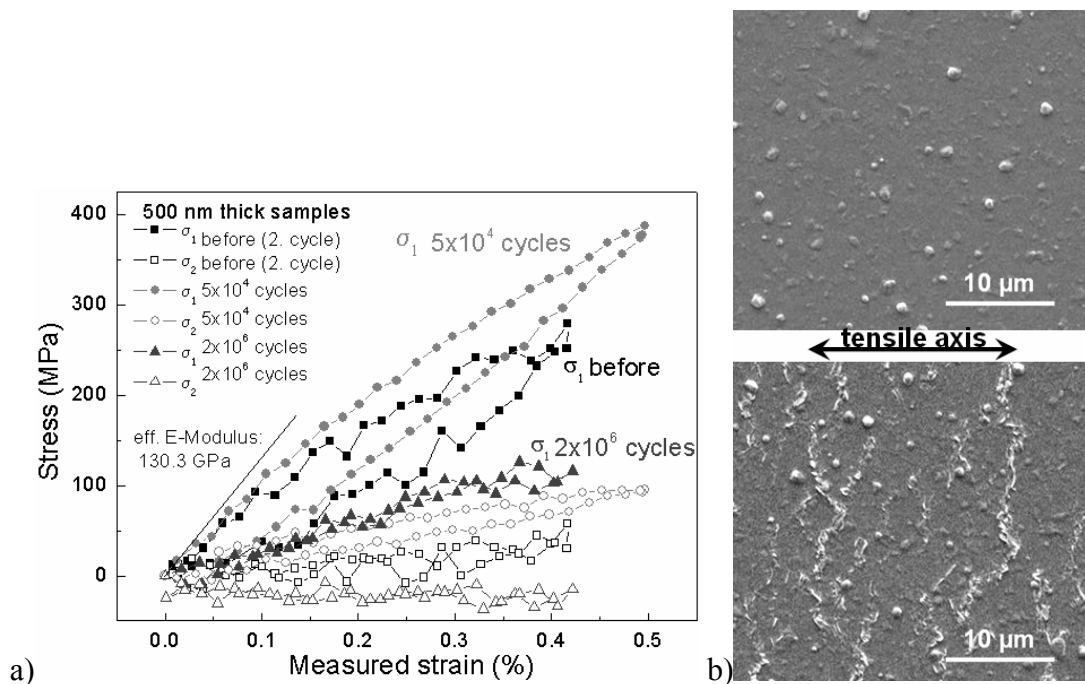

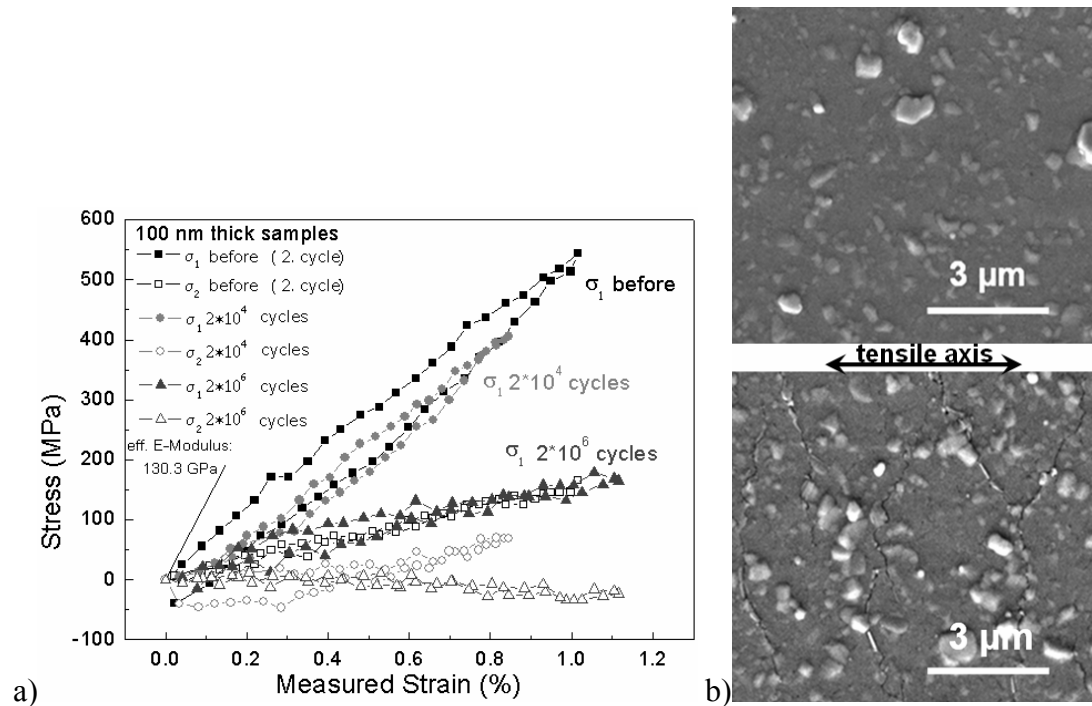Fig. 4-24: Series A 100 nm thick Cu film: (a) In-situ stress-strain curves of samples previously loaded to 2, $2x10^4$, and $2x10^6$ cycles; (b) SEM images of sample surfaces after 2 cycles (upper) and after $2x10^6$ cycles (lower).

Fig. 4-25 shows the in-situ stress-strain curves from a 500 nm thick film for several of the first fourteen cycles. The first cycle has very large hysteresis probably

due to slip of samples during exposition in x-ray and the sample is remounted after the first cycle.

Fig. 4-25 Stress-strain curves of a series A 500 nm thick film during several of the first 14 cycles. Filled symbols indicate σ_1 parallel to tensile axis, open symbols σ_2 perpendicular to loading axis.

To look more carefully for changes in the stress-strain behavior prior to the onset of damage and crack formation, the change in stress-strain behavior at low cycle numbers was investigated by performing in-situ cycling at ANKA. Fig. 4-26 shows the stresses in a 500 nm thick Cu film during the first and 30th loading cycles. Significant plastic deformation occurs in the loading portion of the first cycle. By the 30th cycle, however, the decrease in hysteresis indicates that the amount of plasticity has decreased, probably due to cyclic hardening.
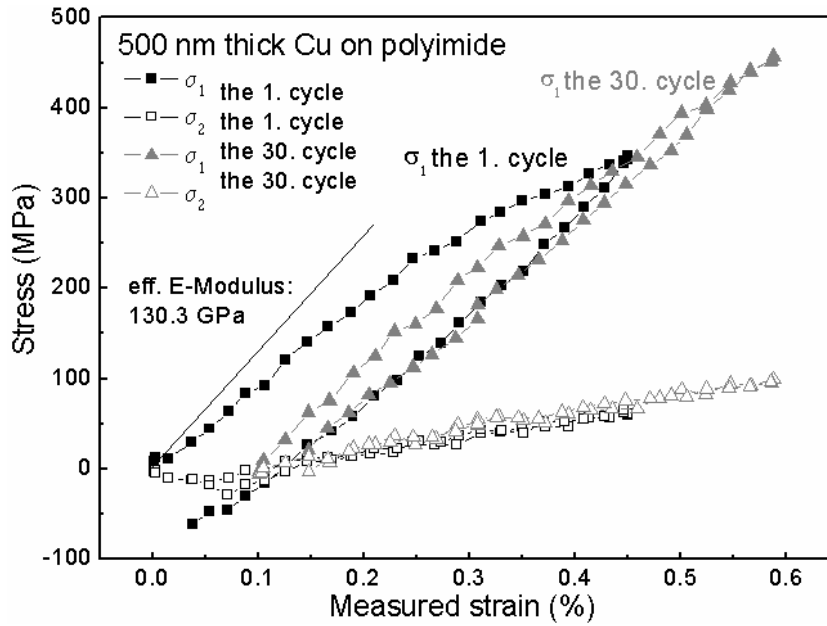
Fig. 4-26 Stress-strain curves of a series A 500 nm thick Cu film in the first and thirtieth cycles. Filled symbols indicate σ_1 parallel to tensile axis, open symbols σ_2 perpendicular to loading axis.

Fig. 4-27 shows the in-situ stress-strain curves in a 100 nm thick film for several of the first fourteen cycles. During cycling, the stresses become progressively more compressive and the hysteresis systematically decreases.

Both the 100 and 500 nm thick films exhibit almost reversible stress-strain behavior with a slope less than that expected based on the calculated Young's modulus of <111> out-of-plane-oriented grains, which has a value of 130.3 GPa. On the one hand, the lower than expected stress-strain slope indicates contributions from plasticity, on the other hand, the small hysteresis indicates a lack of extensive plasticity. This discrepancy will be addressed in the Section 5.2.
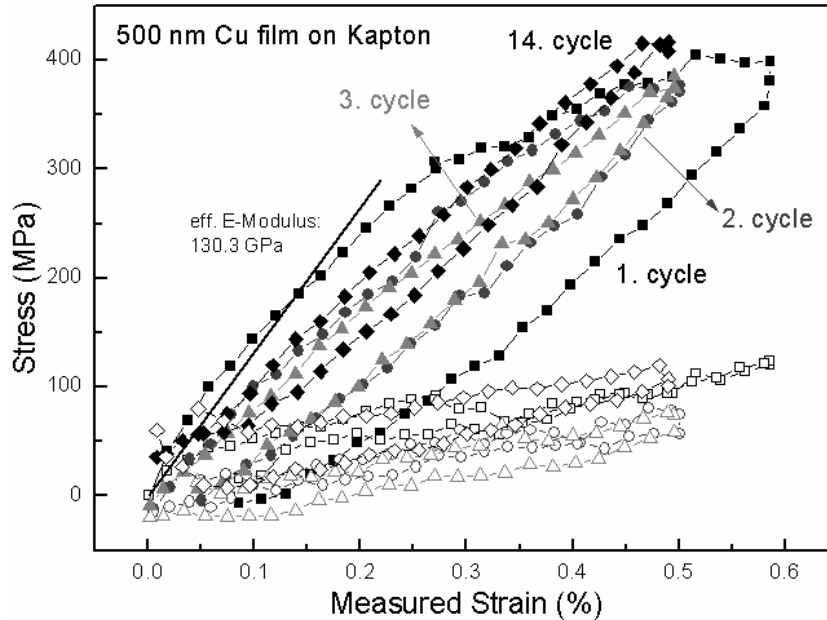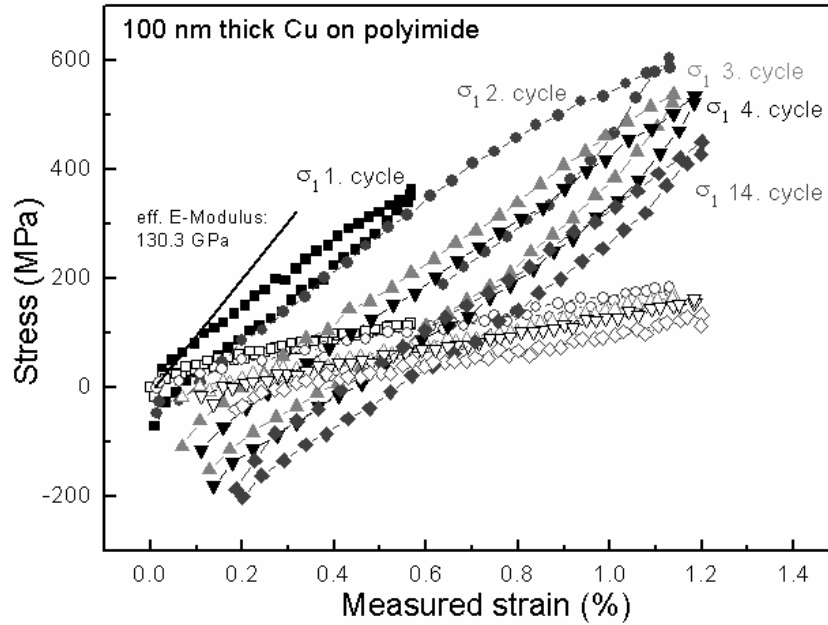
Fig. 4-27: Stress-strain curves of a series A 100 nm thick film during several of the first 14 cycles. Filled symbols indicate σ_1 parallel to tensile axis, open symbols σ_2 perpendicular to loading axis.

4.4 Fatigue behavior of thin Cu films at 200°C

The series A Cu film samples were tested at 200°C under similar loading conditions used for testing the films at room temperature (Table 3.1). A comparison of the fatigue damage in the samples tested at room temperature and 200°C shows that, to first order, the general trends of damage formation are not changed by the increase in temperature. Extrusions are still dominant in the thicker films and cracks in the thinner ones. However, small systematic differences in the damage morphology can be found. For example, a comparison of the images in Fig. 4-28 shows that the extrusions formed at 200°C are more rounded and smaller than those formed at room temperature. There are also fewer at 200°C than at room temperature after similar loading conditions. The many small white spots on the surface of the samples tested at elevated temperature (Fig. 4-28 (a) and Fig. 4-29) may be oxidized regions, which would indicate that the flow of nitrogen gas during the tests was not sufficient to completely avoid oxidation.

tensile axis
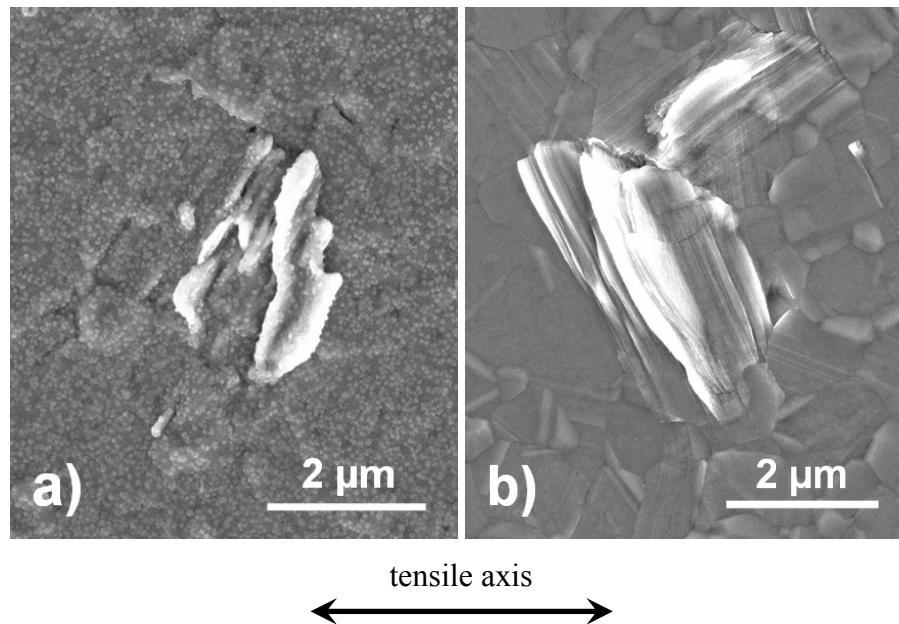
Fig. 4-28 SEM images of extrusions in series A fatigued 1.0 μm thick films: (a) strain range 0.2%; after 8.1×10^5 cycles; at 200°C (b) strain range 0.2%; after 2.8×10^5 cycles; room temperature. The loading axis is horizontal in the images.

Fig. 4-29 shows an SEM image of damage in a fatigued 200 nm thick Cu films. Well defined extrusions and grain boundary grooves or cracks can be seen. A cross-section (Fig. 4-30) of a 200 nm thick Cu film fatigued at 200°C shows that in addition to extrusions (in this case with a height of 100 nm, single arrow) there are intrusions at the Cu/Kapton interface, cracking (tetra-arrows), grain boundary grooving (tri-arrows) and grain thickening (double-arrows).
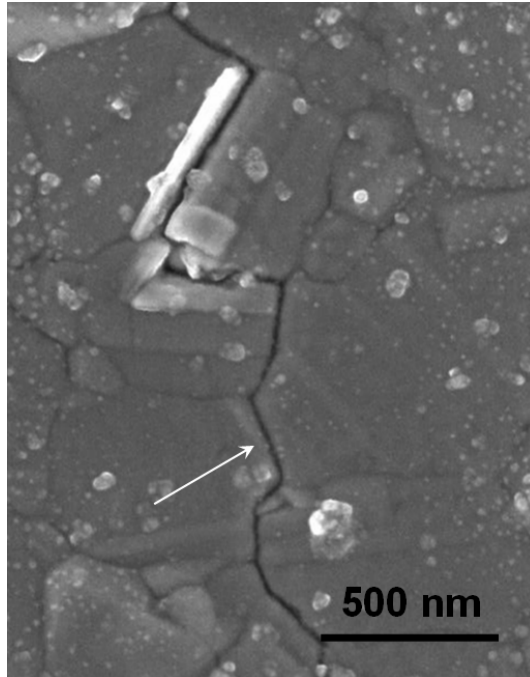
tensile axis

Fig. 4-29 SEM image of a series A fatigued 200 nm thick Cu film (strain range 0.6%, after 5.4×10^4 cycles, at 200°C). The arrow marks a grain boundary crack.
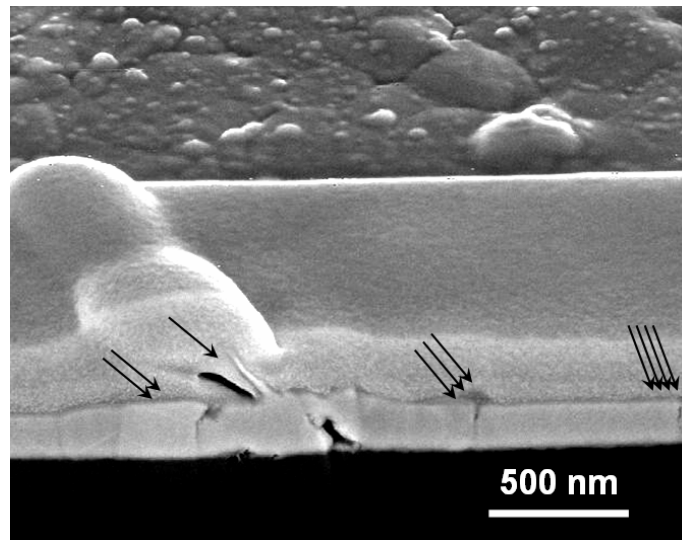
tensile axis

Fig. 4-30 SEM image at 52° tilt of cross-sectioned extrusion in a series A fatigued 200 nm thick Cu film (strain range: 0.6%, after 5.4×10^4 cycles, at 200°C).

49

tensile axis
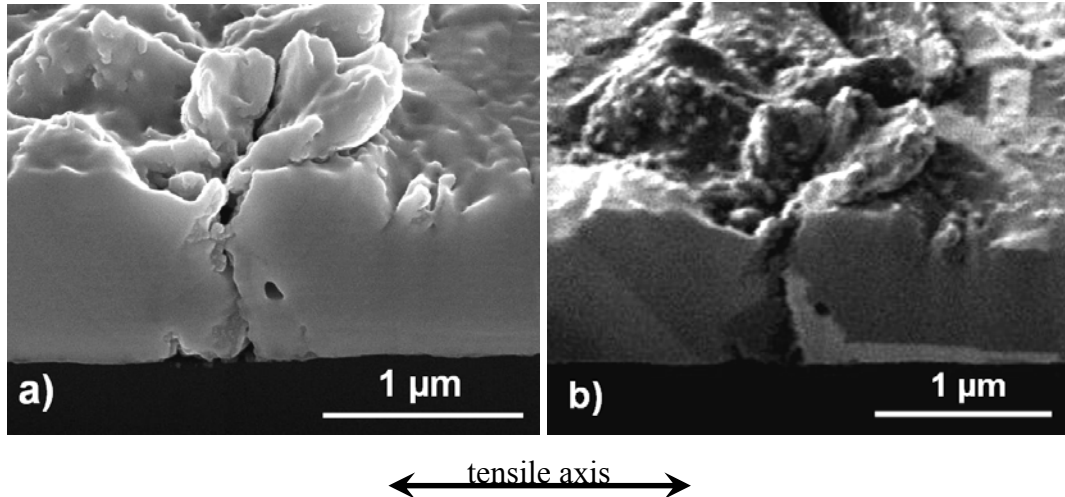
Fig. 4-31 SEM image (a) at 52° tilt and FIB image (b) at 47° tilt of a cross-sectioned extrusion in a series A fatigued 1.0 µm thick Cu film (strain range 0.2%; after 1.89×10^6 cycles; at 200°C).

The cracks formed at elevated temperatures are also slightly different in morphology than those formed at room temperature. In particular, pores were often found near cracks at grain or twin boundaries in films fatigued at 200°C (3.0 µm, 1.0 µm, and 500 nm) but were never found in films fatigued at room temperature. An example of such a pore is shown in Fig. 4-31. In addition, in comparison with the room temperature cracks, the 200°C cracks have rounded edges, suggesting active diffusion during crack formation.

Despite some differences in damage morphology at 200°C compared to room temperature, the same types of damage are observed and fatigue failure can be defined for both temperatures in the same way. Although damage statistics were not measured at 200°C, the fatigue lives could be roughly estimated by a qualitative determination of the number of cycles to reach saturation in crack or extrusion density.

Fatigue lives of the series A Cu films at 200°C are plotted in Fig. 4-32 and compared with room temperature and bulk data. With the exception of the 1.0 µm thick films, the fatigue life is decreased by raising the temperature to 200°C. Although the fatigue failure definition is not always unambiguous, the general effect that increased temperature degrades the fatigue life is clear. The length scale effect on fatigue life is still present at 200°C, in that the fatigue life increases with decreasing film thickness.
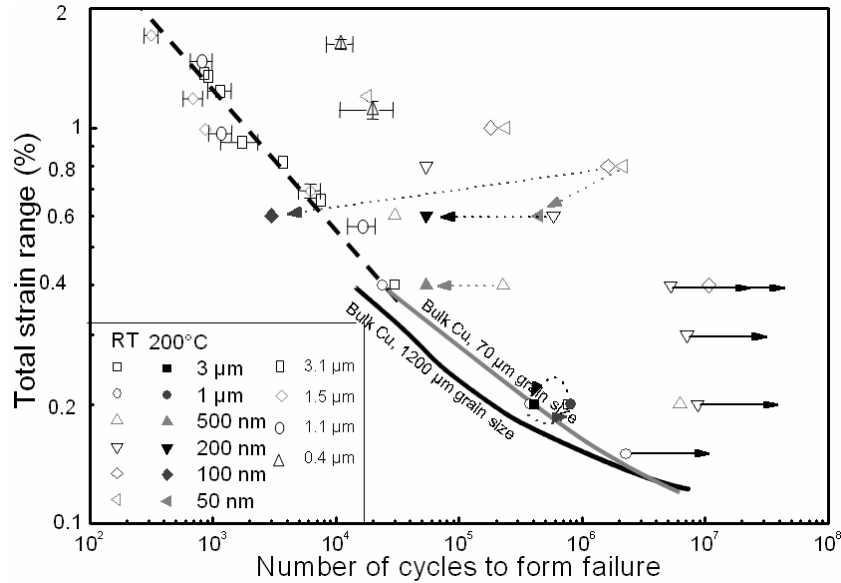
Fig. 4-32 Fatigue life diagram for Cu. Data from tests at room temperature (filled symbols) and 200°C (open symbols). Data from Cu on Kapton samples (open symbols with error bars) [Kraft2002] and from large grained bulk Cu (solid lines) [Lukáš1987] are included for comparison.

4.5 Fatigue behavior of thin Cu films with Ta layers

In order to study the influence of interface character and constraining layers on fatigue damage and fatigue life, 1.0 μm and 100 nm thick Cu films with Ta under- and over-layers were investigated.

4.5.1 Fatigue damage in samples with 1.0 μm thick Cu film

Fig. 4-33 shows SEM images of surface damage in fatigued 1.0 μm thick Cu films with and without Ta under- and over-layers (series B samples). In addition to the similar surface damage of the Cu films, which are chains of extrusions, with or without cracks, surface intrusions (white arrows) and surface roughening (black arrows) can be also observed in Cu/Ta film stacks (Fig. 4-34). The extrusions are often paired with intrusions at the interface between Cu film and Ta under-layer (Fig. 4-35 (a)). But under some extrusions, intrusions are absent (Fig. 4-35 (b)) which has never been observed in Cu films. Surface intrusions can be clearly seen in Fig. 4-35 (c), which are normally paired with surface extrusions. A more diffuse surface

roughening with many but small extrusions and intrusions (Fig. 4-35 (d)) is commonly observed in Cu/Ta film stacks but much less in Cu films without an the Ta under-layer.

tensile axis
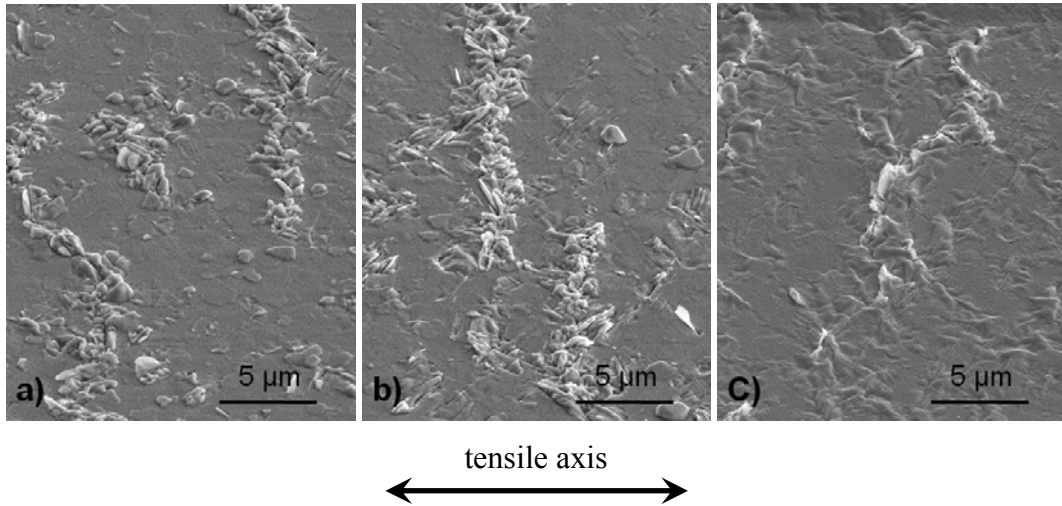
Fig. 4-33 SEM images at 52° tilt of surface damage in fatigued different types (series B) of film stacks with 1.0 μm thick Cu film: (a) Cu (strain range 0.2%; 1.8×10^5 cycles), (b) Cu/Ta (strain range 0.2%; 3.6×10^5 cycles) and (c) Ta/Cu/Ta (strain range 0.4%; 3.6×10^5 cycles).

tensile axis
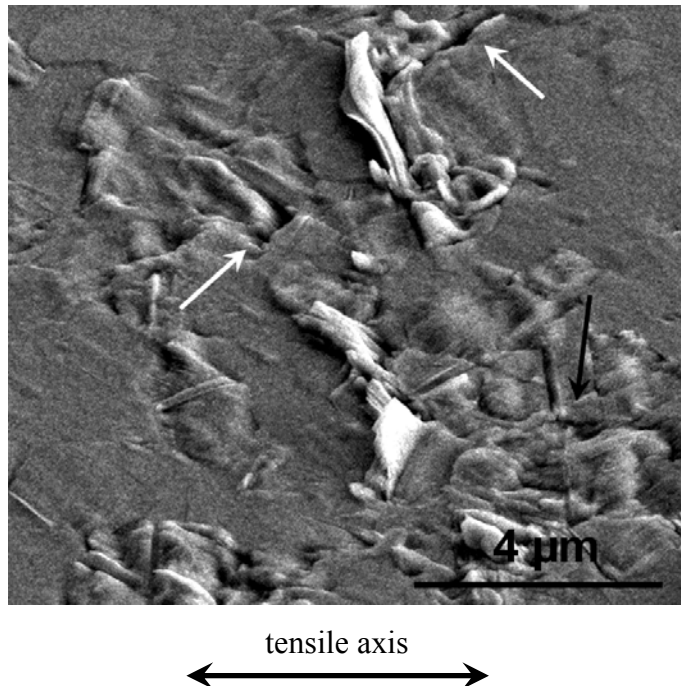
Fig. 4-34 SEM image at 52° tilt of surface damage in a fatigued series B Cu/Ta film stack with 1.0 μm thick Cu film (strain range 0.2%, 3.6×10^5 cycles).

tensile axis
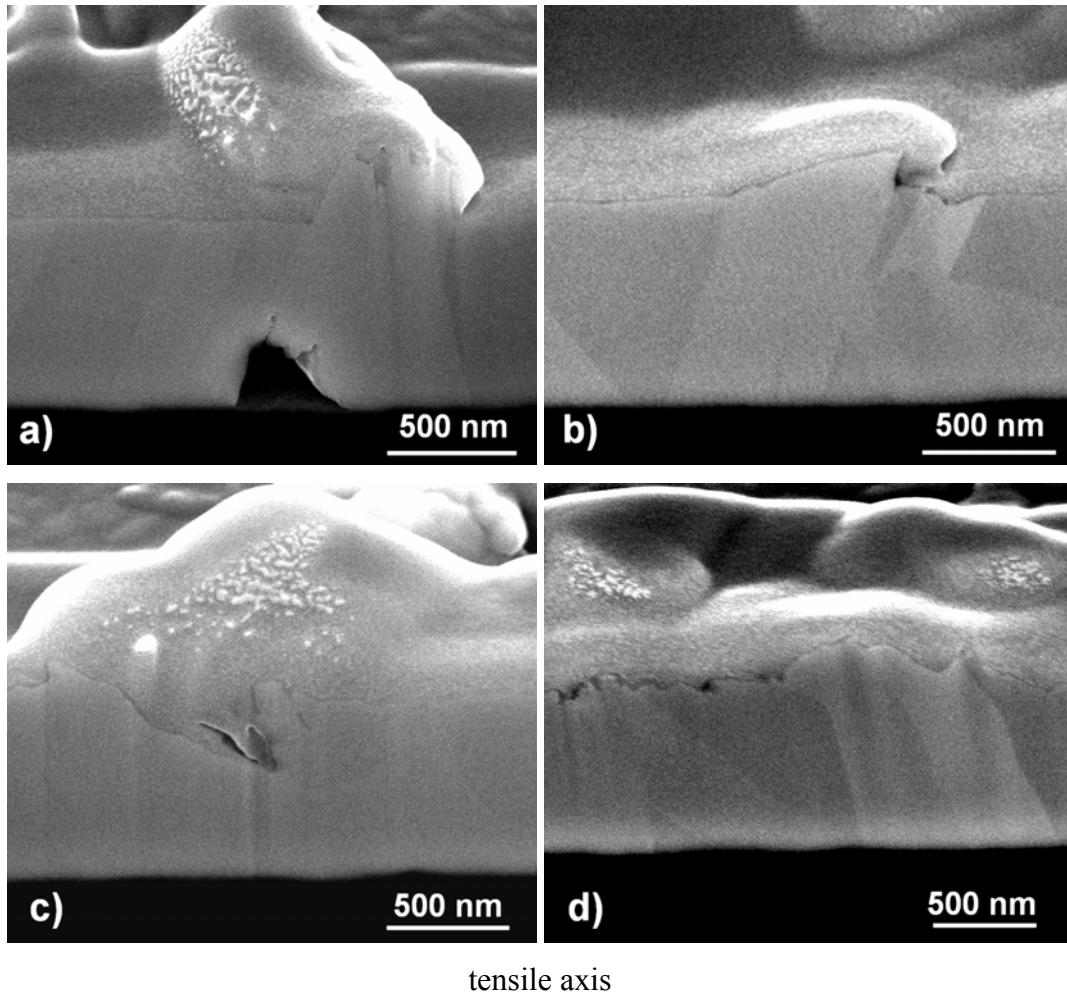
Fig. 4-35 SEM images at 52° tilt of cross-sections in fatigued series B Cu/Ta film stacks with 1.0 µm thick Cu film: (a) and (c) strain range 0.2%, 3.6×10^5 cycles, (b) and (d) strain range 0.3%, 5.4×10^4 cycles.

In contrast, the Ta/Cu/Ta film stacks with 1.0 µm thick Cu films formed fewer and smaller extrusions, and then only after larger strain ranges or cycle numbers than used in the samples without a Ta over-layer. The presence of cracks that are not surrounded by extrusions provides further evidence that extrusion formation is suppressed in the Ta/Cu/Ta film stacks. Instead of extrusions, the samples form uniformly distributed surface wrinkles as are shown in Fig. 4-36 (b). These wrinkles have heights amplitudes that are much smaller than the film thickness (~200 nm) and wavelengths comparable to the grain size (~1 µm). Normally, the regions near cracks are more strongly wrinkled than the crack-free regions. Intrusions are observed under extrusions at the interface between the Cu film and the

Ta under-layer (Fig. 4-37 (a)). Voids or intrusions are observed under the wrinkles at the interface between the Cu film and the Ta under-layer (Fig. 4-37 (b)). The Ta under-layer is deformed and seems to be thicker than 10 nm. This is probably due to the re-deposition from the ion milling process. Delamination at the interfaces of Ta and Kapton (Fig. 4-37 (a) and (b)) is often observed.
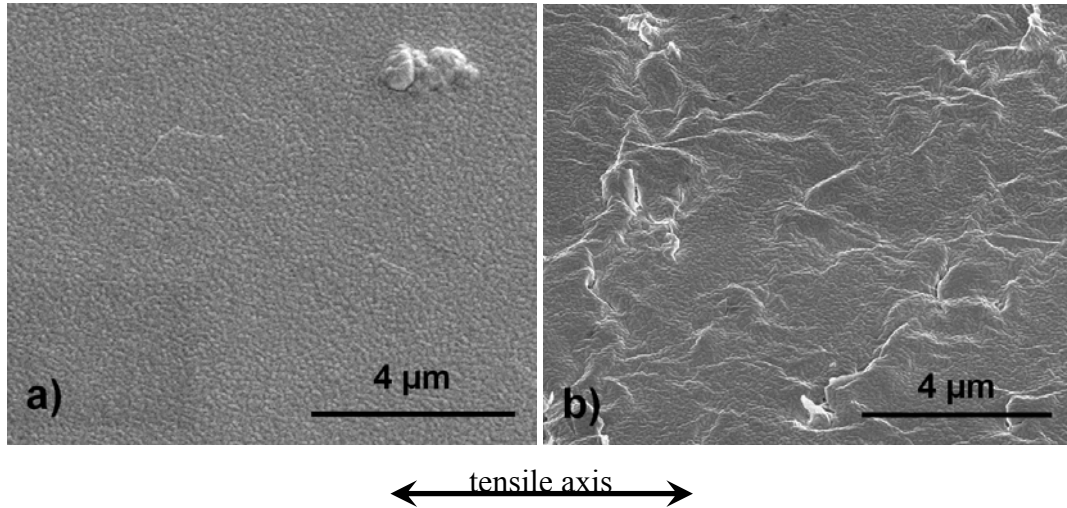
Fig. 4-36 SEM images at 30° of surface before fatigue testing (a) and at 52° tilt of wrinkled surface after fatigue testing (b) (strain range 0.4%, 3.6×10^5 cycles) in a Ta/Cu/Ta film stack (series B) with 1.0 μm thick Cu film.
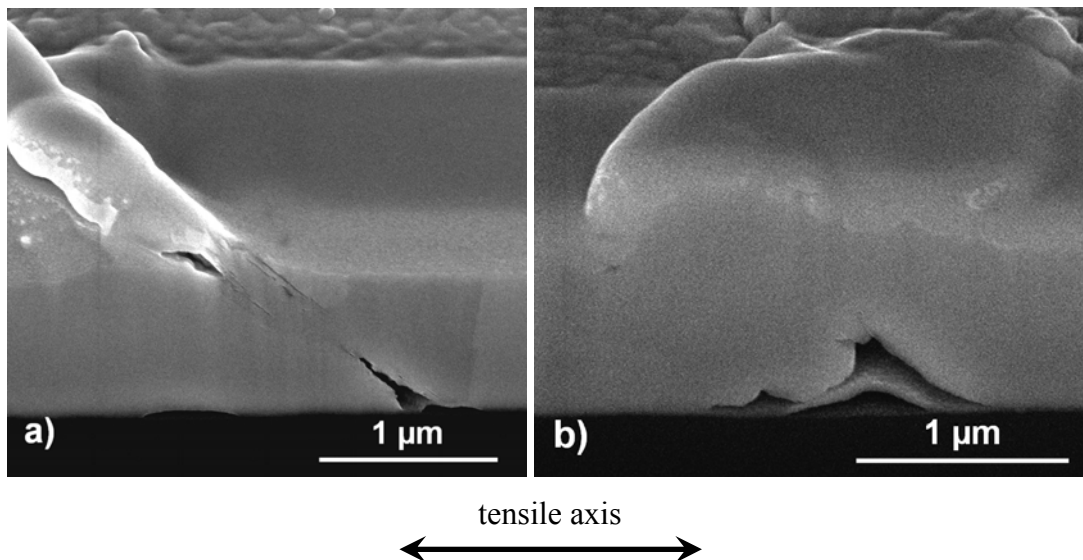

Fig. 4-37 SEM images at 52° tilt in series B fatigued Ta/Cu/Ta film stacks with 1.0 μm thick Cu film: (a) strain range 0.2%; 3.6×10^5 cycles, and (b) strain range 0.4%; 3.6×10^5 cycles.

Not only do the Ta layers influence the nature of the fatigue damage, but also the damage evolution. In Cu films, extrusions first form in single grains paired with intrusions at the Cu/Kapton interface. Then extrusions form in neighboring grains so that chains of extrusions are developed. Finally, cracks initiate from the intrusions and grow along the extrusion chains (Section 4.2.1). The damage evolution in the Cu/Ta film stacks is similar to that in the Cu films despite some absence of intrusions under extrusions at the interface between the Cu film and Ta under-layer. In some cases, the Ta under-layer eventually cracks near extrusions or cracks in the Cu film. The damage evolution in the Ta/Cu/Ta film stacks is quite different and has the following sequence: (i) surface wrinkling and delamination at the interface between the Ta under-layer and Kapton, (ii) cracking in the Ta over-layer at locations of severe wrinkles, (iii) extrusion formation at the surface of the Cu film and intrusion formation at the interface between the Cu film and Ta under-layer at the sites where the Ta over-layer has cracked, (iv) crack nucleation at intrusions and extension from the intrusion to Cu film surface, (v) crack propagation along the film.

4.5.2 Fatigue damage in samples with 100 nm thick Cu film

In all of the series B samples with 100 nm thick Cu film, cracks are the dominant form of fatigue damage. The cracks propagate out perpendicular to the loading axis from pre-existing defects or grain boundaries (Fig. 4-38) and eventually a few extrusions form along the cracks as described in Section 4.2.1.

The detailed morphology of cracks in the three types of series B film stacks is different. Fig. 4-39 shows SEM surface views and cross-sections of cracks in the three types of samples. In the Cu film (no Ta layers) the cracks lie along twin or grain boundaries and are accompanied with some well defined extrusions (Fig. 4-39 (a)). The cross-section shows a clear crack opening displacement (Fig. 4-39 (b)). In the Cu/Ta film stack, cracks are accompanied by rounded hillocks instead of extrusions (Fig. 4-39 (c)). These hillocks are probably caused by friction and wear of the crack faces after crack formation. There is no clear crack opening displacement in the Cu/Ta film stack (Fig. 4-39 (d)) suggesting the presence of compressive stress in the Cu/Ta film stacks during the cyclic testing. In general, more extrusions and hillocks along cracks are observed in series B 100 nm thick Cu and Cu/Ta film stacks than those in series A 100 nm thick Cu films. In the Ta/Cu/Ta film stacks, overlap of

the film at the crack occurs without the presence of extrusions or hillocks (Fig. 4-39 (e) and Fig. 4-39 (f)), suggesting large compressive stresses in Ta/Cu/Ta film stack during cyclic testing.
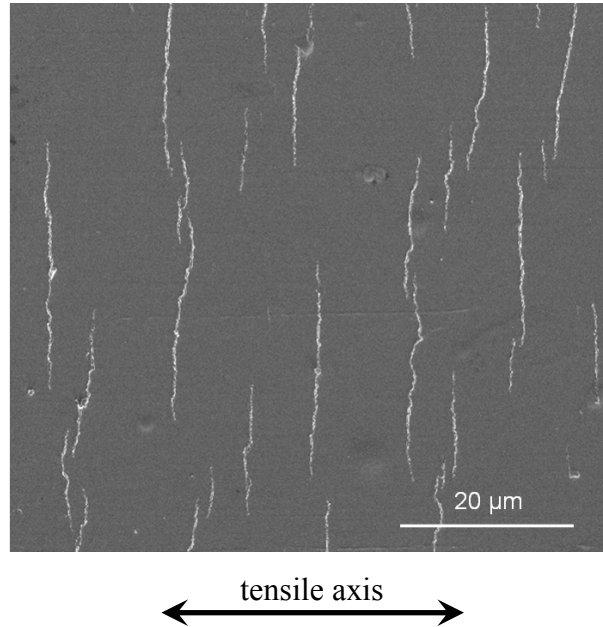
Fig. 4-38 SEM image of surface damage (crack pattern) in Cu/Ta film stack (series B) with 100 nm thick Cu film (strain range: 1%, 1.8×10^5 cycles).
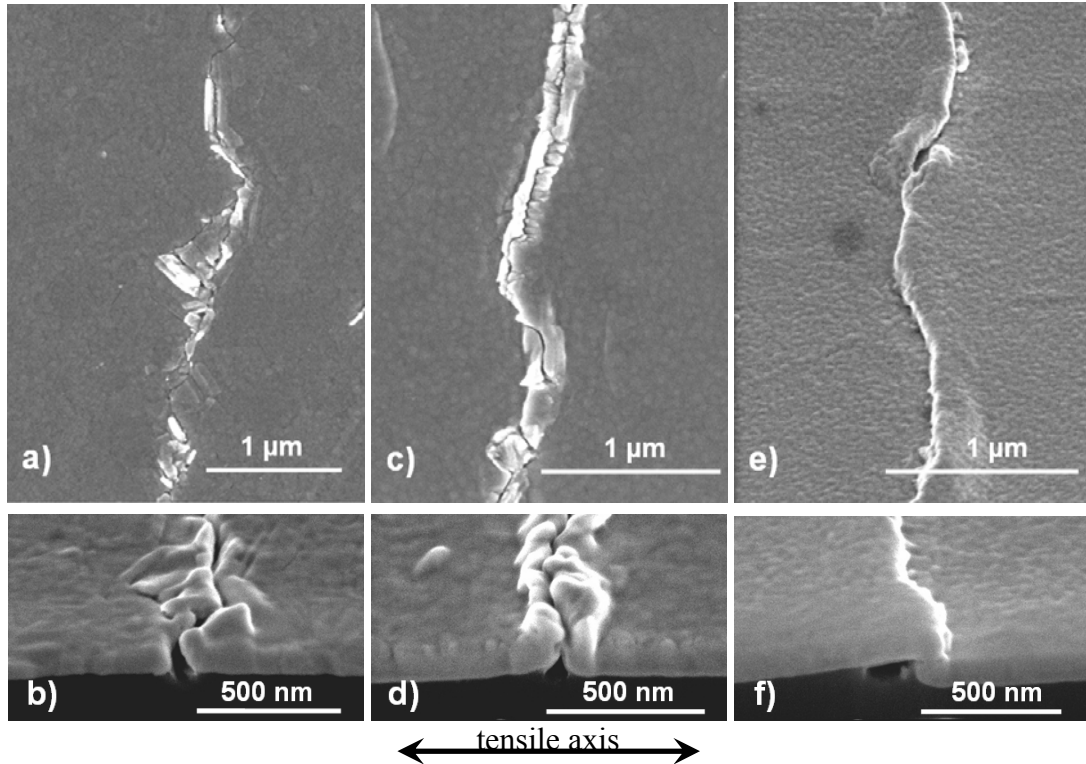
Fig. 4-39 SEM images of cracks and cross-sectioned cracks in series B samples with 100 nm thick Cu film: (a) and (b) Cu film (strain range 1%, 1.2×10^5 cycles), (c) and (d) Cu/Ta film system (strain range 1%, 1.2×10^5 cycles), (e) and (f) Ta/Cu/Ta film system (strain range 1%, 0.6×10^5 cycles). (b), (d), (e) and (f) are at tilt of 52°.

Quantitative analysis of the evolution of crack density was performed during fatigue testing for all series B samples with 100 nm thick Cu films. The crack densities increase linearly with cycle number and reach saturation at around the same cycle number for all three types of samples (Fig. 4-40). The crack density is highest in the Cu films and smallest in the Ta/Cu/Ta film stacks.
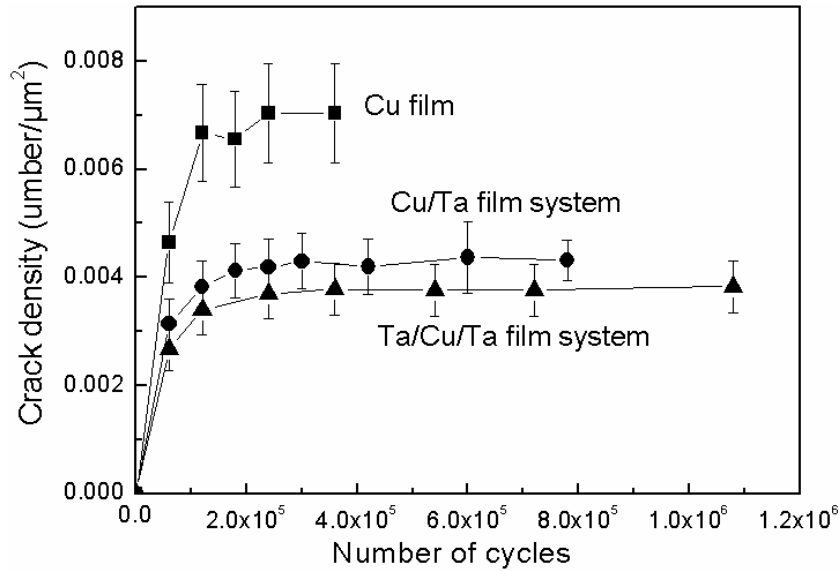
Fig. 4-40 Crack densities in Cu film (■), Cu/Ta film stack (●) and Ta/Cu/Ta film stack (▲) with 100 nm thick Cu film (strain range: 1%) as a function of cycle number. The error bars are calculated with in extrusion density and crack density dividing square roots of number of extrusions or cracks and represent the uncertainties due to finite sampling size.

4.5.3 Fatigue life

Fatigue life in the 100 nm thick series B samples is defined as the onset of saturation of the crack density (Section 4.2.2). Detailed analysis of this saturation point can be found in Appendix B. The definition of fatigue life in series B samples with the 1.0 μm thick Cu film is somewhat more difficult since the extrusions are difficult to identify in the Ta/Cu/Ta film stacks owing to their small size and small number. However, it was observed in the series A 1.0 μm thick Cu films that crack growth only starts after extrusion formation has saturated (Section 4.2). Therefore, the fatigue life of the 1.0 μm thick Cu film samples is defined as the cycle number where cracks first appear in the films or film stacks.

Fatigue lives of the 100 nm and 1.0 μm thick Cu film samples (with and without Ta layers) are plotted in Fig. 4-41. Just as observed in a previous section (Section 4.2), there is a clear length scale effect on fatigue life in Cu films: higher strains or more cycles are required to cause failure in thinner films or film systems, whether they have Ta layers or not. In the 1.0 μm thick Cu film samples, there is a

slight increase in fatigue life due to the Ta under-layer, and a dramatic increase of fatigue life due to a Ta over-layer. Within the 100 nm thick Cu film samples, there is no significant increase in fatigue life due to either the Ta under- of over-layers.
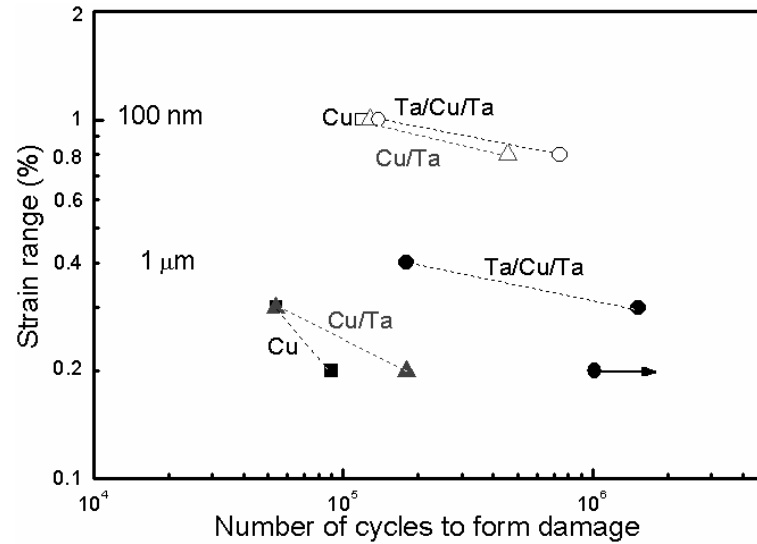
Fig. 4-41 Fatigue life diagram for Cu films (squares), Cu/Ta film stacks (triangles) and Ta/Cu/Ta film stacks (circles) with 1.0 μm (filled symbols) and 100 nm (open symbols) thick Cu film, respectively. The point with the arrow indicates that the corresponding strain and cyclic number did not cause observable surface damage in the film stack.

5 Discussion

In this chapter, interpretations and mechanistic explanations of the experimentally observed trends in fatigue damage evolution and fatigue life in the thin Cu films will be discussed.

5.1 Microstructures

The metal films used in this study have microstructures typical of annealed sputtered Cu films: grains are columnar and in-plane equiaxed; the mean grain size is somewhat larger than and scales with the film thickness (up to some maximum film thickness); and twins are prevalent. The trend that the mean grain size scales with the film thickness [Hommel2001, Yu2004] is typically justified in terms of local minimization of grain boundary energy during grain growth [Mullins1958, Lita2000]. At sufficiently large film thicknesses and grain sizes, grain boundary pinning effects become dominant and presumably account for non-columnar microstructures and a deviation from this scaling behavior.

Numerous twins are observed in the annealed Cu films studied here. In agreement with previous studies on sputtered Cu films, the twin lamella decrease in width and increase in density with decreasing film thickness [Yu2004]. In addition, the average twin size, width and spacing increase with distance from the interface between Cu film and Kapton substrate [Yu2004].

The films used here have mixed (111) and (100) texture with the (111) component being dominant with a fairly constant ratio of <111> to <100> out-of-plane oriented grains, except for in the thinnest films where a stronger (111) texture is observed. A general trend from a (100) to a (111) fiber texture with decreasing film thickness is expected based on a comparison of elastic strain energy with surface and interface energies [Thompson1996] and has recently been observed in Cu films with thicknesses between 3 and 5 μm [Sonnweber-Ribic2006]. Although this model

is consistent with the trends presented here, it is not possible to confirm the model with certainty since studies of the pre-annealing grain sizes and textures were not performed.

When interpreting trends in the influence of film thickness and/or grain size on fatigue behavior, it will be important to recall that: (1) pre-existing defects are found in many of the samples and should be distinguished from fatigue-induced damage; (2) according to recent studies, it is the minimum dimension of the grains in Cu films – either the film thickness or the in-plane grain size – that determines the fatigue behavior, and whether the grains are columnar or non-columnar does not play a role [Zhang2006]; (3) twin width and density change with film thickness in the samples studied here; and (4) (111) texture is stronger in the thinnest films.

5.2 Stress-strain response

Fatigue damage formation and failure are generated by plastic strain. In the tests performed here, loading is applied to the films by controlling the *total* strain in the samples, and an attempt is made to infer the *plastic* strains from synchrotron x-ray diffraction measurements performed during cyclic loading. However, the stress-strain response obtained from the diffraction studies reveals that the plastic strain at the small strains used for the fatigue tests is not unambiguously defined. The following sections will discuss issues with defining plastic strain as well as the measured elastic modulus, stress relief due to crack formation, and cyclic hardening.

5.2.1 Young's modulus

According to the known elastic constants for bulk Cu [Landolt-Bornstein], the Young's modulus for a <111> out-of-plane textured solid with random in-plane orientations is 130.3 GPa [Huang1998]. However, the initial elastic slopes of the stress-strain curves as determined by x-ray diffraction for both 100 nm and 500 nm thick films are considerably smaller than this value. Since the series A Cu films also contain <100> out-of-plane-oriented grains, possible contributions from these grains are estimated to see if they can account for the reduction in modulus. The Young's modulus of <100> out-of-plane-oriented grains with a value of 93.2 GPa [Huang1998] is smaller than that of <111> out-of-plane-oriented grains. The elastic

slope measured using x-ray diffraction is the ratio of measured stress in <111> out-of-plane-oriented grains to total sample strain. There are two extreme cases of distribution of <111> and <100> out-of-plane-oriented grains in films during the loading process (Fig. 5-1). In case (a), the total strain is influenced by <100> out-of-plane-oriented grains and therefore the elastic slope will deviate the Young's modulus of <111> out-of-plane-oriented grains; and in case (b), the total strain has the same value of <111> out-of-plane-oriented grains, so the elastic slope should be the same as the young's modulus of <111> out-of-plane-oriented grains. In case (a), the slope can be calculated from

$$E = \frac{E_{<111>} * E_{<100>}}{V_{<111>} * E_{<100>} + V_{<100>} * E_{<111>}} \tag{5.1}$$

where $V_{<111>}$ and $V_{<100>}$ are volume fractions of <111> and <100> out-of-plane-oriented grains, respectively. It should be noted that this simple analysis neglects the role of the substrate through which the grains are strained. Therefore, we have in general a situation closer to case (b). Nevertheless, Eq. (5.1) gives the lower bound for the modulus.
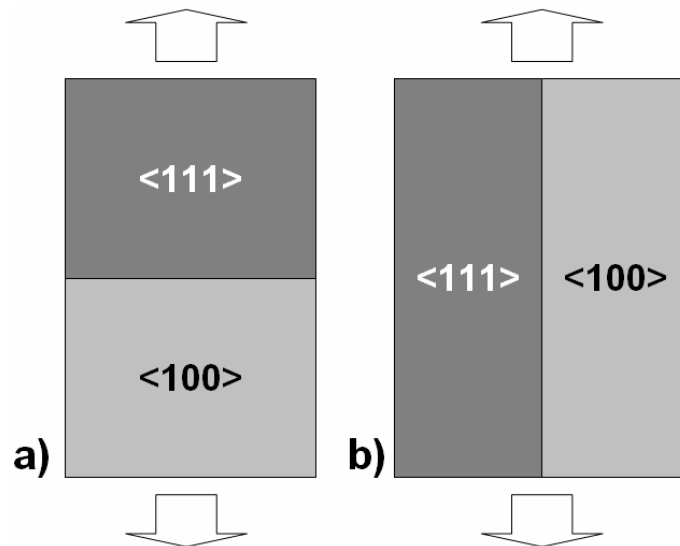
Fig. 5-1 Schematic illustration of two extreme cases which may influence the elastic slope.

Fig. 5-2 is a graph of lower- and upper-bound elastic slope, representing the value calculated in the two extreme cases (Fig. 5-1). The lower-bound is volume fraction dependent. The smallest $V_{<111>}$ is about 0.85 (see Fig. 4-4) for 500 nm thick Cu films and then increases with decreasing film thickness. The corresponding calculated lower bound elastic slope is 122.7 GPa for 500 nm thick Cu films and increases with decreasing film thickness. In addition, Poisson's ratio of <111> out-of-plane-oriented grains is 0.5 [Huang1998] and larger than that of Kapton with a value of 0.34. So the <111> out-of-plane-oriented grains undergo biaxial tension during the loading, and therefore the corresponding lower bound elastic slope should be larger than 122.7 GPa which is calculated in uniaxial condition. However, the elastic slopes measured in unloading slope in stress strain curves after 2 cycles in Fig. 4-23 and Fig. 4-24 are 92 GPa for 500 nm thick Cu films and 66 GPa for 100 nm thick Cu films, and smaller than the calculated lower bound and have inverse trend with thickness. So there is a significant deficit in the Young's modulus.
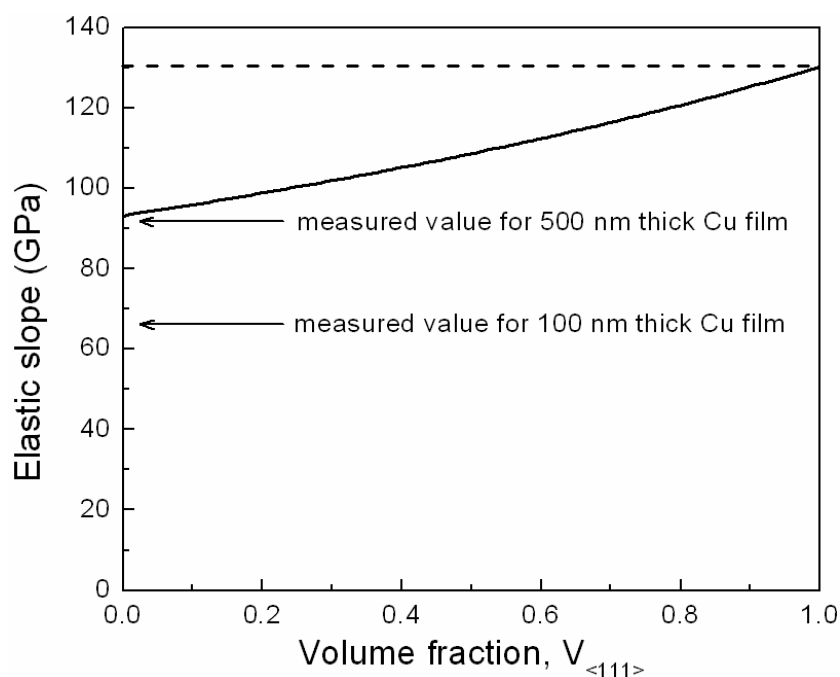
Fig. 5-2 A graph of upper-bound (dashed line, 130.3 GPa) and lower-bound (solid line, Eq. 5.1) elastic slope of Cu films containing both <111> and <100> out-of-plane-oriented grains. Measured values indicated with arrows for both 500 nm and 100 nm thick Cu films (series A) are included.

A reduction of Young's modulus has been observed before in metal thin films [Huang2000, Yu2004, Kalkman2001, Read2001, Read2004, and Espinosa2004] including Cu films on Kapton [Yu2004], and has been attributed to compliant grain boundaries [Huang2000], grain boundary sliding [Kalkman2001] or reversible microplasticity [Huang2000, Nucci2005]. Due to imperfect packing, grain boundaries are more compliant than the bulk crystals and may lead to a decrease in film modulus with decreasing grain size. Similarly, room temperature grain boundary sliding can occur in thin metal films and lead to a significant apparent decrease in modulus for films with small grain sizes [Kalkman2001]. Furthermore, microplastisity such as reversible bowing of dislocation segments can produce reversible strain during loading and thereby reduce the effective stiffness [Huang2000]. Particularly in samples with initial local stress and strain inhomogeneities, such as have been observed in thin films [Phillips2004], microplasticity is expected to play a role [Nucci2005].

5.2.2 Definition of plasticity at small strains

The reduced effective modulus in the films indicates that strain inhomogeneities and microplasticity are present. Therefore, we attempt to quantify the amount of cyclic plasticity is in the films. Although there is no obvious transition from the elastic to the plastic regime, hystereses appear in every stress-strain measurement. If the hystereses are due to plastic dissipation, as schematically shown in Fig. 5-3 (a), plasticity can be quantified by measuring the area of the hysteresis. On the other hand, the elastic slope in the measurements is smaller than that of bulk counterpart, what might be related to microplasticity and reversible grain boundary sliding. This can be quantified as the difference between the bulk elastic slope and the measured stress strain response, schematically shown in Fig. 5-3 (b).

In the following, the hysteresis and the amount of microplasticity with the number of cycles have been studied. The difference of stress between loading and unloading in the same cycle has been determined at half applied total strain (0.6% for 100 nm thick films and 0.25% for 500 nm thick films). This is shown schematically in Fig. 5-4 where (σ_1-σ_2) is the difference of stress characterizing the hysteresis and (σ_3-σ_1) is difference of stress characterizing microplasticity and reversible grain boundary sliding. The change of the differences with testing cycles indicates roughly

the change of hysteresis or microplasticity (and the contribution of reversible grain boundary sliding is ignored for following analysis) with cycles, respectively.
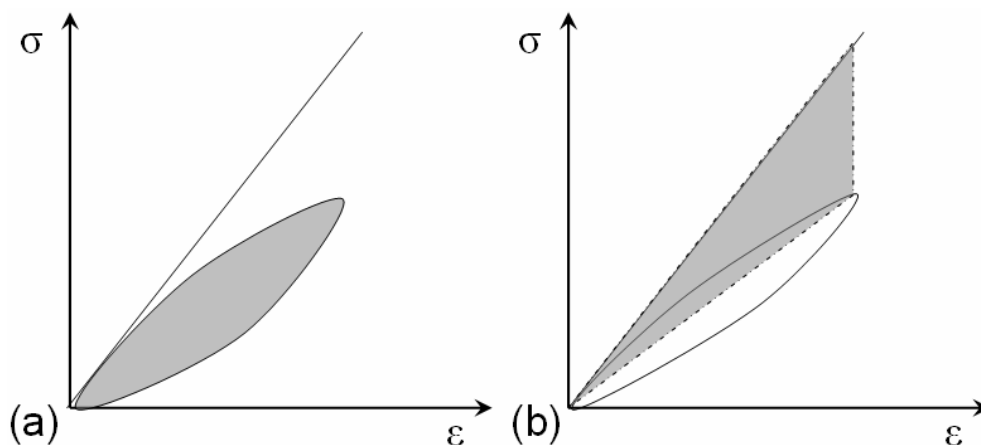
Fig. 5-3 Schematic of plastic dissipation (shaded area) according to (a) hysteresis and (b) microplasticity and reversible grain boundary sliding.
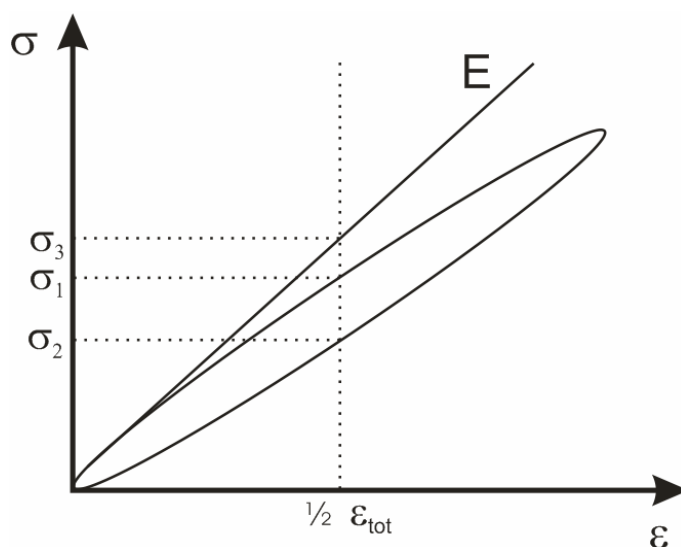
Fig. 5-4 Schematic of the characterization of the hysteresis by σ_1-σ_2, and of the microplasticity by σ_3-σ_1, where σ_1, σ_2 and σ_3 are measured at half of the total applied strain range.

Fig. 5-5 shows the change in stress due to hysteresis, σ_1-σ_2, with cycle number for both 500 nm and 100 nm thick films. The first cycle for both thicknesses is not included due to the measurement failure. In Fig. 5-5 (a), the stress difference

keeps constant with some scatter. For the 100 nm film, Fig. 5-5 (b) shows that the stress difference decreases with increasing number of cycles.

Fig. 5-6 shows the change in stress due to hysteresis for all films that were studied. Both film thicknesses show a clear trend of a decrease in the hysteresis with cycle number.

Fig. 5-5 Change of hysteresis (σ_1-σ_2) during the first 14 consecutive cycles of (a) a 500 nm and (b) a 100 nm thick film.

In contrast, the effect of microplasticity, (σ_3-σ_1) remains almost constant for both the 500 nm and 100 nm thick films from second cycle to 14th cycle, as shown in Fig. 5-7. The first cycle for both thicknesses is not included due to the measurement

failure. It is estimated that the reversible motion of 6 dislocations for 500 nm thick film and 8 dislocations for 100 nm thick film in every grain is required to correspond to the change of microsplasticity (σ_3-σ_1). These values are high but plausible for the grain dimension and estimated by ignoring the contribution of reversible grain boundary sliding. However, in Fig. 5-8 it is seen that the contribution from microplasticity becomes much larger somewhere between 2 - 5x10^4 and two million cycles.
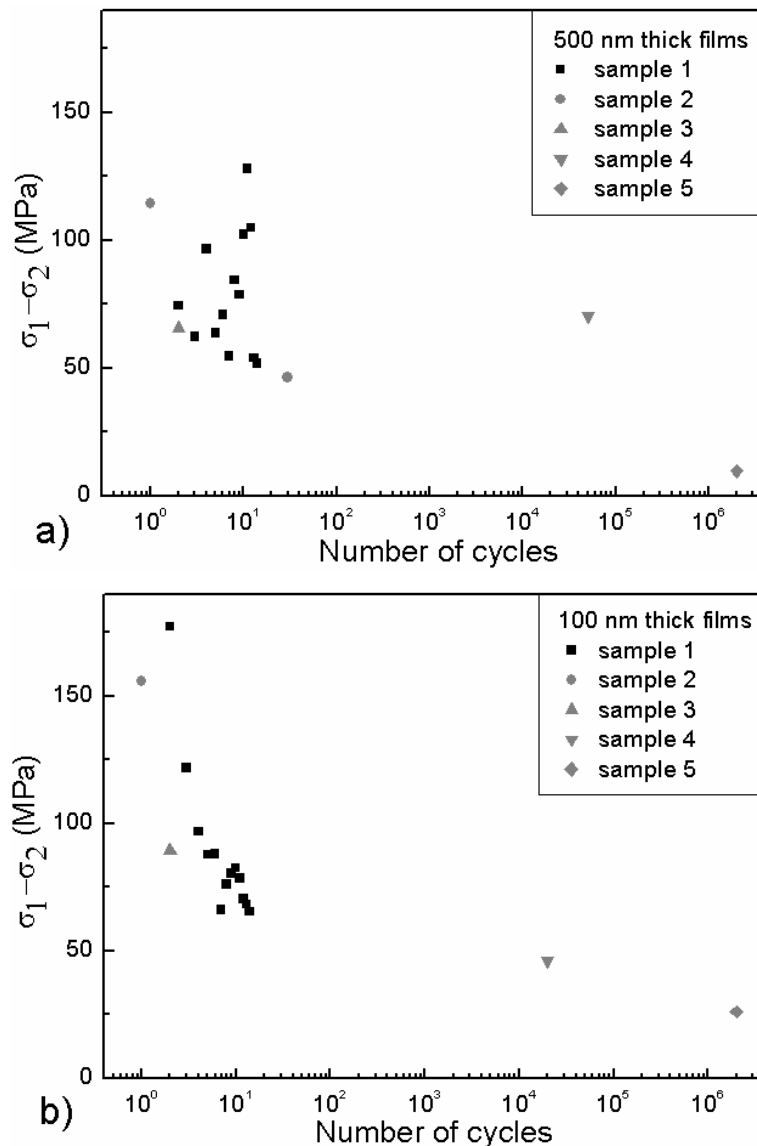
Fig. 5-6 Change of hysteresis (σ_1-σ_2) with cycles in (a) the 500 nm thick films and (b) the 100 nm thick films.

A possible interpretation of these results is presented by the evolution of cracks at the sample surfaces. A sufficient crack density to influence mechanical response (see next section) only evolves after many thousands of cycles at the given strain range. Therefore the cracks can not explain the change in hysteresis, which occurs starting with the first cycle, but can account for the increase in microplasticity. The decrease in hysteresis with cycle number is instead attributed to cyclic hardening, which begins from the first cycle in both 100 and 500 nm thick films.
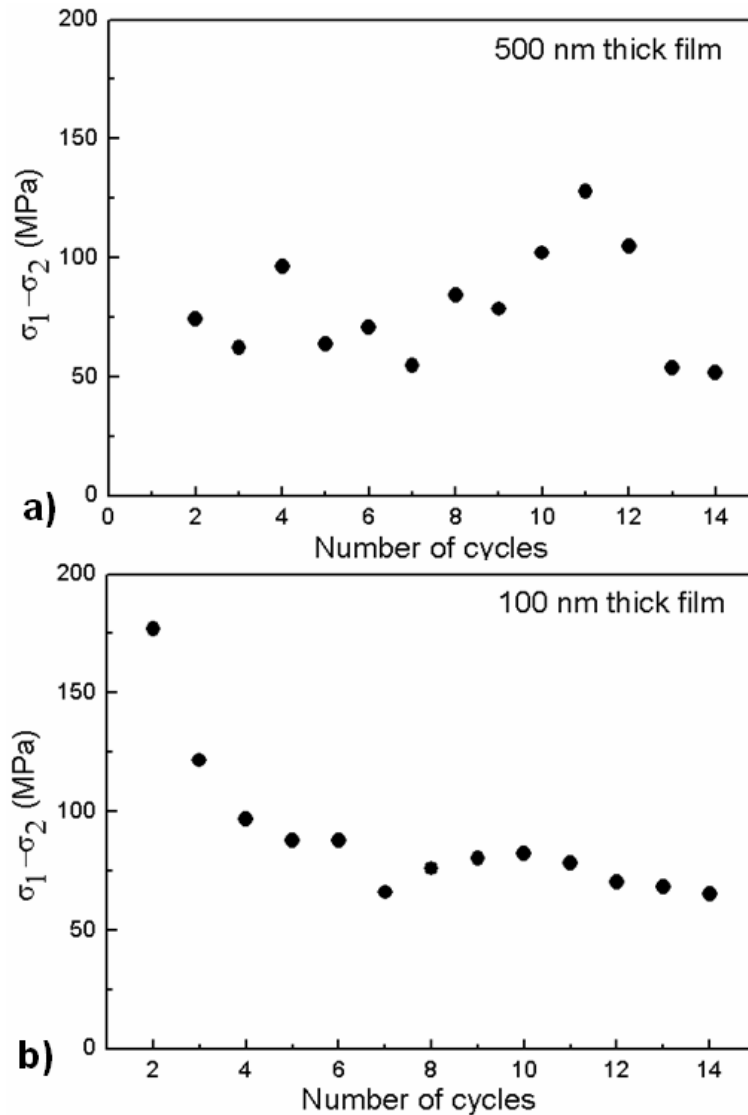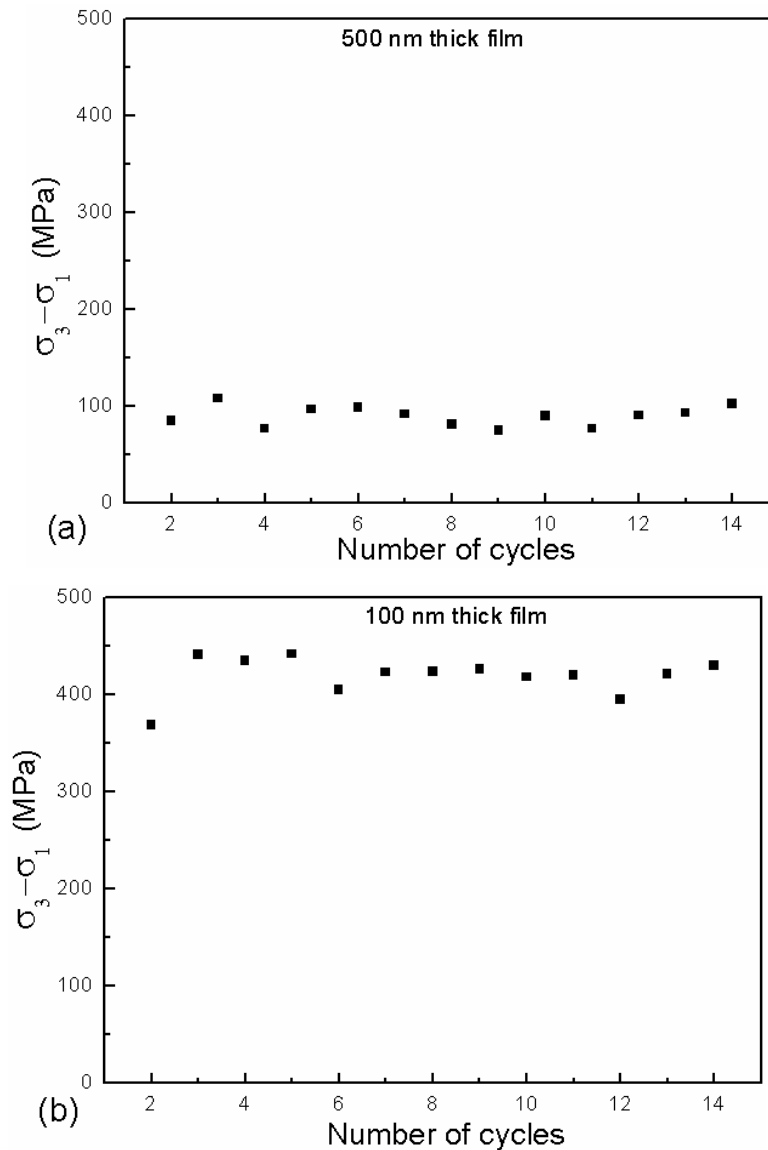

Fig. 5-7 Change of microplasticity (σ_3-σ_1) during the first 14 consecutive cycles of (a) a 500 nm and (b) a 100 nm thick film.

However, the discrepancy is not expected that stronger cyclic hardening occurs in 100 nm thick film but with larger microplasticity. We have not found a good explanation.
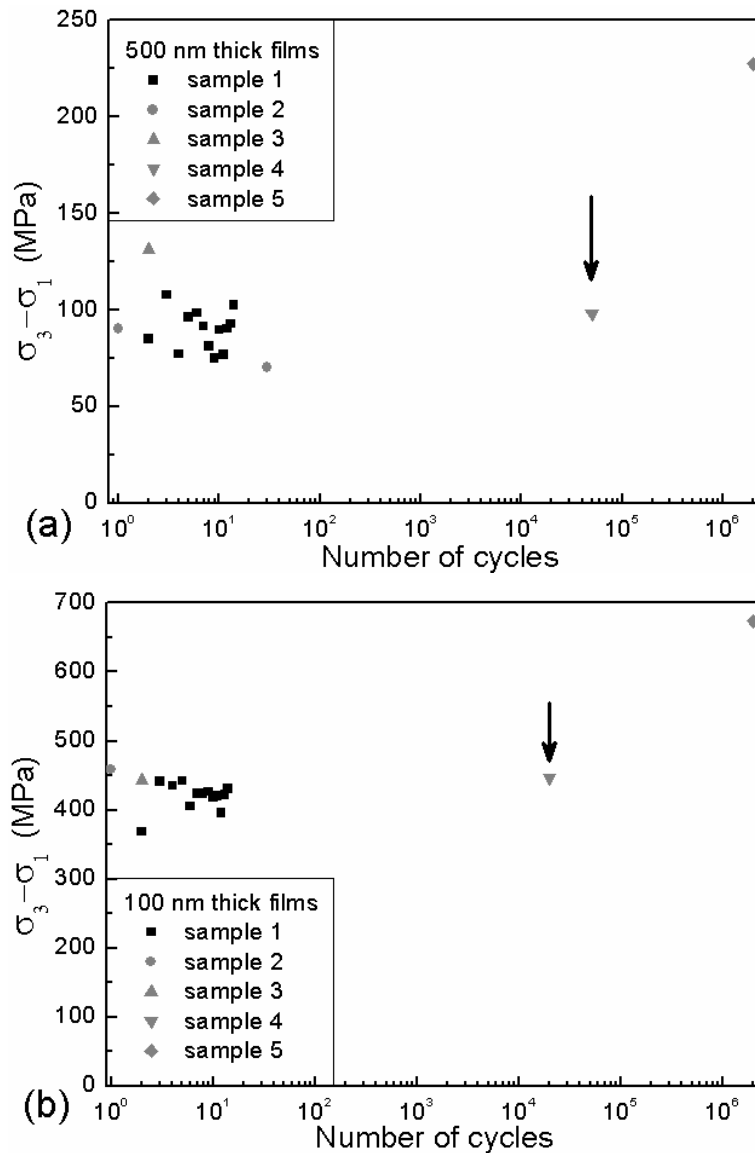
Fig. 5-8 Change of microplasticity (σ_3-σ_1) with cycles in (a) the 500 nm thick films and (b) the 100 nm thick films. The arrows indicate the cycle number at which a significant number of long cracks begin to form in the films.

5.2.3 Cyclic hardening and stress relaxation due to crack formation

The x-ray diffraction data shows that the film stress in the loading direction decreases with increasing cycle number. This decrease is seen in terms of a drop in

the slope in the stress-strain plots (Fig. 4-23 and 4-24), an increase in microplasticity (Fig. 5-8) and a reduction of the hysteresis width (Fig. 5-6) after 2×10^6 cycles. In this condition, images of the film surfaces show numerous cracks perpendicular to the loading direction. The opening of cracks is expected to decrease the tensile stresses in the films and to increase the compliance. The coincidence of the increase in microplasticity with the formation of a high density of long cracks perpendicular to the loading direction provides support for the role of cracks in influencing the mechanical response.

Here a quantitative estimate of the change in compliance and resultant reduction in stress due to crack formation is presented. It is compared with the experimentally measured changes in stress and used estimate the possible contributions from work hardening. A two-dimensional model for crack pattern in thin films [Xia2000] is used. With this model, a stress drop perpendicular to an isolated semi-infinite straight crack can be calculated as:

$$\Delta \sigma_x = -\sigma_0 \exp(\frac{-x}{l}) \qquad\qquad (5.2)$$

where σ_0 is the initial longitudinal stress and l is a reference length which is a measure of the stress relaxation zone in the vicinity of a crack:

$$l = \frac{\pi}{2} g(\alpha, \beta) h \qquad\qquad (5.3)$$

here α, β is Dundur's parameters characterizing the elastic mismatch between the film and the substrate. The function $g(\alpha, \beta)$ given in [Xia2000] depends on α and is equal to 8 for the case of Cu film on Kapton ($\alpha = 0.95$).

According equation (5.3), the reference length l depends on film thickness and this agrees qualitatively with more cracks in thinner film (Fig. 4-20). For 500 nm thick film $l = 6.28$ μm and for 100 nm thick film $l = 1.26$ μm. These values are smaller than the measured mean crack spacing of fatigued 500 nm and 100 nm thick films with value of 9.2 μm and 2.9 μm as shown in Fig. 4-23 (b) and Fig. 4-24 (b). This implies that equation (5.2) can be used here to calculate the stress relaxation by cracking due to fatigue.

If x is the distance perpendicular to the crack and H is mean crack spacing, the average stress perpendicular to cracks σ_x in the film can be calculated:

$$\sigma_x = \sigma_0 + \frac{\int_0^{H/2} \Delta\sigma_x dx}{H/2} = \sigma_0 (1 + \frac{\exp(-H/2l)-1}{H/2l}) \qquad (5.4)$$

This can be written as:

$$r = \frac{\Delta\sigma}{\sigma_0} = \frac{\sigma_0 - \sigma_x}{\sigma_0} = \frac{1-\exp(-H/2l)}{H/2l} \qquad (5.5)$$

As result, $r = 0.71$ and 0.60, respectively, for the 500 nm and 100 nm thick films according.

Using Hook's law the relative stiffness is:

$$r' = \frac{E - E_{eff.}}{E} = \frac{\sigma_0 - \sigma_x}{\sigma_0} \qquad (5.6)$$

where E_{eff} and E are determined from the unloading slope of the stress strain curves after 2×10^6 cycles and 2 cycles, respectively Fig. 4-23 and Fig. 4-24. E_{eff} and E are 26 GPa and 92 GPa for the 500 nm thick film, and 15 GPa and 66 GPa for the 100 nm thick film. Now, we obtain r' as equal to 0.72 and 0.78 for 500 nm and 100 nm thick films, respectively.
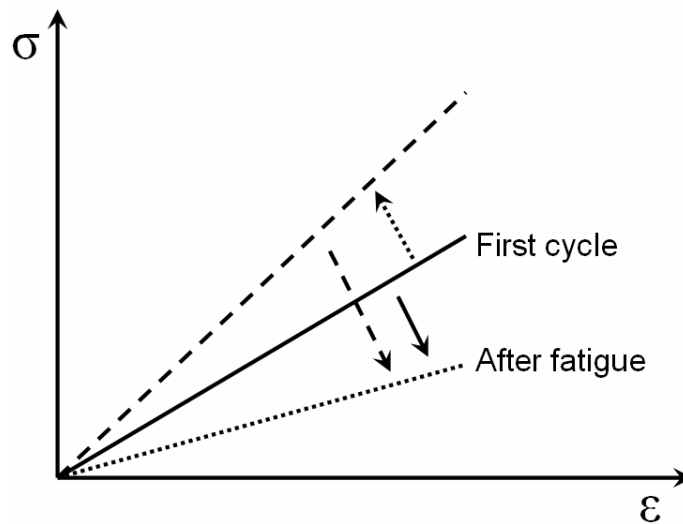

Fig. 5-9 Schematic drawing of the effect of cyclic hardening (dotted arrow) and crack formation (dashed arrow) on the stress-strain response of the Cu films.

We see within the limits of accuracy of this estimate that r' is equal to r for the 500 nm indicating the consistency of the results and, therefore, that most likely

no or very little strain hardening had taken place. In contrast, for the 100 nm thick films *r´* is larger than *r.* This difference is schematically depicted in Fig. 5-9. The solid line indicates the stress in the first cycle and the dotted line the stress after fatigue (with cracks present). It is reasonable that there is a difference indicated by the solid arrow between the stresses in the first cycle and after fatigue due to the stress relaxation related to cracking. But the fact that *r´* is larger than *r* suggests that there is a larger difference indicated by dashed arrow. This implies that prior to the relaxation of stress by crack formation, some cyclic hardening during the fatigue tests in the 100 nm thick film occurred. The very small difference between *r´* and *r* for the 500 nm thick films indicates that the cyclic hardening in 500 nm thick films is not significant compared to that in 100 nm thick films, agreeing with the results of analysis of hysteresis (in Section 5.2.2).

An increase of experimentally determined work hardening rate with decreasing film thickness for monotonic testing from literature [Keller1998, Hommel1999a, Hommel2001, Weiss2001, Weiss2000, and Weihnacht2001] was summarized by Blanckenhagen and his colleagues [Blanckenhagen2004] and compared with the date from discrete dislocation simulation [Blanckenhagen2004]. It is argued that source-controlled deformation mechanism in thin films account for more significant hardening in thinner films, whereat the decrease of the number of dislocation sources with decreasing film thickness/grain size enhances the work hardening [Blanckenhagen2004]. In this work with cyclic testing, the experimental and calculated results show stronger cyclic hardening in thinner films consistently. It is believed that irreversible dislocation motion is responsible for the cyclic hardening, but it is not expected with larger microplasticity in thinner films. This discrepancy is difficult to explain.

5.3 Length scale effect on fatigue behavior of thin Cu films

A clear length scale effect on both fatigue damage morphology and fatigue life has been presented in Section 4.1. Specifically, it has been shown that extrusions form in the thicker films, where they act as sites for crack initiation, whereas in thinner films, extrusions are absent and the cracks form at boundaries and defects. The decrease in film thickness/grain size also leads to a marked increase in fatigue

life. In the following sections, this behavior will be compared with the fatigue behavior of bulk samples and length scale effects on each aspect of damage formation and fatigue life will be discussed. For structural metallic components without large extrinsic defects, different regimes for the evolution of damage during fatigue life can be distinguished in order of increasing cycle number:

- Microstructural changes, such as the formation of *dislocation structures* in the interior of grains.

- *Extrusion and intrusion* formation, at the sites where dislocations structures intersect the sample surface.

- *Crack initiation*, usually at the surface intrusions.

- *Propagation* of short cracks (short compared to microstructural features such as grain size) and then coalescence of small cracks to one large dominant crack, the growth of which can be described by linear elastic fracture mechanics.

- *Rupture* of the specimen or component when the crack reaches a critical length for a given maximum stress according to the critical stress intensity.

In the case of our thin films, the last stage cannot be reached since the film is supported by the substrate and rupture of the specimen does not occur. However, the first four regimes can be identified and they may be all subject to size effects related to film thickness and/or grain size. As a result, the interpretation of length scale on fatigue damage formation and fatigue life requires separate discussions of all of these regimes.

5.3.1 Length scale effects on fatigue damage

5.3.1.1 Dislocation structures

In bulk, large-grained metals, the dominant modes for fatigue damage are the formation of long-range dislocation structures within grains such as persistent slip bands (PSBs). However, the dislocation structure formation is constrained in small crystal volumes. For example, no PSBs are observed in thin, fine-grained Cu films (200 nm to 3.0 μm thick) [Zhang2003, Zhang2005, and Zhang2006]. Nevertheless, dislocation walls are found in the largest grains of the thickest films (3.0 μm), while

only diffuse dislocation structures or individual dislocations are present as the grain size and film thickness decrease [Zhang2003, Zhang2005, and Zhang2006].

In addition, due to the anisotropy in the films, different stress distribution appears in different oriented grains [Baker2001a], and even in the same grains [Phillips2004]. The surface relief observed in earlier stage of fatigue tests in the films (Fig. 4-6) probably can be considered as the results early relaxation of inhomogeneous residual stress at grain boundaries. In general, besides the dominated thickness and grain size effects on fatigue damage, the strain homogeneity induced by structure is also an important factor to be considered.

5.3.1.2 Extrusions and intrusions

The damage that occurs in bulk samples where PSBs intersect the surface is typically in the form of extrusions surrounded by intrusions. This surface structure has been related to the rather complex structure of the PSBs [Essmann1981]. Typically, cracks are initiated at these surface intrusions. Despite the absence of PSBs, extrusions are observed in our films, albeit with decreasing dimensions when grain size and film thickness are decreased. It is argued that extrusion formation is controlled by the amount of local plastic strain in the film, whether carried by individual dislocations or by dislocation structures [Zhang2001]. The work presented here on even thinner films and smaller grains supports this picture: extrusions are very small and form rarely in the thinnest films and are only found in regions where the plastic strain is locally increased, e.g. along cracks. So the decrease of extrusions in size and number can be considered as the reflection of dependence of dislocation motion and nucleation on length scale. Furthermore, the films show extrusions at the surface and intrusions at the film/substrate interface. The fact that extrusions do not form at buried grain boundaries or at film/substrate interfaces, is not surprising given the mechanical constraint from the underlying material, and the known fact that coatings inhibit extrusion formation [Stoudt2000]. The formation of pairs of surface extrusions and interface intrusions in the thin films is an expected consequence of repetitive slip of individual dislocations. The fact that the intrusions form in the Cu on polyimide samples indicates that stress concentration produced by dislocations piling-up against the interface lead to the formation of intrusions. Dislocations

pushed up against interfaces and twin boundaries have been observed in these samples [Zhang2005]. In another thin films system, Ag on SiO$_2$ [Schwaiger2003a], interface voids were found rather than intrusions. It can be argued that the void formation is related to the condensation of vacancies produced by annihilation of dislocations [Schwaiger2003a], or from stress concentrations from dislocation pile-ups. This difference may suggest that the nature of interface damage is influenced by interface quality.

For annealed films, grain size scales with film thickness. In this work, the effects on fatigue damage from thickness and grain size are not separated. However, the grain size clearly affects the extrusion formation based on the fact that extrusions are always found in larger grains [Zhang 2006]. Similar observation is also found in this work. Extrusions can not be observed within the small grains with small plane-view grain size in thicker films (3.0 μm and 1.0 μm), while extrusions can even be observed within large grains with large plane-view grain size in 200 nm thick film. This means the glide length of dislocations in a crystal affects the formation of extrusions in effect. Furthermore, if twin boundaries would have been taken into account for the determined value of grain size, it would have decreased more quickly with film thickness than that plotted in Fig. 4-1 due to increase of twin density with decreasing film thickness. This corresponds to a quicker decrease in glide length of dislocations. In that case, of the change in twin density contributes to the size effect. This would be consistent with a contribution of twin boundaries to the strength of Cu films during monotonic testing as reported in [Yu2004].

Extrusions are found in both <111> and <100> out-of-plane-oriented grains of the Cu films. But the statistic analysis of influence of texture on damage formation has not been performed in presented work. However, <100> out-of-plane-oriented grains are more susceptible to damage formation reported in both Ag films on SiO$_2$ substrate using cyclic bending test [Schwaiger2003a] and Cu films on SiO$_2$ substrate during thermal fatigue [Mönig2005]. It needs more quantitative investigation to know if the change in ratio of the integrated peak intensities I$_{(111)}$ / I$_{(200)}$ (Fig. 4-4) has an influence on damage change with thickness.

Twin boundaries in bulk specimens are well-known sites for crack initiation [Heinz1990, Blochwitz2003, and Blochwitz2005] as well as for early PSB nucleation [Llanes1992, Peralta1994], presumably due to the high local stresses generated by

elastic crystal anisotropy. Twin boundaries play a similar role in the thin Cu films in that cracks often initiate in the boundaries in the thinner films and extrusion-intrusion pairs form next to and parallel to the boundaries in the thicker films.

5.3.1.3   Crack initiation

The studies show that the cracks in the thicker Cu films initiate at the intrusions at the film/substrate interface (Fig. 4-10), and not from the surface as for bulk samples. In the thinner films, the cracks form directly at pre-existing defects or at boundaries, without the aid of extrusions or intrusions. But it is not clear if cracks are initiated first at the surface, in the interior of film or at the interface between film and substrate, as schematically shown in Fig. 5-10. As the film thickness decreases, the ratio of surface roughness (especially at grain boundaries) to thickness becomes higher, and this leads to a more pronounced stress concentration. So it is possible that crack initiates from surface to interface as shown in Fig. 5-10 (a). Also, blocking of dislocations by grain or twin boundary can result in stress concentration in interior of film, and crack may initiate there, as shown in Fig. 5-10 (b). In addition, crack may initiate at the interface to the substrate (Fig. 5-10 (c)).
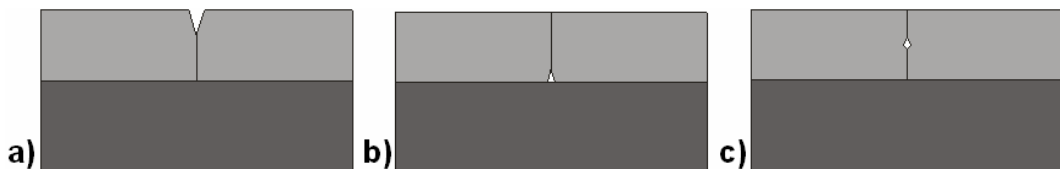
Fig. 5-10 Schematic of crack initiation at boundaries from (a) surface, (b) interior film and (c) interface between film and substrate.

Predicting the film thickness dependence of crack initiation is complicated, but it is expected to be more difficult at smaller length scales. The fact that the crack density at saturation (Fig. 4-20) increases with decreasing film thickness may therefore be a reflection of the increased applied strain range or the increased density of twin and grain boundaries in the thinnest films.

5.3.1.4 Crack propagation

The ease of propagation of a "channel" crack in a film on a substrate depends on the stress and the substrate mechanical properties, among other things [Hutchinson1992, Xia2000]. Here, the large compliance of the polyimide substrate increases the crack opening displacements and the distance over which stresses are relaxed in the neighborhood of a crack. Estimates of the driving forces for channel crack propagation under monotonic loading show that very larges strains are necessary (~10%) in the absence of film delamination [Li2005]. Since we do observe cracks at much smaller strain ranges and we do not observe delamination, we argue that crack propagation under cyclic loading can proceed under much smaller strains, presumably through assistance by dislocation processes ahead of the crack tip. The influence of the film thickness on such a crack propagation mechanism is not obvious because it is influenced by the crack opening displacement, the size of the plastic zone ahead of the crack and the applied stress which all depend on each other in a complicated manner for our sample geometry.

5.3.2 Length scale effect on fatigue life

There is a significant effect of length scale on fatigue life: larger strains are required to cause failure in thinner films. Even though we have used a rather qualitative failure criterion, it is shown in Fig. 4-22 that no damage occurs in thinner films at small strain ranges (data points indicated with arrows), while thicker films have failed under these same conditions. This shows that there is an unambiguous effect of film thickness/grain size on fatigue life in the high cycle fatigue regime.

The fatigue failure data (Fig. 4-22) has been re-plotted in Fig. 5-11 to show the applied strain range required to cause failure after 10^6 cycles. This representation enables the definition of three regimes of fatigue behavior: a bulk-like regime, a transition regime, and a boundary-controlled regime.

Bulk-like regime: Fig. 5-11 shows that the effect of film thickness or grain size on fatigue life is weak at lengths greater than 1.0 μm, in that the applied strain range required to cause failure in 10^6 cycles does not change much. This length scale independence is fairly easily understood in terms of fatigue induced dislocation structures: in samples with thicknesses or grain sizes larger than around 1 μm [Zhang2006], characteristic dislocation structures with length scales smaller than 1

µm form early on during fatigue. These dislocation structures dominate subsequent fatigue behavior and lead to a more or less length scale independent behavior.

Transition regime: In the shaded region of Fig. 5-11 between 1.0 µm and 100 nm, there is a large increase in the applied strain required for causing failure. The total strain required to produce 0.1% plastic strain (yield strain) [Hommel2001] under monotonic loading is also included in the figure and it parallels the strain needed to cause fatigue failure. Presumably, this parallel behavior is an indication that both effects are controlled by the same underlying phenomenon. The mechanisms that have been proposed for the increase in monotonic flow stress with decreasing sample size are most often based on the Orowan stress [Nix1989, Arzt1998] for dislocation motion [Nix1989, Thompson1993] and nucleation [Arzt2001]. This transition regime also corresponds to the length scale over which the nature of the dominant fatigue damage in the Cu films changes from extrusions to cracks. Typically, global or local plastic strains are the driving force for fatigue failure. Therefore, it is not surprising that an increase in applied strain range is required for causing failure since it corresponds to an increase in yield strength under monotonic loading (see solid line in Fig. 5-11). In other words, the effect of length scale on fatigue life is due to the same mechanisms that govern the effect of length scale on film strength, i.e. constraint effects on dislocation nucleation and motion owing to the small dimensions [Nix1989, Arzt1998, Arzt2001 and Blanckenhagen2003].

Boundary-controlled regime: The one data point for the 50 nm thick films is not significantly higher than the data point for the 100 nm thick films, indicating that the effect of length scale on fatigue may be weaker below 100 nm. Although this single data point is not "convincing", in combination with the observed transition in fatigue damage nature and other observations in the literature [Moenig2004], it points to the possibility of a new regime at small length scales.

The change in morphology of fatigue damage, from extrusion to crack dominated, supports the idea of a change in fatigue mechanism. A simple scenario can be developed based on the idea that the stress necessary for dislocation nucleation and motion, and thus for extrusion formation [Zhang2006], increases with decreasing film thickness. When the thickness is below a certain value - 100 nm in our case - the stresses become high enough to allow for crack nucleation at existing

defects or at boundaries. If such a scenario is indeed accurate, predictions of the fatigue behavior for films with thicknesses below roughly 100 nm remains entirely open and will depend on the length scale dependence of crack initiation and propagation.
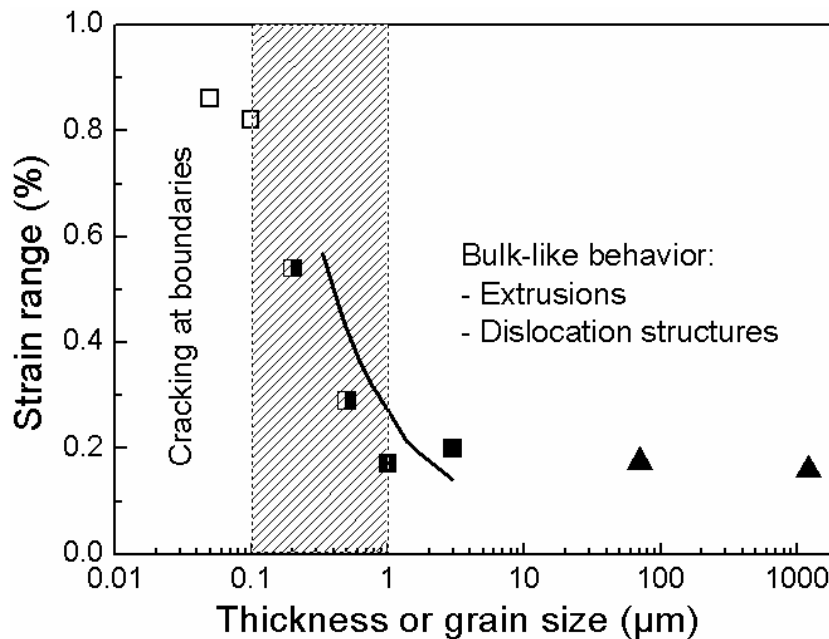
Fig. 5-11 Applied strain range necessary to cause failure in 10^6 cycles in Cu films (square symbols) and in large grained bulk Cu (▲) [Lukáš1987]. The nature of the damage in the films is indicated by the symbols: extrusions (■), cracks with occasional extrusions (◪), cracks along boundaries (□). The solid lines show the strain range at 0.1% yield for Cu films under monotonic loading [Hommel2001].

5.3.3 Columnar structure vs non-columnar structure

It is clear that the extrusion features is dependent dominantly on the volume size of crystals in effect whatever in columnar or non-columnar structures. This means extrusions form preferentially in grains with large volume size. However, Fig. 4-21 shows that the ratio of extrusion height to thickness is much higher in 200 nm, 500 nm and 1.0 μm thick films than in 3.0 μm thick films and strongly dependent on applied strain in 3.0 μm thick films. It is not sure if this is a thickness effect or structure effect (the 3.0 μm thick films have a non-columnar structure). In addition, it is observed that Ta over-layer leads to a more homogeneous plastic deformation in

1.0 μm Cu films. If the non-columnar structure has also a similar effect to lead to a more homogeneous plastic deformation, then we can explain the smaller ratio of extrusion height to thickness in 3.0 μm thick films. If such a scenario is indeed accurate, it may be also explain why the fatigue life of 3.0 μm thick Cu films is little longer than that of 1.0 μm thick films.

5.4 Fatigue behavior of thin Cu films at 200 °C

As temperature is raised, diffusion processes play a more important role. This may account for the more rounded shape of the extrusions and crack edges. It also may lead to stress relief and account for the slightly lower density of extrusions. The grain boundary grooving and local film thickening observed at 200°C may be evidence of stress relief mechanisms. Increased diffusion may also explain why pores are seen near cracks formed at 200°C and not near those formed at room temperature. Presumably, the driving force for pore formation at grain and twin boundaries is local stress concentration such as due to a pile-up of dislocations [Zhang2007].

Yield stress decreases with increasing temperature [eg, Thouless1993], which means that for a given total strain range, the plastic strain range will increase with increasing temperature. If this effect dominates over the possible diffusion-controlled stress relief, it can explain the decrease of fatigue lives at 200 °C. In addition, during the testing starting process as temperature increasing from room temperature to 200 °C, the initial stresses in Cu films should increase or be driven in tension due to lower thermal expansion coefficient in Cu (16.5×10^{-6}/K) than Kapton (20×10^{-6}/K). So, the increasing initial tensile stresses can also have a contribution to a decrease of fatigue lives at 200 °C.

The probable oxide particles (white spots generated during the tests) could have some influence on fatigue life. Increased fatigue life in Cu is reported due to oxidation in literature and interpreted by a mechanism in which the oxide particles act to homogenize the strain and to increase the work-hardening capacity of the material [Eckert1987]. However, it is still not clear here whether the white spots influence the fatigue life of our Cu films at all.

Fig. 5-12 shows fatigue lives of Cu films on Kapton tested at 200 °C and Cu films on Si during thermal fatigue [Mönig2005]. Except that fatigue life of 100 nm thick Cu film at 200 °C is consistent with the data of thermal fatigue, fatigue lives of Cu films at 200 °C are larger than those of thermal fatigue generally. This may be explained by a simple temperature effect as the thermal fatigue is driven by the temperature cycling between room temperature and 400 °C [Mönig2005], reaching much higher temperature than 200 °C.
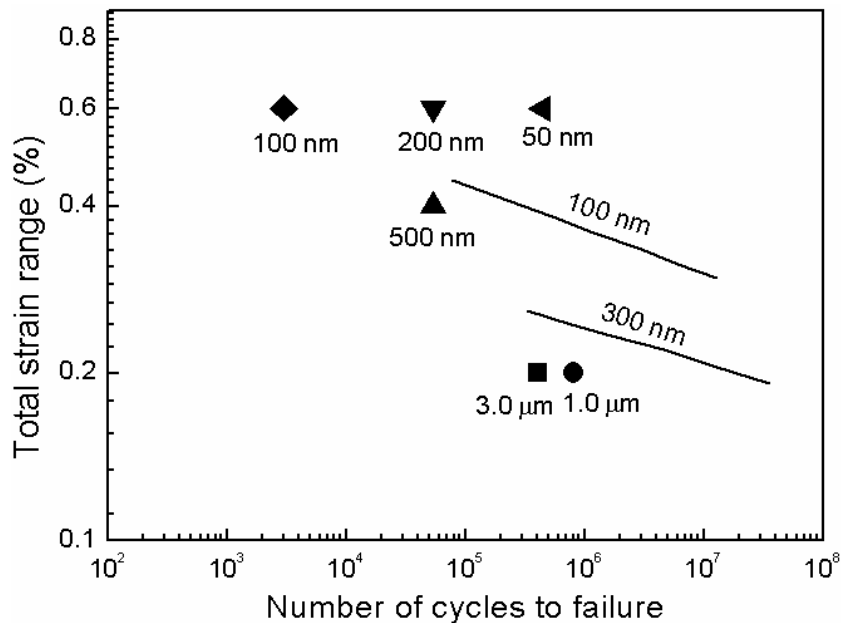
Fig. 5-12 Fatigue life diagram for Cu. Data from tests at 200 °C (shown as filled squares). Data from Cu on Si during thermal fatigue (temperature between room temperature and 400 °C) shown as solid lines [Mönig2005] are included for comparison.

5.5 Influence of Ta under- and over-layers on fatigue behavior

There is a clear effect of Ta under- and over-layers on both fatigue damage and fatigue life in the Cu films. The presence of the Ta layers influences the nature of the damage that is formed, both at the surface and at the buried interface, and the presence of a Ta over-layer is found to improve the fatigue life in the thicker Cu

films. In addition, these influences changes with change of Cu film thickness. Possible explanations for these effects will be discussed in following sections.

5.5.1 Influence of Ta layers on 1.0 μm thick Cu films

Although dislocations pushed up against a Cu/Kapton interface have been observed [Zhang2005], it is still not clear what exact role such a metal/polymer interface plays on dislocation activities. However, the Cu/Ta interface has been studied and can serve as barrier of dislocations [Vidal2006]. The fact that the flow stress is increased due to Ta layers in submicron regime (Fig. 5-13) indicates that the Ta/Cu interface serves much more effectively as blocking boundary for dislocations than Cu/Kapton interface. However, as thickness is increased to 1.0 μm, the influence of Ta layers on flow stress is neglected because boundaries constraint effects on dislocation motion and nucleation are not significant in such length scale. Fig. 5-14 shows schematically the different constraint effects according to the proposed mechanisms for different flow stress shown in Fig. 5-13. The dislocation can glide freely to the Cu surface and Cu/Kapton interface or be partially blocked at the Cu/Kapton interface (Fig. 5-14 (a)). In Cu/Ta/Kapton film stack, dislocations can glide freely to Cu surface but deposit at the Cu/Ta interface surface (Fig. 5-14 (b)). However, dislocations are blocked in both sides at the Cu/Ta interfaces in Ta/Cu/Ta/polyimide film stack (Fig. 5-14 (c)). The absence of intrusions under some extrusions, the surface intrusions paired with surface extrusions and surface roughening (small surface extrusions and intrusions) in Cu/Ta film stacks are evident for more dislocations activity at the surface than at Cu/Ta interface, supporting the interface constraint model illustrated in Fig. 5-14.

The increase of fatigue life in Cu/Ta film stacks with 1.0 μm thick Cu film is probably due to hindrance of intrusion formation at film/substrate interface induced by blocking of dislocations at Cu/Ta interface. Cracks initiate from intrusions to surface (Section 4.2.1) and therefore, the hindrance of intrusion formation can lead to an increase of fatigue life in Cu/Ta film stacks. The more significant increase of fatigue life results from another effect, namely the suppression of extrusion formation by a Ta over-layer. This is similar to the known fact that coatings inhibit extrusion formation [Stoudt2000]. Instead, the surface becomes wrinkled during the cyclic testing. Because strength of Ta is higher than that of Cu, Ta may first deform elastically, while Cu deforms plastically. Then, stress concentrations are produced by

piling-up of dislocations at the interface, so that the stress at the interface becomes high enough to allow plastic deformation in the Ta layer. The stress concentration is partially relaxed by the plastic deformation of Ta over-layer, leading to surface wrinkling. In addition, the replacement of extrusions by surface wrinkling reflects more homogenous plastic deformation due to the constraint of Ta over-layer. Extrusions are considered as the sites where serious stress concentration can result in crack initiation. Therefore, suppression of extrusion formation and more homogenous plastic deformation due to Ta over-layer lead to hindering and deferring the crack initiation and thereby fatigue life is improved dramatically. In addition, the initial stress state in Cu films before testing may be compressive due to Ta layers. The deformed Ta under-layer showed in Fig. 4-37 (b) is evident for the compression state. This compressive initial stress state can also contribute to the increase of fatigue life.
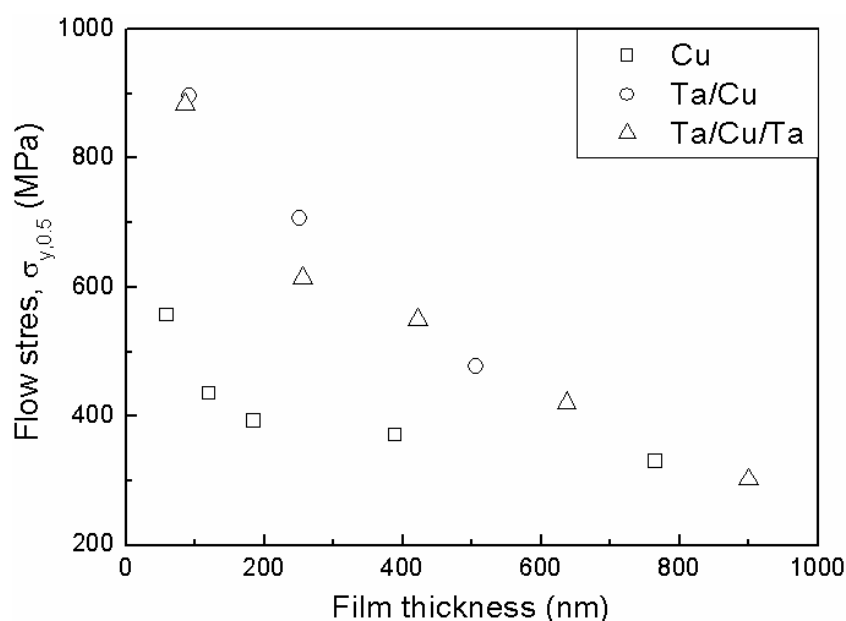
Fig. 5-13 Flow stress at 0.5% plastic strain as a function of film thickness for Cu films, Cu/Ta and Ta/Cu/Ta film stacks. Ta layers are 10 nm thick. These data are replotted data from [Gruber2007].

Delamination has been clearly observed in fatigued Ta/Cu/Ta film stacks at the interface between the Ta under-layer and the polyimide substrate. Delamination suggests that the compressive stress in the films is large enough to reach the fracture

resistance of the interface. Due to the smaller thermal extension coefficient of Ta, it is argued that larger compressive residual stress can evolve in the Ta/Cu/Ta film stacks. But the fact that the delamination occurs at the interfaces under wrinkles or extrusions suggests that the initial compressive stress is not large enough for delamination without an additional driving force due to cyclic deformation.
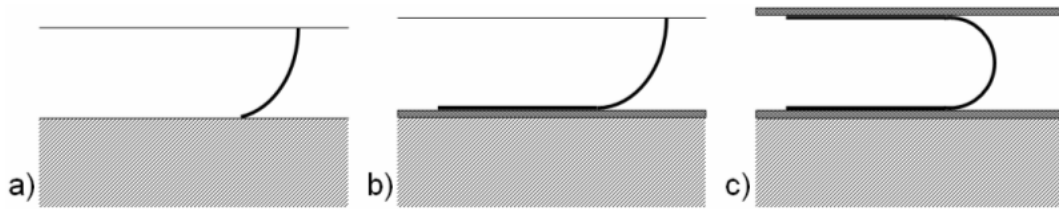

Fig. 5-14 Schematic of constraint effect of interface condition on dislocation motions: (a) unpassivated film on substrate with weak interface, (b) under-layer passivated film and (c) passivated film with both over-and under-layers.

5.5.2 Influence of Ta layers on 100 nm thick films

There is a clear length scale effect on fatigue life and damage in Cu films whatever with or without Ta layers. Fatigue life increases with decreasing film thickness and damage mode changes from extrusions (wrinkles for Ta/Cu/Ta film stacks) dominated to cracks dominated. In addition, we see the influence of Ta layers on fatigue behavior in 100 nm thick Cu films is very different from that in their thicker counterparts (1.0 μm). There is almost no change in fatigue life and nature of damage mode (crack as dominating damage) in 100 nm thick Cu films. Fig. 4-40 shows that the three types of film stacks (Cu, Cu/Ta, and Ta/Cu/Ta) have similar trend of cracks evolution despite different crack density. In other words, the Ta over-layer has large influence on the damage mode in thicker films in terms of suppression of extrusion formation, but much little influence on crack formation in thinner films as they start from pre-existing defects. From energetic viewpoint, the crack growth resistance for a material is given by the sum of plastic dissipation and surface energy of the generated crack faces. The plastic dissipation by cracking is decreased with decreasing film thickness [Litteken2005]. Therefore, it is argued that the Ta layers have almost neither a contribution to plastic dissipation, nor a contribution to surface energy due to their limited thickness. This implies that the Ta

layers almost does not change or influence the crack growth resistance of the film stacks. In summary, the fatigue life is hardly influenced by the Ta layers.

There is a proposed fatigue mechanism transition in thin Cu films from dislocation mediated extrusion formation to crack formation with decreasing film thickness (see Section 5.3). The different influences of Ta layers, especially Ta over-layer on fatigue life and damage in both 1.0 μm and 100 nm thick Cu films confirm this proposed mechanism transition. In addition, the fact that cracks formed in Ta/Cu/Ta film stacks with 100 nm thick Cu film without extrusions or hillocks along cracks as in Cu films or Cu/Ta film stacks support the scenario that when the thickness is below a certain value - 100 nm in our case - the stresses for extrusion formation become high enough to allow for crack nucleation at existing defects or at boundaries without assistance of extrusions. Extrusions formed along cracks in Cu or Cu/Ta film stacks after crack initiation and during crack propagation probably due to stress concentration at crack tip. In addition, the different mechanism (cracking dominated) in fatigue behavior of 100 nm thick film stacks than that (constraint of dislocation motion and nucleation) in flow behavior of monotonic test account for the increased flow stress of 100 nm thick Cu films due to Ta layers has no influence on fatigue life.

The different crack densities (Fig. 4-40) are probably due to compressive stress states in Cu/Ta and Ta/Cu/Ta film stacks. The hillocks along cracks in Cu/Ta film stacks and the overlap of crack faces in Ta/Cu/Ta film stacks suggests compressive stress state in both Cu/Ta and Ta/Cu/Ta film stacks.

6 Summary and conclusion

The ultimate goal of this work has been to gain insights into the mechanisms responsible for the length scale dependence of fatigue damage formation and failure. To this end, the fatigue behavior of Cu films with thicknesses between 50nm and 3.0 µm has been investigated at both room temperature and 200°C. Through the incorporation of surrounding Ta layers, the influence of interfaces on fatigue behavior in Cu films has also been studied. The stress-strain response of the Cu films during in-situ fatigue testing has been determined using synchrotron x-ray diffraction and used to interpret the damage morphologies and failure lives.

To study length scale effect on fatigue behavior in thin Cu films systematically, cyclic tensile testing of 50 nm to 3.0 µm thick Cu films deposited on compliant Kapton substrate was performed, and periodically interrupted to investigate fatigue damage evolution using SEM and FIB. There are clear length scale effects on both damage morphology and fatigue life. Extrusions decrease in number and size with decrease of thickness/grain size. More cracks are observed in thinner films. In thicker films, cracks initiate first from the locations of extrusion/intrusion pair and then propagate. But in very thin films (100 nm and 50 nm), cracks initiate directly at pre-existing defects or grain or twin boundaries, and then few extrusions are formed after crack initiation and during crack propagation. There is a clear length scale effect on fatigue life in film thickness between 1.0 µm and 100 nm: higher strain or more cycles are required for thinner films to form damage. But the data of fatigue life in 50 nm thick films is not significantly higher than the data for the 100 nm thick films. Based on the observation of change in both damage morphology and fatigue life, we have proposed that there is fatigue mechanism transition from dislocation mediated extrusion formation to crack formation with decreasing film thickness. A simple scenario can be developed based on the idea that the stress necessary for dislocation nucleation and motion, and thus for extrusion formation, increases with decreasing film thickness. When the

thickness is below a certain value - 100 nm in our case - the stresses become high enough to allow for crack nucleation at existing defects or at boundaries. If such a scenario is indeed accurate, predictions of the fatigue behavior for films with thicknesses below roughly 100 nm remains entirely open and will depend on the length scale dependence of crack initiation and propagation.

A similar investigation of fatigue behavior in thin Cu films (50 nm to 3.0 μm) has also been performed at 200°C. The same trend of length scale effects has been observed that fatigue damage changes from extrusion dominated to crack dominated as film thickness decreases and that higher strain or more cycles are required in thinner films to form damage. However, the fatigue damage at 200°C differs from that at room temperature clearly in that rounded extrusions, pores interior of Cu films, and grain boundary grooves are observed. All these differences support that diffusion processes are involved in damage formation. In addition, the fatigue life is clearly reduced at 200°C.

100 nm and 1.0 μm thick Cu films were passivated with 10 nm thick Ta layers to study the interface effect on fatigue behavior in thin Cu films. Ta layers influence both fatigue damage and fatigue life. For Ta over-layers on 1.0 μm thick Cu films fewer and smaller extrusions, wrinkled surface and delamination at film/substrate interfaces were observed. In contrast, Ta layers do not change the dominance of cracks in fatigue damage for 100 nm thick Cu films, but influence the crack morphology. In the 1.0 μm thick Cu films passivated with both Ta over-and under-layers, there is a dramatic increase of fatigue life due to depression of extrusion formation owing to Ta over-layer. However, Ta layers have much smaller influence on fatigue life in 100 nm thick Cu films in which cracks are dominated damage. This indicates that the Ta over-layer have a large influence on extrusion formation but almost no influence on crack formation. The different influence of Ta over-layer on fatigue behavior between 1.0 μm and 100 nm thick Cu films confirms the proposed fatigue mechanism transition from dislocation mediated extrusion formation to crack formation as film thickness is decreased.

Bibliography

F. Ackermann, L.P. Kubin, J. Lepinoux, and H. Mughrabi. Dependence of dislocation microstructure on plastic strain amplitude in cyclically strained copper single crystals. *Acta Metall*, 32(5):715–725, 1984.

E. Arzt. Size effects in materials due to microstructural and dimensional constraints: A comparative review. *Acta Mater*, 46(16):5611–5626, 1998.

E. Arzt, G. Dehm, P. Gumbsch, O. Kraft, and D. Weiss. Interface controlled plasticity in metals: dispersion hardening and thin film deformation. *Progress in Materials Science*, 46(3-4):283–307, 2001.

S.P. Baker. Plastic deformation and strength of materials in small dimensions. *Mater Sci Eng A*, 319-321:16–23, 2001.

S.P. Baker, A. Kretschmann, and E. Arzt. Thermomechanical behavior of different texture components in Cu thin films. *Acta Mater*, 49:2145–2160, 2001a.

O.H. Basquin. The exponential law of endurance tests. *Proc. Of the ASTM*, 10:625-630, 1910.

C. Blochwitz and W. Tirschler. Influence of texture on twin boundary cracks in fatigued austenitic stainless steel. *Mater Sci Eng A*, 339(1-2):318–327, 2003.

C. Blochwitz and W. Tirschler. Twin boundaries as crack nucleation sites. *Cryst Res Technol*, 40(1-2):32–41, 2005.

J. Böhm, P. Gruber, R. Spolenak, A. Stierle, A. Wanner, and E. Arzt. Tensile testing of ultrathin polycrystalline films: A synchrotron-based technique. *Rev Sci Instrum*, 75(4):1110–1119, 2004.

F.R. Brotzen and S.C. Moore. Mechanical testing of thin films. *Int Mater Rev*, 39(1):24–45, 1994.

L.F. Coffin Jr, L.F. A study of the effects of cyclic thermal stresses on a ductile metal. *Trans. ASME*, 76:931–950, 1954.

C. Eberl, R. Spolenak, E. Arzt, F. Kubat, A. Leidl, W. Ruile, and O. Kraft. Ultra high-cycle fatigue in pure Al thin films and line structures. *Mater Sci Eng A*, 421(1-2):68–76, 2006

C. Eberl, R. Spolenak, O. Kraft, F. Kubat, W. Ruile, and E. Arzt. Damage analysis in Al thin films fatigued at ultrahigh frequencies. *J Appl Phys,* 99 (11), 2006a.

R. Eckert, C. Laird and J.L. Bassani. Fracture mechanisms in Cu-O and Cu-Pb alloys fatigued with a positive mean stress. *Mater Sci Eng*, 91:19-28, 1987.

H.D. Espinosa, B.C. Prorok, and B. Peng. Plasticity size effects in free-standing submicron polycrystalline FCC films subjected to pure tension. *J Mech Phys Solids*, 52: 667-689, 2004.

U. Essmann, U. Goesele, and H. Mughrabi. Model of extrusions and intrusions in fatigued metals - 1. point-defect production and the growth of extrusions. *Phil Mag A*, 44(2):405–426, 1981.

A.G. Evans and J.W. Hutchinson. The thermomechanical integrity of thin films and multilayers. *Acta Metall Mater*, 43:2507–2530, 1995.

J.N. Florando and W.D. Nix. A microbeam bending method for studying stress-strain relations for metal thin films on silicon substrates. *J Mech Phys Solids*, 53: 619-638, 2005

Paul A. Flinn, Donald S. Gardner, and William D. Nix. Measurement and interpretation of stress in aluminum-based metallization as a function of thermal history. *IEEE Trans Electron Devices*, ED-34(3):689–699, 1987.

P. Gruber, J. Böhm, A. Wanner, L. Sauter, R. Spolenak, and E. Arzt. Size effect on crack formation in Cu/Ta and Ta/Cu/Ta thin film systems. *Mat Res Soc Symp Proc*, 821, 272–277, 2004.

P. Gruber. Private communication. 2007.

A. Heinz and P. Neumann. Crack initiation during high cycle fatigue of an austenitic steel. *Acta Metall Mater*, 38(10):1933–1940, 1990.

M. Hommel, O. Kraft, and E. Arzt. A new method to study cyclic deformation of thin films in tension and compression. *J Mater Res*, 14(6): 2373–2376, 1999.

M. Hommel. Röntgenographische Untersuchung des monotonen und zyklischen Verformungsverhaltens dünner Metallschichten auf Substrate. *Dissertation an der Universität Stuttgart*, 1999a.

M. Hommel and O. Kraft. Deformation behavior of thin copper films on deformable substrates. *Acta Mater*, 49(19):3935–3947, 2001.

H.B. Huang. Mechanical properties of free-standing polycrystalline metallic thin films and multilayers. Dissertation, Harvard University, 1998.

H.B. Huang and F. Spaepen. Tensile testing of free-standing Cu, Ag and al thin films and Ag/Cu multilayers. *Acta Mater*, 48(12):3261–3269, 2000.

J.W. Hutchinson and Z. Suo. Mixed mode cracking in layered materials. *Adv Appl Mech*, 29:63–191, 1992.

A. J. Kalkman, A. H. Verbruggen, and G. C. A. M. Janssen. Young's modulus measurements and grain boundary sliding in free-standing thin metal films. *Appl Phys Lett*, 78(18):2673–2675, 2001.

R. M. Keller, S. P. Baker, and E. Arzt. Quantitative analysis of strengthening mechanisms in thin Cu films: Effects of film thickness, grain size, and passivation. *J Mater Res*, 13(5):1307–1317, 1998.

R. M. Keller, S. P. Baker, and E. Arzt. Stress-temperature behavior of unpassivated thin copper films. *Acta Mater*, 47(2):415–426, 1999.

O. Kraft, M. Hommel, and E. Arzt. X-ray diffraction as a tool to study the mechanical behaviour of thin films. *Mater Sci Eng A*, 288(2):209–216, 2000.

O. Kraft, R. Schwaiger, and P. Wellner. Fatigue in thin films: lifetime and damage formation. *Mater Sci Eng A*, 319:919–923, 2001.

O. Kraft and C. A. Volkert. Mechanical testing of thin films and small structures. *Adv Eng Mater*, 3(3):99–110, 2001a.

O. Kraft, P. Wellner, M. Hommel, R. Schwaiger, and E. Arzt. Fatigue behaviour of polycrystalline thin copper films. *Z Metall*, 93(5):392–400, 2002.

Landolt-Bornstein. Numerical Data and functional relationships in science and technology. New Series, *Springer-Verlag*, Berlin, 1979.

S. P. Lacour, D. Chan, S. Wagner, T. Li, and Z. G. Suo. Mechanisms of reversible stretchability of thin metal films on elastomeric substrates. *Appl Phys Lett*, 88(20), 2006.

H-J. Lee, K-W. Kwon, C. Ryu, and R. Sinclair. Thermal stability of a Cu/Ta multilayer: an intriguing interfacial reaction. *Acta Mater*, 47(15): 3965-3975, 1999.

T. Li, Z. G. Suo, S. P. Lacour, and S. Wagner. Compliant thin film patterns of stiff materials as platforms for stretchable electronics. *J Mater Res*, 20(12):3274–3277, 2005.

A.E. Lita and J.E. Sanchez, Jr. Effects of grain growth on dynamic surface scaling during the deposition of Al polycrystalline thin films. *Phys Rev B*, 61(11):7692-7699, 2000.

C.S. Litteken, S. Strohband and R.H. Dauskardt. Residual stress effects on plastic deformation and interfacial fracture in thin-film structures. *Acta Mater*, 53: 1955-1961, 2005.

L. Llanes and C. Laird. Role of annealing twin boundaries in the cyclic deformation of f.c.c. materials. *Mater Sci Eng A*, A157 (1):21–27, 1992.

P. Lukáš and L. Kunz. Effect of grain-size on the high cycle fatigue behavior of polycrystalline copper. *Mater Sci Eng*, 85(1-2):67–75, 1987.

P. Lukáš and L. Kunz. Role of persistent slip bands in fatigue. *Phil Mag*, 84(3-5):317–330, 2004.

B.T. Ma and C. Laird. Overview of fatigue behavior in copper single crystals. i. surface morphology and stage i crack initiation sites for tests at constant strain amplitude. *Acta Metall*, 37(2):325–336, 1989.

S.S. Manson. Behavior of materials under conditions of thermal stress. Technical report, National advisory commission on aeronautics: Report 1170 (Lewis flight propulsion laboratory, Cleveland), 1954.

R. Mönig, R.R. Keller, and C.A. Volkert. Thermal fatigue testing of thin metal films. *Rev Sci Instrum*, 75(11):4997–5004, 2004.

R. Mönig. Thermal fatigue of Cu thin films. *Dissertation an der Universität Stuttgart*, 2005.

H. Mughrabi, F. Ackermann, and K. Herz. Persistent slipbands in fatigued face-centered and body-centered cubic metals. *ASTM Spec Tech Publ*, (675):69–105, 1979.

W.W. Mullins. The Effect of Thermal Grooving on Grain Boundary Motion. *Acta Metall*, 6:414, 1958.

L. Nicola, Y. Xiang, J.J. Vlassak, E. Van der Giessen, and A. Needleman. Plastic deformation of freestanding thin films: Experiments and modeling. *J Mech Phys Solids*, 54(10):2089–2110, 2006.

W.D. Nix. Mechanical-properties of thin-films. *Metall Trans A*, 20(11):2217–2245, 1989.

W.D. Nix. Yielding and strain hardening of thin metal films on substrates. *Scripta Mater*, 39(4-5):545–554, 1998.

J. Nucci, S. Kramer, E. Arzt, and C. A. Volkert. Local strains measured in Al lines during thermal cycling and electromigration using convergent-beam electron diffraction. *J Mater Res*, 20(7):1851–1859, 2005.

H.M. Otte. Lattice Parameter Determinations with an X-Ray Spectrogoniometer by the Debye-Scherrer Method and the Effect of Specimen Condition. *J Appl Phys*, 32(8):1536-1546, 1961.

N.-J. Park and D.P. Field. Predicting thickness dependent twin boundary formation in sputtered Cu films. *Scripta Mater*, 54(6):999–1003, 2006a.

Y.-B. Park, R. Mönig, and C.A. Volkert. Thermal fatigue as a possible failure mechanism in copper interconnects. *Thin Solid Films*, 504(1-2):321–324, 2006.

Y.B. Park, R. Mönig, and C.A. Volkert. Frequency effect on thermal fatigue damage in Cu interconnects. *Thin Solid Films*, 515:3253–3258, 2007.

P. Peralta, L. Llanes, J. Basani, and C. Laird. Deformation from twin-boundary stresses and the role of texture: application to fatigue. *Phil Mag A*, 70(1):219–232, 1994.

M.A. Phillips, R. Spolenak, N. Tamura, W. L. Brown, A.A. MacDowell, R.S. Celestre, H.A. Padmore, B.W. Batterman, E. Arzt, and J.R. Patel. X-ray microdiffraction: local stress distributions in polycrystalline and epitaxial thin films. *Microelectronic Engineering*, 75(1):117–126, 2004.

D.T. Read. Tension-tension fatigue of copper thin films. *Int J Fatigue*, 20(3): 203–209, 1998.

D.T. Read, Y.W. Cheng, R.R. Keller, J.D. McColskey. Tensile properties of free-standing aluminum thin films. *Scripta Mater*, 45: 583-589, 2001.

D.T. Read, Y.W. Cheng, and R. Geiss. Morphology, microstructure, and mechanical properties of a copper electrodeposit. *Microelectron Eng*, 75: 63-70, 2004.

R. Schwaiger and O. Kraft. High cycle fatigue of thin silver films investigated by dynamic microbeam deflection. *Scripta Mater*, 41(8):823–829, 1999.

R. Schwaiger, G. Dehm, and O. Kraft. Cyclic deformation of polycrystalline Cu film. *Phil Mag*, 83(6):693–710, 2003.

R. Schwaiger and O. Kraft. Size effects in the fatigue behavior of thin Ag films. *Acta Mater*, 51(1):195–206, 2003a.

P. Sonnweber-Ribic, P. Gruber, G. Dehm, and E. Arzt. Texture transition in Cu thin films: Electron backscatter diffraction vs. X-ray diffraction. *Acta Mater*, 54 (15):3863–3870, 2006.

M.R. Stoudt, R.C. Cammarata, and R.E. Ricker. Suppression of fatigue cracking with nanometer-scale multilayered coatings. *Scripta Mater*, 43:491–496, 2000.

S. Suresh. *Fatigue of Materials*. Cambridge University Press, 1998.

C.V. Thompson. The yield stress of polycrystalline thin films. *J Mater Res*, 8(2): 237–238, 1993.

C.V. Thompson and R. Carel. Grain Growth and Texture Evolution in Thin Films. *Materials Science Forums* (Proceedings of the 2nd International Conference on Grain Growth, Kitakyushu, Japan), 83:204-206, 1996.

M.D. Thouless, J. Gupta, and J.M.E. Harper. Stress development and relaxation in copper films during thermal cycling. *J Mater Res*, 8(8):1845–1852, 1993.

R. Venkatraman and J. C. Bravman. Separation of film thickness and grainboundary strengthening effects in Al thin-films on Si. *J Mater Res*, 7(8):2040–2048, 1992.

J.J. Vlassak and W.D. Nix. New bulge test technique for the determination of young's modulus and poisson's ratio of thin films. *J Mater Res*, 7(12):3242–3249, 1992.

B. von Blanckenhagen, P. Gumbsch, and E. Arzt. Dislocation sources in discrete dislocation simulations of thin-film plasticity and the hall-petch relation. *Modelling and Simulation in Materials Science and Engineering*, 9(3):157–169, 2001.

B. von Blanckenhagen, P. Gumbsch, and E. Arzt. Dislocation sources and the flow stress of polycrystalline thin metal films. *Phil Mag Lett*, 83(1): 1–8, 2003.

V. Weihnacht and W. Brückner. Dislocation accumulation and strengthening in Cu thin films. *Acta Mater*, 49:2365-2372, 2001.

T.P. Weihs, S. Hong, J.C. Bravman, and W.D. Nix. Mechanical deflection of cantilever microbeams: A new technique for testing the mechanical properties of thin films. *J Mater Res*, 3(5):931–942, 1988.

D. Weiss. Deformation mechanisms in pure and alloyed copper films. *Dissertation an der Universität Stuttgart*, 2000.

D. Weiss, H. Gao and E. Arzt. Constrained diffusional creep in UHV-produced copper thin films. *Acta Mater*, 49:2395-2403, 2001.

A. Wöhler. Versuche zur Ermittelung der auf die Eisenbahnwagen-Achsen einwirkenden Kräfte und der Widerstandsfähigkeit der Wagen-Achsen. *Zeitschrift für Bauwesen*, 10, 1860.

Z. C. Xia and J. W. Hutchinson. Crack patterns in thin films. *J Mech Phys Solids*, 48(6-7):1107–1131, 2000.

Y. Xiang, X. Chen, and J.J. Vlassak. The mechanical properties of electroplated Cu thin films measured by means of the bulge test techniques. *Mater Res Soc Symp Proc* 695: 189–194, Boston, MA, 2002.

Y. Xiang, X. Chen, and J. J. Vlassak. Plane-strain bulge test for thin films. *J Mater Res*, 20(9):2360–2370, 2005.

Y. Xiang, T. Li, Z. Suo, and J.J. Vlassak. High ductility of a metal film adherent on a polymer substrate. *Appl Phys Lett*, **87,** 2005a.

V. Vidal, L. Thilly, F. Lecouturier and P.-O. Renault. Effects of size and geometry on the plasticity of high-strength copper/tantalum nanofilamentary conductors obtained by severe plastic deformation. *Acta Mater*, 54:1063-1075, 2006.

D. Y. W. Yu and F. Spaepen. The yield strength of thin copper films on kapton. *J Appl Phys*, 95(6):2991–2997, 2004.

Z.F. Zhang, Z.G. Wang, and Y.M. Hu. Fatigue crack initiation and fracture behavior of a copper bicrystal with a perpendicular grain boundary. *Mater Sci Eng A*, 269(1-2):136–141, 1999.

G. P. Zhang, R. Schwaiger, C. A. Volkert, and O. Kraft. Effect of film thickness and grain size on fatigue-induced dislocation structures in Cu thin films. *Phil Mag Lett*, 83(8):477–483, 2003.

G. P. Zhang, C. A. Volkert, R. Schwaiger, E. Arzt, and O. Kraft. Damage behaviour of 200-nm thin copper films under cyclic loading. *J Mater Res*, 20(1):201–207, 2005.

G. P. Zhang, C. A. Volkert, R. Schwaiger, P. Wellner, E. Arzt, and O. Kraft. Length-scale-controlled fatigue mechanisms in thin copper films. *Acta Mater*, 54(11):3127–3139, 2006.

G.P. Zhang, R. Moenig, Y.B. Park, E. Arzt and C.A. Volkert: Transmission electron microscopy investigation of thermomechanical fatigue damage in Cu films (to be published), 2007.

Appendix A.   Determination of fatigue failure in Cu films

In Section 4.2.2, the fatigue failure is defined as onset of saturation of extrusion evolution (500 nm, 1.0 μm and 3.0 μm) and crack evolution (50 nm, 100 nm and 200 nm). Fatigue lives of 100 nm (strain range 0.8%), 200 nm (strain range 0.6%) and 1.0 μm (strain range 0.2%) have also been thereby determined. Here the determination of fatigue lives of other films under other strain ranges is listed.

Fig. A-1 through Fig. A-4 show evolution of extrusion (3.0 μm and 500 nm) and crack (50 nm) density as a function of number cycles. Fatigue failure is indicated with arrows as damage evolution reaches to saturation.
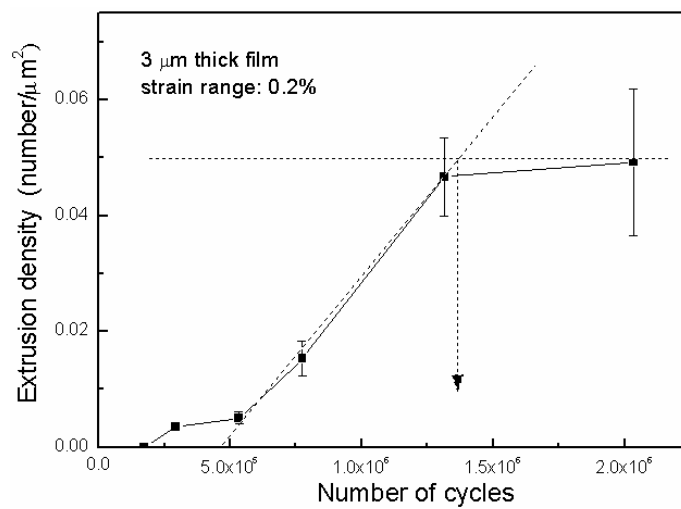
Fig. A-1 Extrusion density in a series A 3.0 μm thick Cu film (strain range 0.2%) as a function of cycle numbers. Fatigue failure is indicated with arrow.
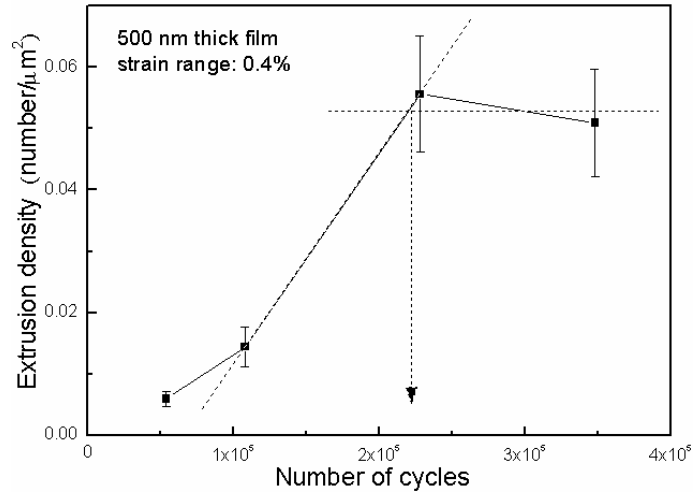
Fig. A-2 Extrusion density in a series A 500 nm thick Cu film (strain range 0.4%) as a function of cycle numbers. Fatigue failure is indicated with arrow.
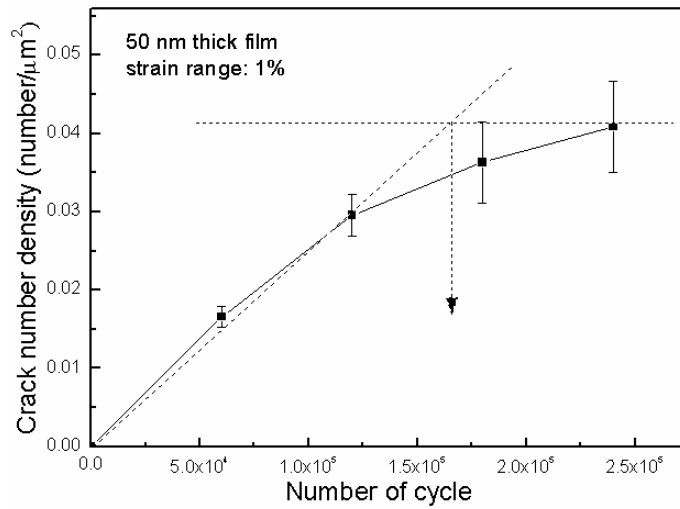

Fig. A-3 Crack density in a series A 50 nm thick Cu film (strain range 1%) as a function of cycle numbers. Fatigue failure is indicated with arrow.
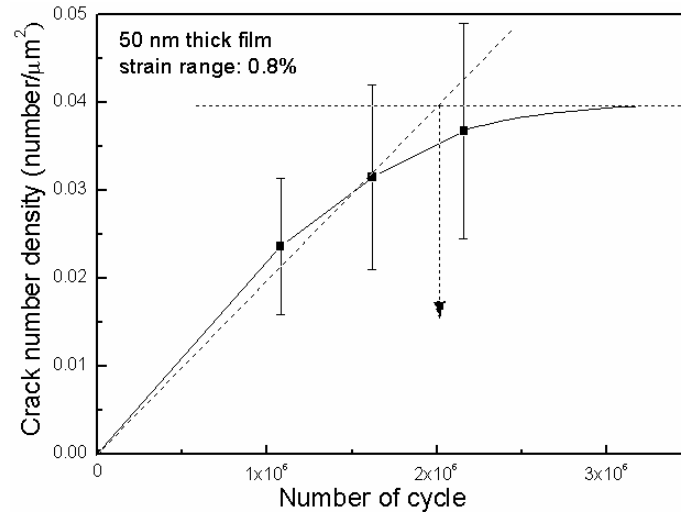
Fig. A-4 Crack density in a series A 50 nm thick Cu film (strain range 0.8%) as a function of cycle numbers. Fatigue failure is indicated with arrow.

Several data (3.0 μm and 1.0 μm, strain range: 0.4%; 500 nm, strain range: 0.6%; 200 nm, strain range: 0.8%; 100 nm, strain range: 1%; 50 nm, strain range: 1.2%) in fatigue life plot (Fig. 4-22) are not determined directly using damage evolution plots like showed in above 4 figures, because fatigue damage in these films after first testing interval using DMA, which is about 10^4 cycles (minimum of interval), is clear enough and qualitatively comparable with the damage state at saturation in other films. In these cases, the number of cycles in first interval is defined as fatigue life.

Appendix B.   Determination of fatigue failure in Cu films with Ta layers

Fatigue failure determined here is also based on the principle of onset of saturation in damage evolution introduced in Section 4.2.2. Crack densities of 100 nm thick Cu, Cu/Ta, and Ta/Cu/Ta film stacks under different strain ranges are plotted in Fig. B-1 to Fig. B-5 as function of number of cycles. Fatigue failure is indicated with arrows showing the onset of saturation of crack density.
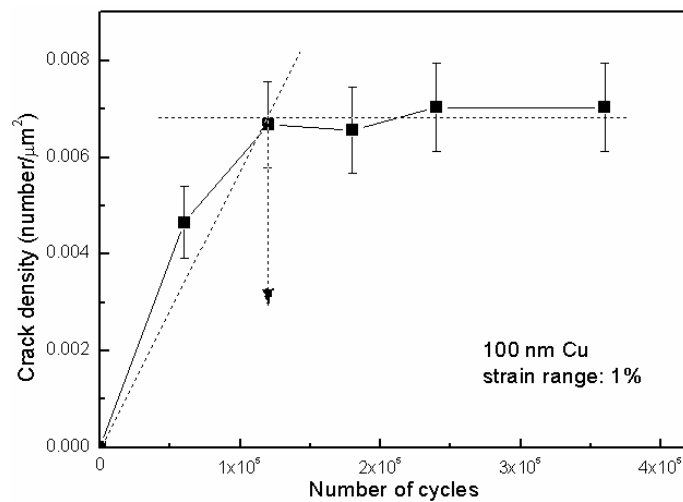

Fig. B-1 Crack density in a series B 100 nm thick Cu film (strain range 1%) as a function of cycle numbers. Fatigue failure is indicated with arrow.
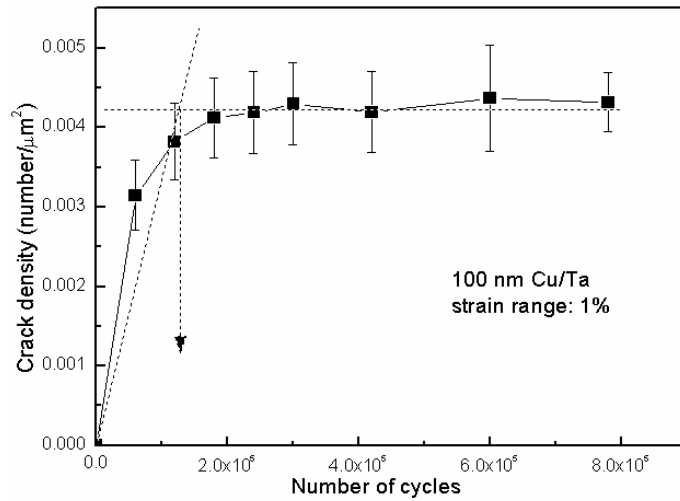
Fig. B-2 Crack density in a series B Cu/Ta film stack with 100 nm thick Cu film (strain range 1%) as a function of cycle numbers. Fatigue failure is indicated with arrow.
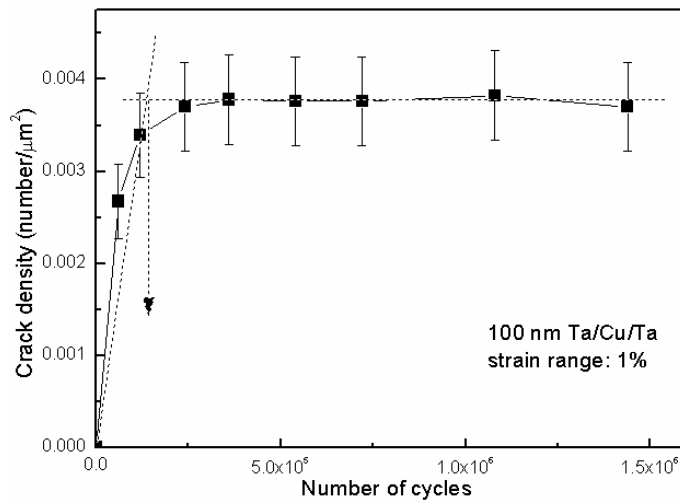

Fig. B-3 Crack density in a series B Ta/Cu/Ta film stack with 100 nm thick Cu film (strain range 1%) as a function of cycle numbers. Fatigue failure is indicated with arrow.
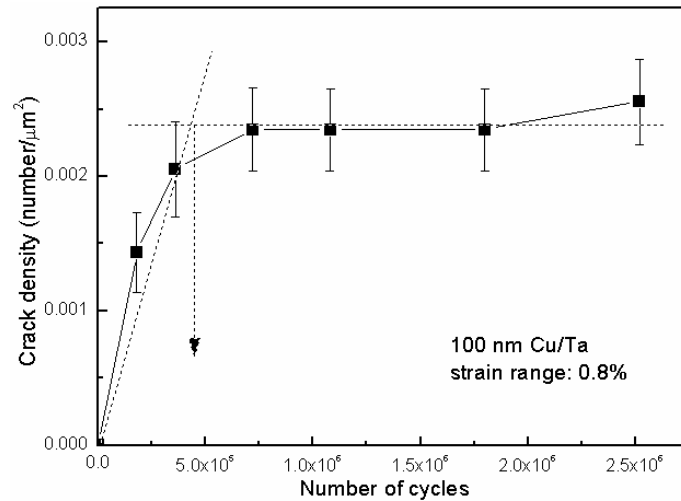
Fig. B-4 Crack density in a series B Cu/Ta film stack with 100 nm thick Cu film (strain range 0.8%) as a function of cycle numbers. Fatigue failure is indicated with arrow.
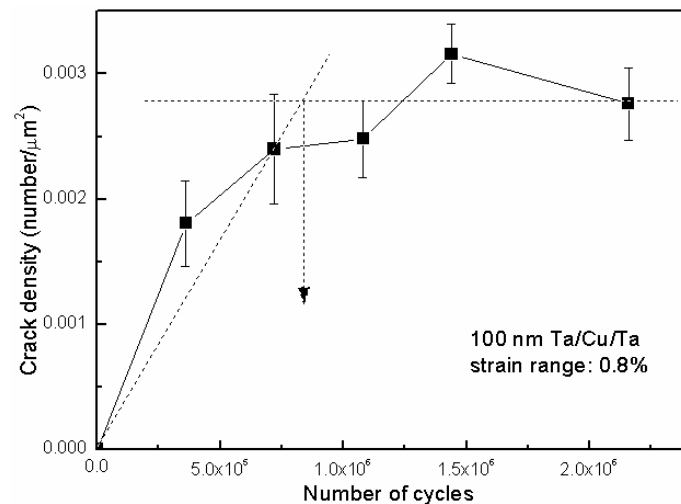

Fig. B-5 Crack density in a series B Ta/Cu/Ta film stack with 100 nm thick Cu film (strain range 0.8%) as a function of cycle numbers. Fatigue failure is indicated with arrow.

In Section 4.2.2, fatigue failure in 1.0 μm thick films is been defined as onset of saturation of extrusion density. But here in 1.0 μm thick Ta/Cu/Ta film stacks, extrusions are depressed by Ta over-layer and difficult to identify. But in Section4.2.2, we see the cracks appear at the site of saturation of extrusion density. So the fatigue failure here in 1.0 μm thick Cu, Cu/Ta and Ta/Cu/Ta film stacks is defined as appearance of cracks.

Resume

Personal Details

Name:	Dong Wang
Date / Place of birth:	07 Nov 1977 / Nei Mongol, China
Marital status:	Married since 10 Nov 2004 to Ying Liu
Adress:	Max-Planck-Str. 14, 76344 Eggenstein-Leopoldshafen

Education

1984 – 1990	Primary school, Linhe, Nei Mongol, China
1990 – 1993	Middle school, Linhe, Nei Mongol, China
1993 – 1996	High school, Linhe, Nei Mongol, China
1996 – 2000	Wuhan University of Technology, Wuhan, China *Bachelor of fine chemical engineering*
2001 – 2004	RWTH Aachen, Aachen, Germany *Master of materials science*
2004 – 2007	Forschungszentrum Karlsruhe, Karlsruhe, Germany *Ph.d. candidate*

Karlsruhe, May 22nd 2007